

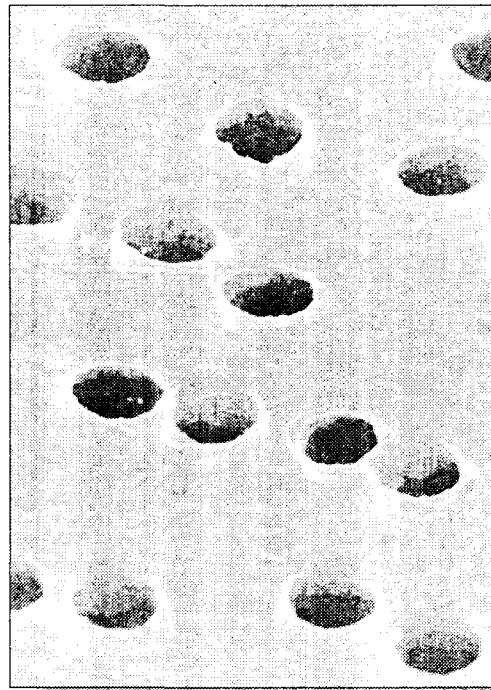
The Ministry of Russian Federation for Atomic Energy
The State Scientific Center of Russian Federation
INSTITUTE FOR PHYSICS AND POWER ENGINEERING
named after Acad. A.I.Leipunsky

Nuclear Physics Department

ANNUAL REPORT

1999

Surface of the track membrane "REATRACK"



OBNINSK

Annual Report

Nuclear Physics Department

**The Ministry of Russian Federation for Atomic Energy
The State Scientific Center of Russian Federation
INSTITUTE FOR PHYSICS AND POWER
ENGINEERING
named after Acad. A.I.Leipunsky**

For the year 1 January to 31 December 1999

Contacts:

**Nuclear Physics Department
The State Scientific Center of Russian Federation
Institute for Physics and Power Engineering
named after Acad. A.I.Leipunsky.
The Ministry of the Russian Federation for Atomic
Energy.
249020, Obninsk, Kaluga Region, Russia
FAX: (095) 230 23 26, 8833112
e-mail: kuzminov@ippe.obninsk.ru**

Editor:

B.D.Kuzminov

CONTENTS

PREFACE

1. DEPARTMENT STRUCTURE	5
2. SCIENTIFIC RESEARCH	
2.1 Nuclear Fission.....	7
2.2 Nuclear Structure and Nuclear Reactions.....	16
2.3 Nuclear Data.....	32
2.4 Transmutation	54
2.5 Condensed Matter Physics.....	60
2.6 Mathematical Modeling	83
2.7 Applied Research.....	102
2.8 High-Voltage Accelerators.....	109
2.9 Instruments and Methods.....	116
3. ACCELERATOR COMPLEX.....	121
4. PUBLICATIONS.....	122
5. MEETINGS AND CONFERENCES.....	133
6. PARTICIPATION IN INTERNATIONAL AND NATIONAL CONFERENCES AND MEETINGS	134
7. COOPERATION	135

P R E F A C E

As at previous years this annual report has been prepared to promote exchange of information between the IPPE Nuclear Physics Department and other Russian and foreign Scientific Centers. The scope of activity of Nuclear Physics Department is: measurement, compilation and evaluation of nuclear data for nuclear power technology and applied science; the experimental and theoretical research of nuclear fission, nuclear structure and nuclear reactions; condensed matter physics; mathematical modeling; high voltage accelerators and applied research.

The main results of work in 1999 year are as follows:

- The physical experiment using pulsed proton beam of tandem-generator EGP-15 was started;
- Measurements of delayed neutron yield for set of actinides were continued in wide energy range;
- The files of evaluated nuclear data for $^{241,243}\text{Am}$ were prepared;
- Structural and dynamical properties of some condensed matter were researched in neutron scattering experiments;
- Mathematical modelling of some complex processes connected with fast reactor physics, fluid mechanics, heat and mass transfer, single crystal growth etc. was realised;
- High selectivity polymer track membranes were prepared for sterilising filtration of liquid and gaseous media.



B. Fursov

Director of Nuclear Physics Department

1. DEPARTMENT STRUCTURE

DIRECTORATE:

Director: B.I.FURSOV
Deputy Directors: B.D.KUZMINOV
V.E.RUDNIKOV

THEORETICAL NUCLEAR PHYSICS DIVISION

Head: A.V.IGNATYUK

THEORETICAL NUCLEAR PHYSICS LABORATORY

Head: Yu.N.SHUBIN

NUCLEAR DATA CENTER

Head: V.N.MANOKHIN

EXPERIMENTAL NUCLEAR PHYSICS DIVISION

Head: A.A.GOVERDOVSKI

NUCLEAR FISSION PHYSICS LABORATORY

Head: M.I.SVIRIN

NEUTRON SPECTROMETRY LABORATORY

Head: B.V.ZHURAVLEV

NUCLEAR REACTIONS LABORATORY

Head: V.M.PIKSAIKIN

NUCLEAR FISSION DYNAMICS LABORATORY

Head: Yu.B.OSTAPENKO

APPLIED NUCLEAR PHYSICS LABORATORY

Head: A.A.TUMANOV

HIGH-VOLTAGE ACCELERATORS DIVISION

Head: A.I.GLOTOV

CONDENCED MATTER PHYSICS LABORATORY

Head: A.V.PUCHKOV

MATHEMATICS AND SOFTWARE DIVISION

Head: V.P.GINKIN

NUMERICAL METHODS LABORATORY

Head: V.P.GINKIN

PRECISION METHODS LABORATORY

Head: V.K.ARTEMYEV

STATISTICAL METHODS LABORATORY

Head: S.V.PUPKO

2. SCIENTIFIC RESEARCH

2.1 NUCLEAR FISSION

Photofission Cross Section of Americium Isotopes in the Energy Range from 6 to 12 MeV

A.S. Soldatov

The photofission cross-sections for ^{241}Am , $^{242\text{m}}\text{Am}$ and ^{243}Am were measured in energy range from 6 to 12 MeV at the bremsstrahlung beams of the SSC RF IPPE microtron with energy step from of 50 to 200 keV (Fig. 1). The measurements were performed with relative method by using of the photofission cross-section of ^{238}U as a cross-section standard [1,2]. The photofission cross-section of $^{242\text{m}}\text{Am}$ in energy region of 6-12 MeV and the photofission cross-section of ^{243}Am in energy region of 6-7 MeV were measured first. New measurements for ^{241}Am showed that our previous results of measurements of the photofission cross-sections for ^{241}Am [1] were too high. The results of present measurements of the photofission cross-sections for ^{241}Am agree with the results of other works [3,4]. We got the argument for existing a resonans of the photofission cross-sections for ^{241}Am in the 6 MeV energy region, it is more believed to appear because of the low energy resonances structure of the dipol photoabsorbtion cross-section. The fact that fissility for ^{243}Am is more then the fissility for ^{241}Am [3] was not confirmed. The comparison of energy dependence of fissilitties for americium isotopes from photofission and from reactions like $^{240}\text{Pu}(^3\text{He},\text{df})^{241}\text{Am}$ [5,6] showed the coincidence of the observed fission thresholds and the plateaus in the energy dependence for $E > 7.5$ MeV range (Fig. 2).

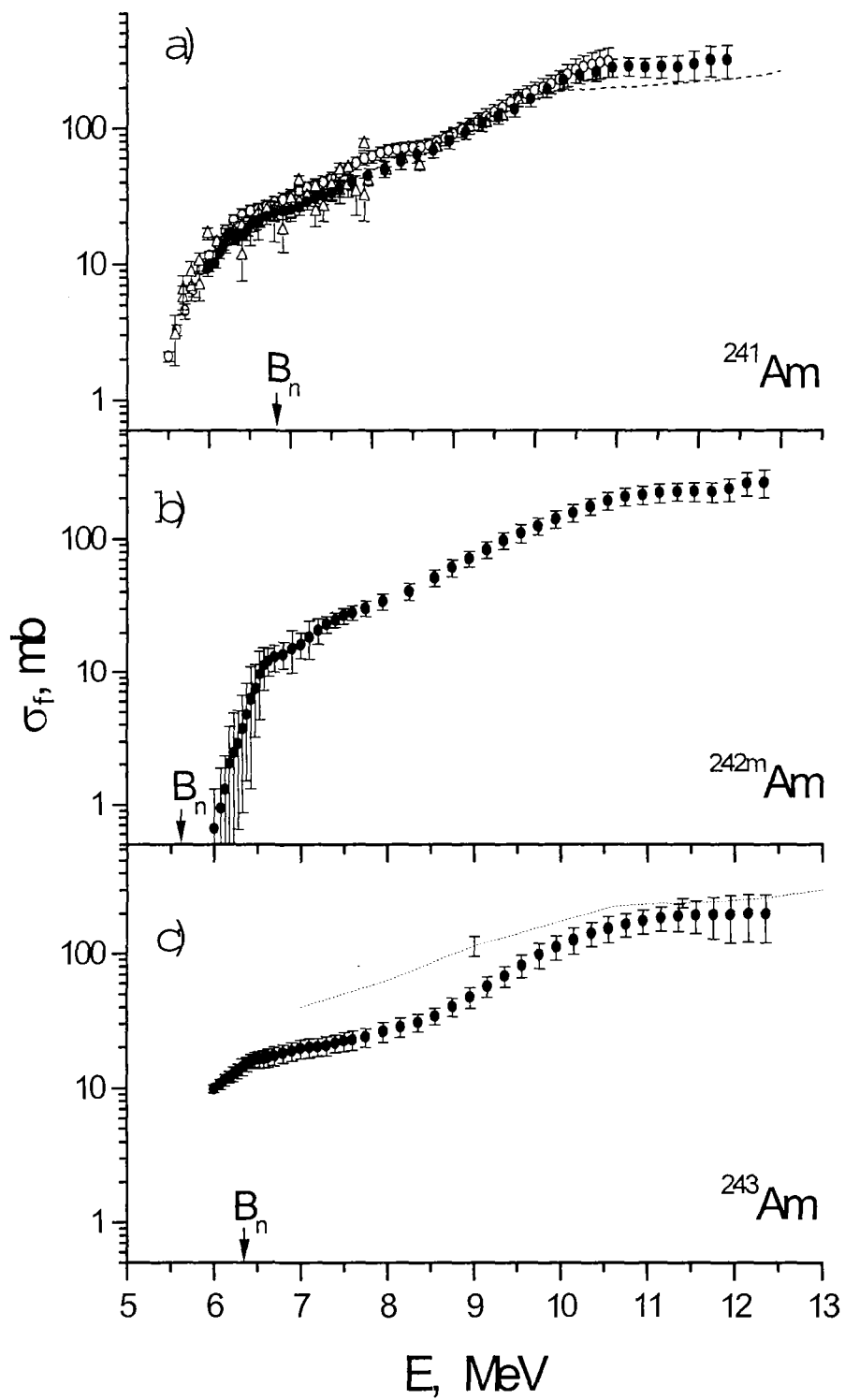


Fig. 1. The energy dependence of photofission cross section: (a) for ^{241}Am , (b) - for ^{242m}Am , (c) - for ^{243}Am , \bullet - data from present work, \circ - data from [1], ∇ - data from [4], dashed curve - data from [8], B_n - neutron binding energy

New Evidence of Scission Neutron Existence

N.V. Kornilov, A.B. Kagalenko, F.-J. Hambsch¹

¹*Institute for Reference Materials and Measurements (IRMM), Geel, Belgium
(This paper was submitted for ISINN-7, Dubna)*

The investigations of the fission neutron angular-energy distribution relative to the fragment direction depending on mass split and fragment kinetic energy gives unique information about the neutron emission mechanism and the fission process. However, these experiments are very complicated and time consuming which may explain some contradictions between individual experimental results and rather different conclusions made by the authors.

The fission neutrons may be emitted from three different sources.

1. The main part of the neutrons are evaporated from moving fragments including possible emission during fragment acceleration if the neutron life time in exited fragments is comparable with their acceleration time. The incorporation of the neutron emission during fragment acceleration does not change very much the main features of the angular- energy distribution which may be described by a reduction of the fragment Center of Mass (CMS) velocity.
2. Neutrons accompanying ternary fission. These neutrons are emitted from neutron-unstable light charged particles, e.g. ^5He , ^7He and they are collimated around $\sim 90^\circ$ due to the charged particle movement. However, their contribution is very small.
3. Neutrons emitted from the compound system during descent from saddle (exit point of the tunneling mechanism for spontaneous fission) to scission or at the moment of scission (Scission Neutrons, SCN). However, experimental knowledge about the fraction of SCN and their energy spectrum is scarce and very contradictory.

In this paper we analyzed the results of three independent experiments [1-3] which measured the neutron energy- angular distribution relative to the fragment direction of $^{252}\text{Cf}(\text{SF})$. The results of these experiments being in reasonable agreement allow us to conclude that a $(30\pm 5)\%$ neutron surplus exists at $\sim 90^\circ$, which can not be accounted for with the assumption that all neutrons are emitted from fully accelerated fragments. This experimental fact required the incorporation of neutron emission during fragment acceleration or the existence of an additional source of neutrons (SCN). It was shown that the assumption of SCN gives a more reliable explanation of all experimental peculiarities. Angular and energy distributions of additional neutrons were evaluated from IRMM experimental data [3] and were compared with the results of previous experiments [1,2].

References

1. Bowman H. R., Milton J.C.D., et al., Velocity and angular distributions of prompt neutrons from spontaneous fission of ^{252}Cf , Phys. Rev. 126,2120, 1962.
2. Piksaikin Y.M., et al., J. Nucl. Phys. 1977, 25(4), 723.;
Seregina E.A., Djatchenko P.P., J. Nucl. Phys. 1985, 42, 6(12), 1337;
Seregina E.A. Measurements and analysis of angular-energy distribution for $^{252}\text{Cf}(\text{SF})$ neutrons, PhD thesis, Obninsk, 1985.
3. Budtz-Jorgensen C., Knitter H-H. Simultaneous investigation of fission fragments and neutrons in $^{252}\text{Cf}(\text{SF})$, Nucl. Phys. A490, 307, 1988.

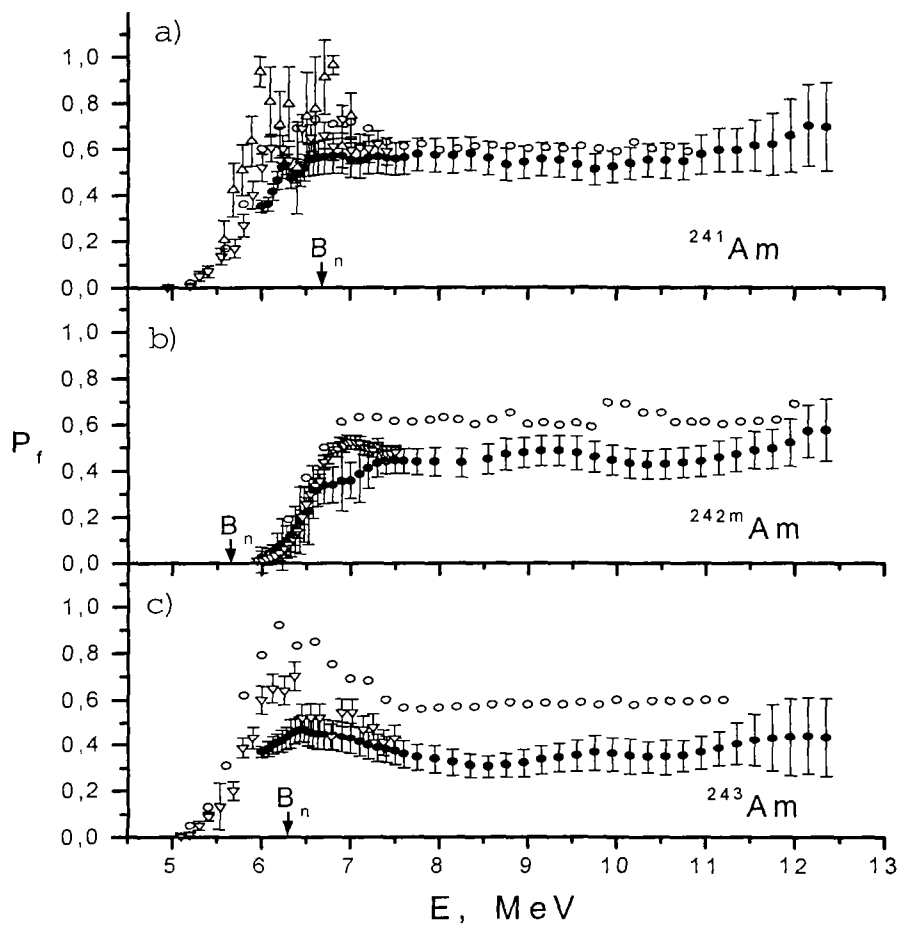


Fig. 2. Comparison of energy dependence of fissilities for americium isotopes from photofission and from reactions like $^{240}\text{Pu}(^3\text{He},\text{df})^{241}\text{Am}$: (a) - for ^{241}Am , (b) - for $^{242\text{m}}\text{Am}$, (c) - for ^{243}Am . . data from present work, o - data from [6], ~ - data from [4], ∇ - data from [5]. B_n - neutron binding energy .

References

1. A.S.Soldatov, G.N.Smirenkin, Yad. Fiz. 1992 V.55. p.3153.
2. A.S.Soldatov et al., Yad. Fiz. 1993. V.56. p.16.
3. I.S.Koretskaya et al., Yad. Fiz. 1979. V.30. p.910.
4. S.J. Watson, D.J.S. Findlay and M.R. Sene //Nucl. Phys. 1992. V.A548. p.365.
5. B.B.Back et al.// Proc. Of Int. Symp. on Phys. and Chem. Fission React. 1973. Vienna. IAEA. 1974. V.I. p.3.
6. A.Gavron et al.// Phys. Rev. 1976. V.C13. p.2374.

Relative Abundance and Periods of Delayed Neutrons from Fission of ^{239}Pu by Fast Neutrons

*V.M. Piksaikin, L.E. Kazakov, S.G. Isaev, G.G. Korolev,
V.A. Roshenko, M.Z. Tarasko, R.G. Tertytchnyi*

The fundamental role of delayed neutrons in the kinetic behavior, control, and safety of nuclear reactors is well known today, being a matter of practical experience in hundreds of installations around the world. In spite of great efforts devoted to the investigation of delayed-neutron physics, the fundamental delayed-neutron parameters of several of the most common fissionable isotopes encountered in reactor systems are still poorly known. For example, delayed-neutron parameters used in most reactor physics applications are usually associated with either thermal or fast fission spectrum. It is difficult for the reactor designer to select the most applicable delayed neutron data set for an intermediate-spectrum system. In cases like this, the problem is further exacerbated because there is no clear-cut method to combine thermal and fast delayed-neutron sets since the group decay constants are different. This variation in decay constants is the direct result of the high correlation that naturally occurs amongst the various parameters (i.e., the group abundance and decay constants) in the delayed neutron model when performing the least-squares fit. Without the benefit of a consistent set of decay constants from energy-to-energy, the choice of which decay constants best characterize the delayed neutrons for a particular energy spectrum may not be obvious.

The primary objective of the present work was to measure the energy-dependent delayed neutron group parameters for ^{239}Pu for incident-neutron energies ranging from thermal spectrum up to 4.9 MeV.

The method that will be used to perform these new measurements will be based on a periodic irradiation technique in which samples of each isotope will be fissioned by mono-energetic neutrons from T(p,n), D(d,n) and T(d,n) reactions produced by an electrostatic accelerator. The accelerator, the KG-2.5 at IPPE (Obninsk), uses 300 mA of ion current, and, because of the experimental setup, the sample can be transferred out of the beam in 150 milliseconds. Following irradiation, the samples were counted by 30 BF₃ neutron counters uniformly distributed in three concentric circles in a polyethylene block.

Analysis of delayed neutron decay curves for each isotope were performed by using a generalized least-squares fitting procedure to obtain the traditional 6-group decay constants and relative abundance at each incident-neutron energy.

Experimentally determined delayed neutron parameters for neutron-induced fission of ^{239}Pu in the energy range from thermal energies to 4.9 MeV are presented as a traditional 6-group model. The comparison of the obtained energy-dependent DN group parameters with data of other authors was performed in the terms of the average half-life of the DN precursors. Energy dependence of the average half-life of DN precursors for neutron-induced fission of ^{239}Pu is shown on Fig. 1.

It is shown, that there is a significant energy dependence of DN group parameters in the energy range of primary neutrons from thermal up to 4.9 MeV, which appears as 10% decrease of the average half-life of DN precursors in the studied energy range of primary neutrons. It is obvious, that such modification of DN group parameters must be taken into account in reactor calculations. The data obtained in present work can be used

for deriving the group constants for reactors with an intermediate neutron spectrum, which differ from both thermal and fast.

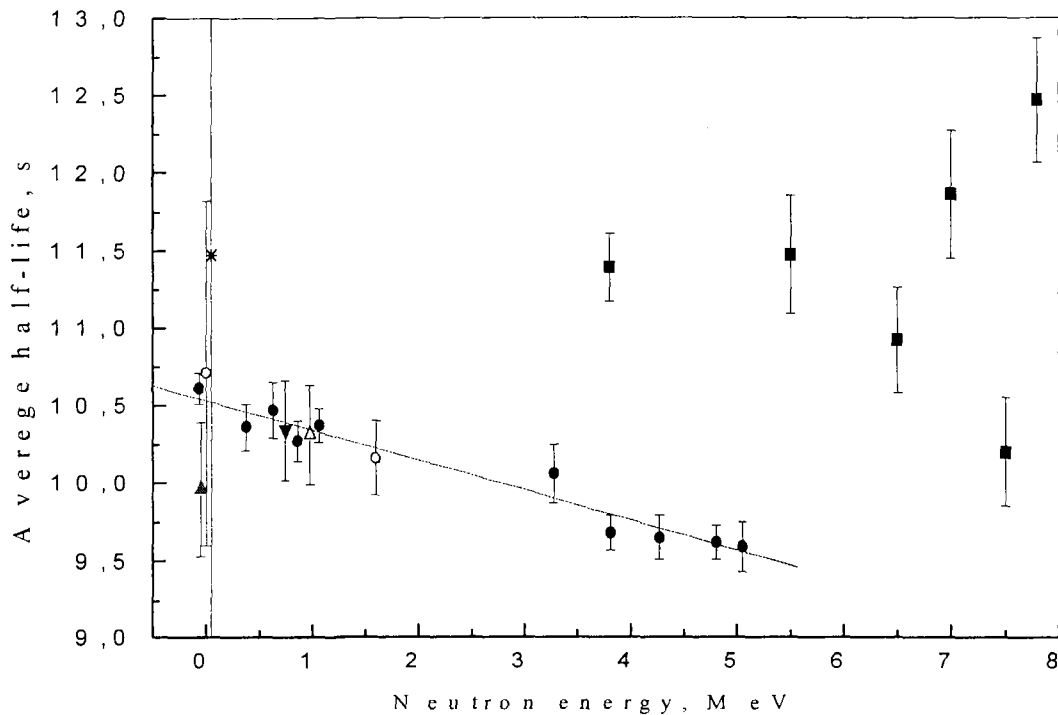


Fig. 1. Energy dependence of the average half-life of DN precursors for neutron-induced fission of ^{239}Pu .

- - present work
- ▲ - Waldo
- △ - Rose
- - Keepin
- - Maksyutenko
- * - Huizinga
- - approximation by function $\langle T \rangle = a + b \cdot E_n$
- ▼ - Besant

References

- H. Rose and R. D. Smith, "Delayed Neutron Investigations with the ZEPHYR Fast Reactor, Part II - The Delayed Neutrons Arising from Fast Fission in ^{235}U , ^{233}U , ^{238}U , ^{239}Pu and ^{232}Th ", J. Nucl. Energy, 4, p.133 (1957).
- B.P. Maksyutenko, "Delayed neutrons from ^{239}Pu ", *Yadernaya Fizika* (English translation), V.15, No.2, p.848 (August 1, 1963).
- R.W. Waldo, R.A. Karam, R.A. Meyer, "Delayed Neutron Yields: Time Dependent Measurements and a Predictive Model", Physical Review C, 23, No.3, p.1113 (March, 1981).
- G.R. Keepin, T.F. Wimett, and R.K. Zeigler, "Delayed Neutrons from Fissionable Isotopes of Uranium, Plutonium and Thorium", Physical Review, 107, 4, p.1044 (Aug. 15, 1957).
- M. Huizinga, R.J. Onega, G.E. Rambo, and A. Robeson, "Delayed Neutron Half-Lives for ^{233}U , ^{235}U , and ^{239}Pu ," Trans.Am.Nucl.Soc., V.12, 1, p.289, 1969.
- C.B. Besant, P.J. Challen, M.H. McTaggart, P. Tavoularidis, J.G. Williams, "Absolute Yields and Group Constants of Delayed Neutrons in Fast Fission of ^{235}U , ^{238}U and ^{239}Pu ", J. Br. Nucl. Energy Soc., 16, p.161 (1977).

Angular Anisotropy of Fission Fragments from the Resonance Neutron Induced Fission of Aligned ^{235}U Target and the Role of $J^\pi K$ Fission Channels

*D.I. Tambovtsev, L.K. Kozlovsky, N.N. Gonin, W.I. Furman¹, Yu.N. Kopach¹,
A.B. Popov¹ and J. Kliman^{1,2}*

¹*Joint Institute for Nuclear Research, Dubna, Russia*

²*Institute of Physics SAS Bratislava, Slovakia*

Fission induced by slow neutrons is one of the unique tools for studying the quantum-mechanical aspects of the fission process. It gives a possibility to obtain information about the fission amplitudes $\gamma_{J^\pi K}^{\lambda}$ for a given resonance λ . These parameters form a basis for a quantitative description of the fission process induced by resonance neutrons.

We performed an experimental study of the energy dependence of the differential fission cross section (fission fragment angular anisotropy) of ^{235}U resonance neutron induced fission using an aligned target and unpolarized neutrons.

The experiment has been performed at the booster IBR-30 + LEA-40 in Dubna. The detailed description of the experimental set-up can be found in [1] and the previous data analysis in [2]. The experimental data at end of 1999 of the energy dependence of the A_2 coefficient, which characterizes the angular anisotropy of fission fragments, is shown in Fig. 1.

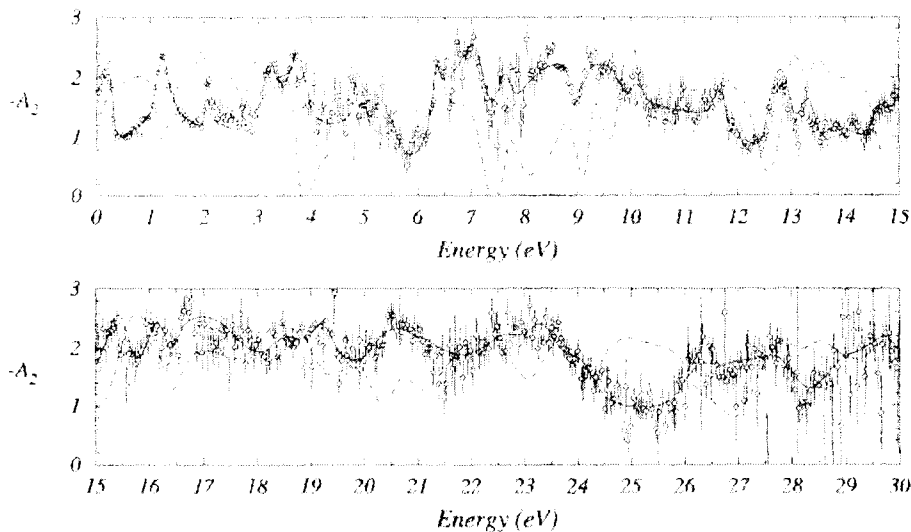


Fig. 1: The results of the fit (solid curve) for $A_2(E)$, circles are experimental data. Dashed line is calculated using the resonance parameters from the ENDF /B-VI library.

For a combined analysis, we used the experimental data of the A_2 coefficient and known data of total neutron, total and spin-separated fission cross section. These experimental data sets were fitted over the energy region 0-30 eV using the R-matrix formalism in the Reich-Moore approximation with the inclusion of formulae for $A_2(E)$

derived in ref. [2]. In the fit, each resonance λ was described by six resonance parameters: E_λ , $\Gamma_{\gamma\lambda}$, $\gamma_{n\lambda}$, $\gamma_{f\lambda}$, Φ_λ and θ_λ . The radiative width $\Gamma_{\gamma\lambda}$ was fixed and equals 0.039 eV for all resonances. All other parameters were varied.

First we analyzed the data assuming that three channels are open for the spin group $J=3$ ($K=0,1,2$) and two for the spin group $J=4$ ($K=1,2$) [2]. According to the commonly used assumption [4], the $J^\pi K = 4^0$ state is forbidden by parity conservation. The integral distributions of the partial fission widths for the spin group $J=4$ obtained in such approximation turned out to be not consistent with the Porter-Thomas distribution (see Fig. 2, right column). An additional fission channel seems to be open for this spin group.

It is necessary to note that the conclusion [4] about absolute forbiddenness of the 4^0 channel was based on A.Bohr hypothesis [3] that the fissioning nucleus at saddle point was mirror symmetric with respect to the plane perpendicular to the fission axis. However, more careful examination of the problem (see for details [5]) leads to a conclusion that the 4^0 channel has higher first fission barrier and relatively low second one for asymmetric fission modes. Thus, one would expect the $J^\pi K=4^0$ channel to be at least partially open for our case. So we reanalyzed the data assuming that all three channels are open for both spin groups.

The results of the final fit for $A_2(E)$ are shown in Fig. 1. All other cross sections are also well reproduced. The dashed line is calculated using a set of resonance parameters from the ENDF/B-VI library which also describes all other cross sections quite well, but obviously fails to reproduce the A_2 energy dependence.

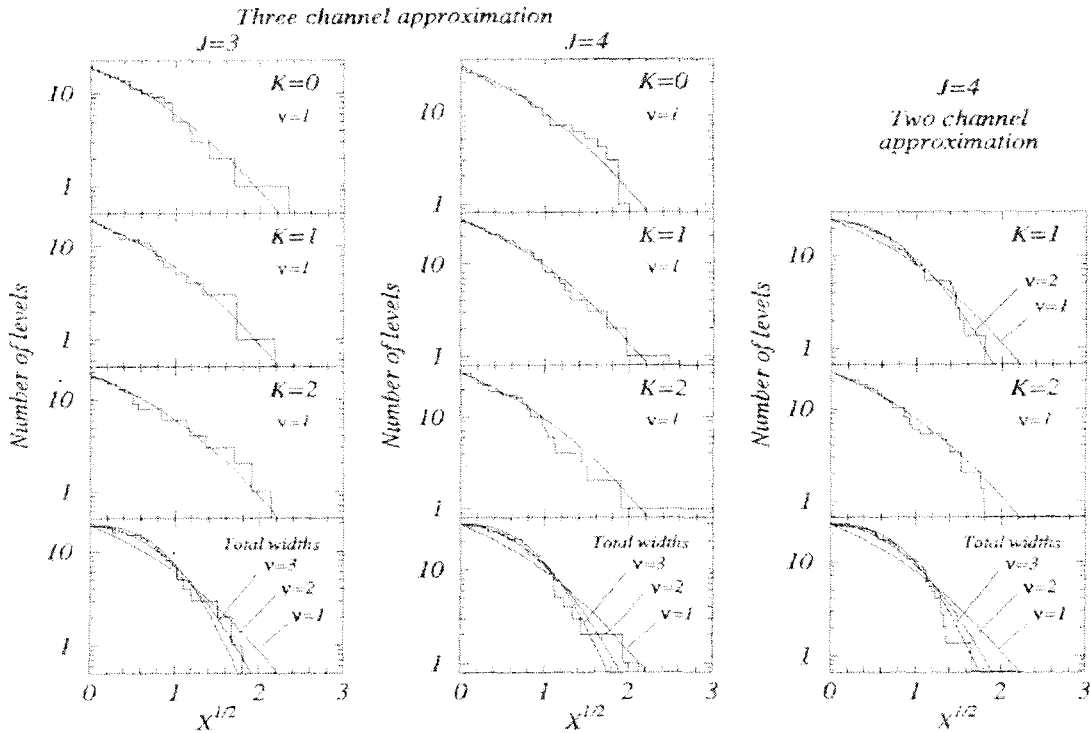


Fig. 2. Integral distributions of partial and total fission widths (number of resonances with $\langle \Gamma_{f\lambda} / \Gamma_{\text{fl}} \rangle X$). Solid lines are the χ^2 -distributions with ν degrees of freedom.

The integral distributions of the partial and total fission widths of resonances in the energy interval 0-30 eV are given in Fig. 2 (left and middle). The experimental distributions for each separate $J^{\pi}K$ channel now are in good agreement with the Porter-Thomas distribution. The integral distributions of the total fission widths for both channels fluctuate according to the χ^2 -distribution with the number of degrees of freedom being between $\nu=2$ and 3.

The average contributions of different fission channels, which can be regarded as a measure of the degree of openness of a given channel are shown in Tab.1. One can see that these values are almost equal for both spin groups. The $K=0$ channel seems to be somewhat suppressed, which is consistent with modern theoretical considerations [5].

Table 1. Degrees of openness of different fission channels (%)

	K=0	K=1	K=2
J=3	25	39	35
J=4	26	40	34
J=3+4	26	40	34

Finally, it should be noted that the obtained set of resonance parameters is not uniquely determined while. It depends on the choice of negative resonances as well as on inclusion of resonances with small neutron and large total fission widths. However, since this parameter set includes all possible K channels, it forms the most reliable basis for quantitative analysis of s - and p -resonance interference. A combined study of neutron energy dependence of fragment mass-TKE distributions together with an angular anisotropy coefficient can give new information about the interconnection of the Bohr fission channels and fission modes.

References

1. D.I. Tambovtsev, L.K. Kozlovsky, N.N. Gonin, N.S. Rabotnov, Yu.N. Kopach, A.B. Popov, W.I. Furman, J. Kliman, H. Postma, A.A. Bogdzal, and M.A. Guseinov, Phys. At. Nucl. 60/6, 877 (1997).
2. Yu.N. Kopach, A.B. Popov, W.I. Furman, N.N. Gonin, L.K. Kozlovsky, D.I. Tambovtsev, and J. Kliman, Phys. At. Nucl. 62/5, 900 (1999)
3. A. Bohr, in Proc. 1st Int. Conf. Peaceful Uses At. Energy, Geneva, Vol.2, p.151 (1956).
4. J.E. Lynn, "Theory of Neutron Resonance Reactions", (Clarendon Press, Oxford, 1968).
5. W.I. Furman and A.L. Barabanov, in Proc. of the Sem. on Fission Pont d'Oye III, edited by C. Wagemans, Castle of Pont d'Oye, Habay-la-Neuve, Belgium, Oct. 24-26, 1999, to be published.

2.2 NUCLEAR STRUCTURE AND NUCLEAR REACTIONS

Level Density of ^{59}Ni

B.V. Zhuravlev, N.N. Titarenko, V.I. Trykova

Absolute level density of ^{59}Ni , its energy and spin dependence, model parameters have been determined from the measurements of neutron emission spectra and angular distribution in (α, n) reaction. Previous studies [1,2,3] had shown that level density of ^{59}Ni from evaporation spectra does not agree with value obtained by neutron resonance counting, and the value of effective moment of inertia varies by about a factor of two, being below a rigid body value. The aim of present work was a study of level density of ^{59}Ni at excitation energy range of (0-15) MeV on the basis of the measurements performed by us earlier [4,5] and the new neutron resonance data [6].

Neutron spectra and angular distributions from reaction $^{56}\text{Fe}(\alpha, n)^{59}\text{Ni}$ at α -particle energies of 12.3, 16.3, 18.3 MeV were measured on HI-13 tandem Van-de-Graaff accelerator of China Institute of Atomic Energy [4] and at α -particle energy of 26.6 MeV on 150 cm cyclotron of Institute of Physics and Power Engineering [5] by means of time-of flight technique. The new neutron resonance data for ^{59}Ni were obtained in the work [6] from very high resolution transmission measurements on GELINA facility.

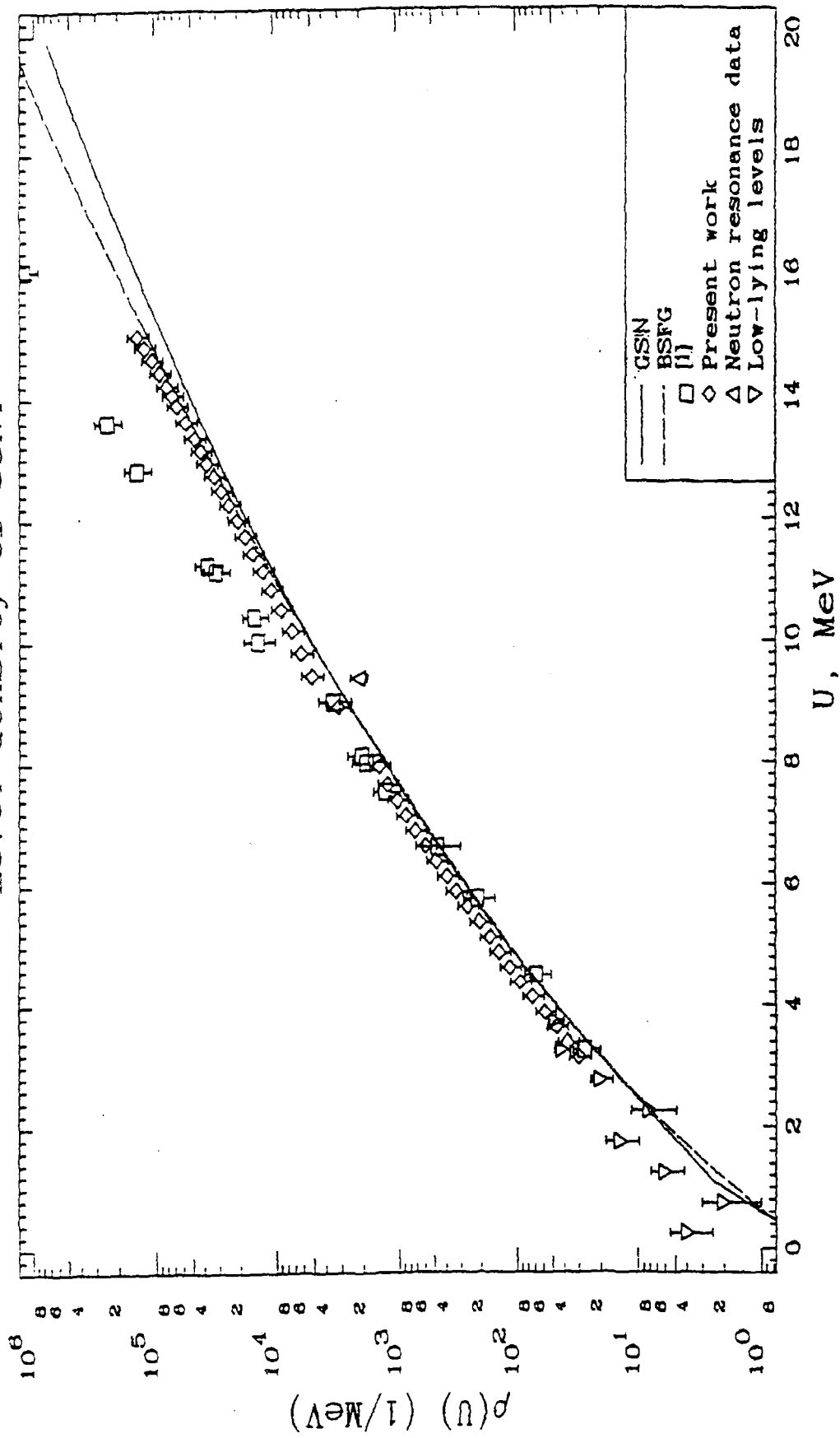
The method of nuclear level density extraction from evaporation spectra is based on the fact that the level density is one of the most critical components of the statistical model calculations. To determine the level density of a residual nucleus we proceeded in two steps:

1. The model dependence of level density is chosen and the parameters are adjusted such that the cross-section calculated by means of Hauser-Feshbach formula fits the measured value in the energy range of discrete levels. It means that the total decay width of compound nucleus is determined,
2. Using this model of level density we calculate by means of Hauser-Feshbach formalism the cross-section for continuum part of spectrum and absolute level density was determined in a wide range of excitation energy from comparison of the spectra measured and calculated.

The angular distributions were calculated as a function of ratio of effective moment of inertia to its rigid sphere value as a variable parameter to determine from comparison with experimental data the spin cut-off parameter and effective moment of inertia. All calculations in the framework of an optic-statistical approach have been carried out with the PEAK-98 code [8] provided with automatic search of the parameters on the experimental data.

The obtained results on level density of ^{59}Ni is presented in fig. The uncertainty is ~20%. As can be seen from fig., the our data are in an agreement in the limits of errors with the results of ref.[1] at excitation energy <10 MeV and with low-lying level data. The increased divergence at excitation energies >10 MeV is connected, obviously, with the level density derivation procedure from composite spectra in ref.[1] used the approximation of "constant nuclear temperature", which leads to higher values of level density. It can be seen also that the values of level density obtained from our analysis of evaporation spectra and from neutron resonance data differ in 2 times.

Level density of ^{59}Ni



The reason of such difference can be connected with the assumption about equal probability of both parities at determination of total level density from a count of neutron resonances. In the experiment only S-wave resonances of ^{59}Ni of positive parity are observed, just as negative parity is dominate up to excitation energy of 4.5 MeV. The spin cut-off parameter and effective moment of inertia were determined from analysis of the measured angular distribution of neutron at α -particle energy of 16.3 MeV. $\sigma=3.43\pm 0.27$, $I_{\text{ef}}/I_{\text{rig}}=0.75\pm 0.1$ at average excitation energy of 6 MeV and $r_0=1.25$ fm. The analysis of the spin distribution of low-lying levels had shown that the best agreement is obtained also at $I_{\text{ef}} / I_{\text{rig}} = 0.75$. The new model evaluations of ^{59}Ni level density have been carried out and also presented in the Fig.

References

1. S.M. Grimes, et al. Phys. Rev.C, 1971,V.3, N2, P.645; 1974,V.10, N6, P.2373.
2. M.T. Magda, A. Alevra et al. Nucl.Phys.A, 1970, V.140, P.23.
3. P. Hille, R. Sperr et al. Nucl.Phys.A, 1974, V.232, P.157.
4. B.V. Zhuravlev et al. Proc.of the 6 Inter. Seminar on Interaction of Neutrons with Nuclei. Dubna, May 13-16, 1998, JIRN-E3-98-202, P.151.
5. N.S. Biryukov, B.V. Zhuravlev et al. Neutron Physics. Proc. of the 6 All-Union Conf. on Neutron Physics, Kiev, October 3-6, 1983, Moscow, 1984, V.3, P.290.
6. A. Brusegan, G. Rohr et al. Proc. of the Inter. Conf. on Nuclear Data for Science and Technology, Gatlinburg, Tennessee, May 9-13, 1994, V.1, P.224.

Weak Interaction Rates of Neutron-Rich Nuclei and the R-process Nucleosynthesis

I.N. Borzov^{1,2}, S. Goriely²

¹*State Scientific Centre - Institute of Physics & Power Engineering*

²*Institut d'Astronomie et d'Astrophysique, Université Libre de Bruxelles, Belgium*

The rapid neutron-capture process, or r-process, is known to be of fundamental importance for explaining the origin of about half of the stable nuclides heavier than iron observed in nature. Weak interaction rates for very short-lived neutron-rich nuclides involved in the r-process are mostly beyond the experimental reach at the present time. Accurate theoretical predictions demand a coherent extrapolation of different nuclear properties away from the experimentally known regions.

We are involved in a program aiming at studies of a wide variety of phenomena encountered at subnuclear and nuclear densities during and after the stellar collapse associated with the supernova event in terms of a single, universal, effective nuclear interaction. Because of the huge number of nuclei relevant to the r-process, an efficient procedure has been found to be the so-called Extended Tomas-Fermi approach plus Strutinski Integral correction (ETFSI). The main achievement so far has been the development, for the first time, of a mass formula based entirely on a microscopic force, the ETFSI-1 mass formula ([2] and refs. therein).

In order to increase the reliability of the predictions, improvements have been brought to the ETFSI approach. In particular, the Skyrme force parameters are subject to the constraint that the neutron matter does not collapse at nuclear and sub-nuclear densities (see [3] and Refs. therein). The ETFSI model can also be used to predict all ground-state properties of interest in the estimate of weak interaction rates. The aim of the paper is to present the results obtained within ETFSI-based approximation to the self-consistent calculation of β -decay and ν -capture rates in the framework of the continuum quasi-particle random phase approximation (cQRPA) (see [3]). We emphasize the predictive power of this method by comparing the results of large-scale ETFSI+cQRPA calculations with recent experimental data, as well as with the predictions obtained by (phenomenological [4] and microscopic [5] global calculations, the microscopic HFB+cQRPA [6] and shell model [7] approaches.

β -decay rates near the closed shells

Recently much experimental effort has been devoted to the study of the nuclear properties in the vicinity of the doubly magic ^{78}Ni and ^{132}Sn . These data provide a clear basis both for application of the self-consistent QRPA and for the comparison between different methods. Most of the nuclei involved have a spherical ground state; hence their β -decay half-life is very sensitive to nuclear structure effects. Moreover, the nuclei with $Z \approx 28$ and $Z < 50$ in the ^{78}Ni and ^{132}Sn region, respectively, are predicted to undergo a high-energy GT β -decay $\omega \approx Q_\beta$. In these conditions, the QRPA is expected to give a reasonable description of the β -decay half-lives.

The discrepancies between the different microscopic and phenomenological models tend to decrease when approaching the neutron drip line, since an appreciable portion of the GT sum rule for such nuclei is contained within the Q_β -window. In contrast, the microscopic calculations systematically overestimate (by a factor of 2-3) the experimental half-lives near the closed shells nuclei undergoing a high-energy β -decay.

To improve the description of the half-lives near the closed shells, an additional transition strength within the Q_{β} -window or/and a shift of the strength to higher transition energies is certainly needed. It is clear that the impact of the additional strength depends strongly on the specific shell sequence. As mentioned above, in the vicinity of the $Z=28$ closed shell, our calculations predict the existence of a high-energy GT β -decay transition both for isotopes below and above the proton shell closure. On the contrary, for the $Z>50$ nuclides in the region of the doubly magic ^{132}Sn , a switch to the low-energy GT β -decay regime is observed by all QRPA approaches, as well as a large overestimate of the experimental half-lives.

Three major additional sources can be at the origin of a half-life reduction. First, in the cases of favorable selection rules, an additional strength comes from the contribution of forbidden transitions. The experimental evidence of such high energy first forbidden transitions near the $Z=50$, $N=82$ shell has been widely discussed. Second, effects beyond the QRPA should also be considered. These result mainly in the spreading of the $1p-1h$ strength over $np-nh$ configurations. For some nuclei, it pushes the strength outside the Q_{β} -window, making the half-lives longer. It may also cause the appearance of an additional GT strength due to $np-nh$ correlations in the ground state which, on the contrary, would reduce the half-lives. Third, a major modification of the half-lives is due to the onset of nuclear deformation which has not been included in our calculations. The deformation causes an additional spreading of the GT strength which reduces the half-lives [5]. The spherical order of the quasi-particle levels occupancy is also affected by the onset of deformation. This effect influences the half-lives dramatically. Such a decrease of the β -decay half-lives seems to be experimentally observed for Mn isotopes in [8] who reported much shorter half-lives compared to previous measurements. Since different possible remedies exist to improve the agreement between the experimental and theoretical β -decay half-lives, the direct adjustment of the pp interaction strength to measured β -decay data [6] has to be taken with some reservation, especially if extrapolated or applied to large-scale calculations.

In Fig. 1, the β -decay half-lives for the $N=82$ isotopes (of importance for the r -process analysis) obtained within the ETFSI+cQRPA approach are compared with FRDM+QRPA [5], ETFSI+GT2 [4], shell-model [7] and HFB+cQRPA [6]. Our results are rather close to the one obtained within the HFB+cQRPA [6] (note a 30-40% reduction of the ETFSI+cQRPA half-lives due to the larger value of spin-isospin Landau-Migdal parameter g'_{ξ} used by [6]) The present prediction gives half-lives with a Z -dependence very similar to HFB+cQRPA [6] and DF3+cQRPA [9]. In comparison with shell-model results [7], we obtain longer half-lives in the $N=82$ region. This partially reflects the QRPA neglect of more complex configurations than $1p-1h$. In particular, it would be of great interest to compare QRPA and shell-model predictions for nuclei with $Z>50$ near ^{132}Sn , where complex configurations, as discussed above, are expected to give a predominant contribution.

The updated predictions of the ETFSI+cQRPA β -decay half-lives for about 700 spherical and quasi-spherical ($\beta_2<0.1$, $\beta_4<0.02$) short-lived nuclides ($T_{1/2}<1\text{s}$) ranging from Fe to U are available at the following web-sites: <http://www-astro.ulb.ac.be> and <http://www.rndc.obninsk.ru>.

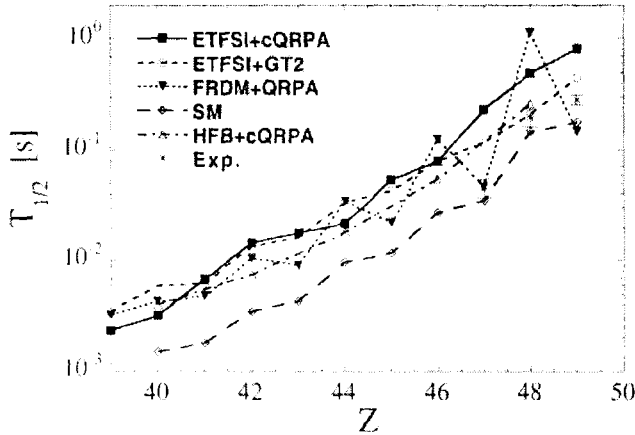


Fig. 1. Comparison between the ETFSI+cQRPA, ETFSI+GT2 [4], FRDM+QRPA [5], shell model [7] and HFB+cQRPA [6] predictions of the β -decay half-lives along the $N=82$ isotope chain

Electron neutrino capture cross sections

Within the same scheme, we also consider the electron neutrino capture rate in the neutrino-driven wind environment of exploding massive stars that has been envisioned as a possible astrophysical site of the r -process nucleosynthesis. The aim is to study in detail the possibility of competition of the β -decay and ν -capture - the processes which enable a nuclear flow to higher Z numbers.

The averaged neutrino capture cross sections σ_ν have been calculated for about 2500 nuclei with $26 < Z < 92$ and neutron numbers from $N=Z+1$ up to the neutron drip-line. The electronic data files for GT strength functions and energy dependent neutrino capture cross sections are available on request to I.B. These data can also be used to estimate neutrino capture rates for various neutrino energy spectra (supernovae neutrinos, solar neutrinos, electron neutrino from KARMEN etc.).

Finally, with our new predictions of the β -decay rates and neutrino capture cross sections we have performed the calculations of the r -process elemental abundances using two parametric r -process models, namely the canonical non-equilibrium model and the ν -driven wind model [5].

Acknowledgments

The authors are grateful to Prof. M. Arnould, A.V. Ignatyuk and J.M. Pearson for their continuous interests in this work. IB acknowledge discussions with Profs. J. Dobaczewski, W. Nazarewicz and Drs. M. Rayet, T. Tachibana. The work was supported in part by FNRS, Belgium.

References

1. S.E. Woosley, J.R. Wilson, G.J. Mathews, R.D. Hoffman, B.S. Meyer, *Ap. J.*, 229 (1994).
2. Y. Aboussir, J. M. Pearson, A.K. Dutta, and F. Tondeur, *ADDT* 61, 127 (1995).
3. I.N. Borzov, S. Goriely, and J.M. Pearson, *Nucl. Phys.*, A621, 307c (1997).
4. I.N. Borzov, S. Goriely, J.M. Pearson, and M. Arnould., in *Proc. Int.Conf. Nucl. Data in Science and Technology*, Trieste, Italy, p.1509 (1997),
I.N. Borzov, in *Proc. Int. Workshop on "Beta-decay: from weak interaction to nuclear properties"*, Strasbourg, France, p. 43 (1999).
5. T. Tachibana, M. Yamada, and N. Yoshida, *Prog. Theor. Phys.*, 84, 641 (1990).
6. P. Moeller, J.R. Nix, and K.-L. Kratz. *At. Data Nucl. Data Tables*, 66, 131 (1997).
7. G. Martinez-Pinedo, and K. Langanke, *Phys. Rev. Lett.*, 83, 4502 (1999).
8. J. Engel, M. Bender, J. Dobaczewski, W. Nazarewicz, T. Surm, *Phys. Rev.*, 60, 1432 (1999).
9. M. Hannawald, T. Kautzsch, A. Wöhr et al., *Phys.Rev.Lett.*, 82, 1391 (1999)
10. I.N. Borzov, S.A. Fayans, E. Kromer, and D. Zawischa, *Z. Phys.*, A335, 127, 1996.

Gamow-Teller Beta-Decay Strengths of Neutron-Deficient Tin Isotopes: Comparison of FFST and pnBCS+QRPA Results

A. Bobyk¹, W.A. Kaminski¹, I.N. Borzov

¹*Department of Theoretical Physics, Maria Curie-Skłodowska, University, Lublin, Poland*

Evolution of shell structure of exotic nuclei near new double-shell closures with total isospin is an attractive problem. The interest in this field is mainly related with the progress in radioactive beams experiments and the important role of the exotic nuclei in explosive astrophysical processes. Study of the β -decay modes is often the only way to extend our knowledge of nuclear properties to region far from stability. For the proton rich nuclei the β -decay is dominated by the Gamow-Teller (GT) transitions. This is the fastest channel of the β -decay in the region of nuclei where super-allowed Fermi decay is suppressed by isospin selection rules

In the region of doubly-magic very neutron deficient ^{100}Sn the Gamow-Teller β -transition is built on $(1\pi g_{9/2}, 1\nu g_{7/2})$ shell-model configuration. The simplicity of the decay mode and the selectivity of the GT-transitions ($\Delta L=0$, $\Delta S=1$, $\Delta\pi=\text{no}$) is a good reference point for checking various microscopic approaches to exotic nuclei

In the present work a microscopic analysis of recent data on beta-decay of even-even neutron-deficient nuclides between ^{100}Sn and ^{108}Sn is performed within FFS (self-consistent finite Fermi-system theory) and BCS+QRPA (Quasiparticle Random Phase Approximation) with G-matrix interaction and proton--neutron pairing. Strength functions of Gamow--Teller β -decay are calculated. The mechanisms of reduction of the GT-strength are discussed.

FFS theory

In the present work we have used the density functional fitted to the ground state properties of spin-zero nuclei as used in [1]. As a consequence, the scheme is not fully self-consistent in the case of spin-isospin excitations, and one has some freedom in choosing the effective spin-isospin NN-interaction. In general, the method includes the description of the ground states of superfluid nuclei and excited states of even and odd-A nuclei with pairing correlations [2].

The effective interaction in the particle--hole spin-isospin channel is chosen as local δ -part with Landau-Migdal parameter g' and renormalized one-pion exchange amplitude. The effective spin-isospin interaction in the particle-particle channel entering FFS theory equations for the charge-exchange excitations is chosen in the simplest form similar to that of pairing.

QRPA excited states

The QRPA formalism accounts not only for the particle-hole diagrams but for particle-particle ones as well. The excited states are constructed as one-phonon excitations generated from the ground state of the initial nucleus. The usual proton-neutron QRPA formalism has been extended to a full form, taking into account the possibility of mixing between protons and neutrons [3]. Treating X and Y amplitudes as independent variational parameters one gets a matrix equation for them and for the excitation energy $\omega(I^{\pi})=E(I^{\pi})-E^{\circ}$.

For our calculations we have taken the realistic hamiltonian with interaction part based on the G-matrix calculated using the Bethe--Goldstone equation with one-boson

exchange nucleon--nucleon potential of Bonn type [4], and Woods--Saxon potential with Bertsch parametrization as the single-particle part. For comparison with FFS results, the strength of the spin-isospin effective interaction in the pp-channel has been chosen the same as in FFS.

Results

Some of the results of the calculations within the FFS are given in Table 1 where the total GT-strength within the Q_{EC} - window for the β -decay of even $^{100-108}\text{Sn}$ are presented. For all available cases the experimental distributions are also analyzed (for review see [5]).

Table.1.Total B(GT) strength, calculated within the FFST and QRPA without (b) and with (c) p--n pairing, together with the experimental values . The strength of the spin-isospin interaction in the pp-channel is $60 \text{ MeV}\cdot\text{fm}^3$

A	a)	b)	c)	Exp.
100	7.63	9.27	8.95	-
102	6.08	8.02	7.69	-
104	5.30	6.75	6.49	2.63 ± 0.4
106	4.37	5.43	5.24	2.44 ± 0.3
108	3.53	3.99	3.85	1.37 ± 0.1

The total GT-strength observed below decay energy threshold is substantially lower than calculated in FFS and BCS+pnQRPA approaches. The mechanisms of the strength renormalisation has been intensively studied recently. The main source of the GT-strength reduction in is the "core-polarization" mechanism due to the effective interactions in ph and pp channels and the continuum effect

We have studied also an influence of the proton-neutron pairing on the B(GT) values by switching off the p-n interaction, what corresponds to taking non-diagonal elements of the u and v matrices equal to zero and restricting the isospin indices to values p and n . The results are summarized in Table 1. One can notice slight reduction of B(GT) values when p--n pairing is included. This is due to the fact that the strength is redistributed because of the increased number of possible excitations. But still they overestimate both FFS results and experimental data.

In order to explain the fragmentation of the GT-strength in terms of QRPA-like schemes one should include the effect of coupling of single-particle and phonon modes. The self-consistent approach of this type in nuclei with pairing is still missing. The principal attempts to extend the QRPA model in this direction are known [6], but quantitative analysis has been not performed yet. Also recently discussed problem of the violation of Pauli principle in the QRPA approach [7] may influence the results. These and many other questions remain therefore still open.

Summary and conclusions

The analysis of recent experiments on the β -decay of neutron- deficient tin isotopes near ^{100}Sn were performed in order to understand the details of the GT-decays in even-even nuclei in this region. The results are consistent with the overall picture of GT-decay governed by the $g_{9/2} \rightarrow g_{7/2}$ transition.

The effect of proton--neutron pairing on low-spin 1^+ excitations is found to be small. Although the change in the total strength caused by the pn-pairing is in the right direction, it is clearly not enough to solve the problem of the universal quenching of GT-strength. The latter seems to be also an experimental issue. To explain the rest of

difference in total GT-strength for even-even tin isotopes one should include in reliable way the quasiparticle-phonon correlation in the QRPA-like schemes. This can also provide the link with the shell-model approaches, which forms a basis for understanding of the role of strength splitting in the observed quenching effect. On the other hand, further experimental developments, like the application of well calibrated total gamma absorption spectrometers will help to improve our knowledge on the β -decay properties of exotic nuclei in the region of doubly-magic ^{100}Sn .

References

1. Smirnov A.V., Tolokonnikov S.V., S. A. Fayans Sov.J.Nucl.Phys.1988.V.48 P. 1661.
2. Borzov I.N., Trykov E.L. Sov.J.Nucl. Phys.1992.V.52 P. 33.
Borzov I.N., Trykov E.L., Fayans S.A. Nucl. Phys. A. 1995. V584. P. 335.
3. Teneva G., Shimkovic F, Bobyk A., Cheoun M.K., Faessler A., Khadkikar S.B., Nucl.Phys. A.1995.V.586.P. 249.
4. Machleidt R., Holinde K., Elster Ch. Phys.Rev .1987.V.149 P.~1.
5. Rykaczewski K.Proc. Int. Conf. "Nuclei far from stability»,Bernkastel-Kues, Germany, 1992.
6. Hara K., Iwasaki S. Nucl.Phys.A. 1979. V.332. P.61.
7. Toivanen J., Suhonen J. Phys.Rev.Let.B.1995.V.75.P. 410.

Nuclear Structure Effects in Electron Neutrino Capture by Heavy Nuclei

^{1,2}*I.N. Borzov*

*State Scientific Centre - Institute of Physics & Power Engineering
Institut d'Astronomie et d'Astrophysique, Université Libre de Bruxelles, Belgium*

Microscopic studies of neutrino capture rates by complex nuclei are required for a reliable calibration of solar neutrino detectors as well as for the accelerator-based experiments searching for neutrino oscillations. Neutrino capture processes also play an important role in astrophysical r-process nucleosynthesis. Recent developments in astrophysical modeling have led to new suggestions for the site of the r-process. In particular, the neutrino-driven wind streaming out of the neutron star forming at the center of a Type II supernova has been shown to be a promising candidate for the r-process [1].

Accurate theoretical predictions of neutrino capture rates for very neutron-rich nuclides of relevance to the r-process demand a coherent extrapolation of different nuclear properties away from the experimentally known regions. So far, the neutrino capture cross sections for astrophysical applications have mainly been estimated within the "gross-theory"-like model [2]. These calculations are based on simplified approximations which remain valid only for nuclei relatively close to the β -stability line.

The aim of the paper is to apply the ETFSI+cQRPA approximation (see [3,4] and Refs. therein) to supernovae neutrino capture by nuclides of relevance to the r-process nucleosynthesis. Manifestation of nuclear structure effects in isotopic dependence of spectrum-averaged neutrino capture rates is studied.

Electron neutrino capture rates

Electron neutrino capture $\nu_e + A_Z \rightarrow e^- + A_{Z+1}$ which takes place through weak charged current can be seen as an inelastic scattering process with a discrete energy spectrum of the emitted electron. In the allowed transitions approximation the energy dependent ν -capture cross section can be expressed through the integrals of Fermi and Gamow-Teller strength functions on the excitation energy in the daughter nucleus $\omega_x = Q - \omega$ (here ω - is the transition energy, Q - is the isobar pair mass difference, and the integration on ω_x runs over all energetically possible final states in the daughter nucleus). For stable nuclei ($Q < 0$), the ν -induced excitation of the states in the daughter nucleus corresponds to nuclear transitions with a negative Q -value ($\omega < m_e c^2$). For unstable nuclei ($Q > 0$), we consider the contributions of both the ν -induced excitations ($\omega < m_e c^2$) and the ν -mediated de-excitations ($\omega > m_e c^2$), where lepton final states correspond to nuclear transitions to the discrete states in the daughter nucleus with a positive Q -values.

For applications the spectrum-averaged neutrino capture cross section is usually of need:

$$\langle \sigma_\nu \rangle = A^{-1} \int_{E_{TH}}^{E_{max}} \varphi(E_\nu, T_\nu) \sigma_\nu(E_\nu) dE_\nu$$

where $E_{TH} = |Q|$ is the reaction energy threshold for stable nuclei ($E_{TH} = 0$, otherwise). The neutrino energy spectrum $\varphi_\nu(E_\nu, T_\nu)$ is taken as a zero-chemical-potential Fermi-Dirac distribution, where T_ν is the neutrino temperature.

Electron neutrino capture cross sections

Using the ETFSI+cQRPA framework we have developed the ETFSI-based model for charged-current neutrino capture [4] and performed a large-scale calculation of the neutrino energy-dependent cross sections for stable and unstable neutron-rich nuclei. The GT strength function is calculated within ETFSI+cQRPA approach in the excitation energy range from the ground state of the daughter nucleus up to about 40 MeV. The IAS energies are taken from the experimental systematics of Coulomb displacement energies. The Fermi strength included in the IAS of the daughter nucleus is taken as $M_F^2=N-Z$. The averaged neutrino capture cross sections and their partial components are shown as a function of A for the Ni-isotopic chains in Fig. 1.

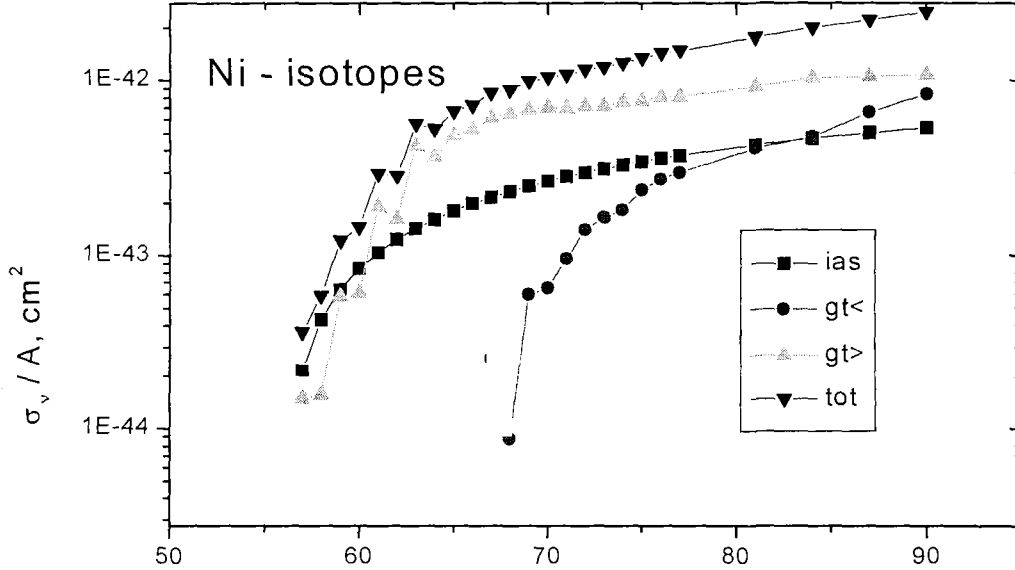


Fig. 1 The total and partial ν -capture cross sections for Ni-isotopic chain.

In stable nuclei, the IAS and ν -induced excitation components of the total cross section increase with $N-Z$ due to the corresponding shift of the IAS and GTR down in energy and towards the maximum of the neutrino energy spectrum. For stable nuclei, the contribution of the neutrino excitation of the low energy states in the daughter nucleus cannot be neglected. Such a contribution is responsible for the systematic odd-even effect in the total cross section, as illustrated in Fig. 1.

In unstable nuclei, at increasing neutron excesses, the IAS and GT-excitation contributions to the cross section become rather smooth and flat. At relatively small charge numbers Z , the GT-excitation component may even decrease with increasing neutron numbers, at least if the super-allowed GTR is energetically possible (note that for these nuclei the empirical systematic of the IAS energy may fail). At the same time, the GT de-excitation component of the cross section in unstable nuclei increases with neutron excesses, as the $Q\beta$ -value (and available phase-space) becomes larger.

For relatively small Z , the de-excitation part of the total cross section can not be neglected. As seen in Fig. 1, for Ni isotopes, it exceeds the IAS contribution well before the neutron drip-line is reached. This is mainly due to the increasing portion of the GT sum rule shifted within the $Q\beta$ -window at increasing $N-Z$ values. The impact of the de-excitation component is smaller for heavy isotopic chains $Z>50$ for which the super-allowed GT transitions is not possible for neutron-stable nuclei. For heavy nuclei, like Pb-isotopes our predictions agree well with the schematic estimate of the de-excitation

contribution by [3], while in the ^{132}Sn region, the calculated neutrino capture rates are rather close to the one derived from shell-model calculations [5].

Acknowledgments

The author is grateful to Prof. M.Arnoold for many stimulating discussions. Discussions with Profs. P.Vogel, K.Langanke and Drs. S.Goriely and M.Rayet are acknowledged. The work was supported in part by FNRS, Belgium.

References

1. S.E. Woosley, J.R Wilson, G.J. Mathews, R.D. Hoffman, B.S. Meyer, *Astroph. J.* 433, 229 (1994).
2. G.M. Fuller, and B.S. Meyer, *Astrophys. J.* 453, 792 (1995);
3. I.N. Borzov, and S. Goriely, in *Proc. of the 5th International Conference on Nuclei in the Cosmos*, Volos, Greece (Editions Frontieres, eds. N. Prantzos, S. Harissopoulos), 303 (1998).
4. I.N. Borzov, in *Proc. Int. Workshop on "Beta-decay: from weak interaction to nuclear properties"*, P.Dessagne, A. Michalon, C.Miehe (eds.), Strasbourg, France, p. 43 (1999).
5. Y.-Z.Qian, W.C. Haxton, K.-H. Langanke, and P. Vogel, *Phys. Rev. C* 55, 1532 (1997).

On "Quasiparticle+Two-Phonon" Excitations in Odd-Mass Nuclei with Pairing

A.V.Avdeenkov, I.V.Bundin, S.P.Kamerdzhiev*

**Obninsk Institute of Nuclear Power Engineering*

At present, there are new and excellent experimental possibilities to measure two-phonon excitations in even- even nuclei and quasiparticle+two-phonon excitations in odd- mass ones. These results "require" an improved microscopic description of the excitations as compared with that obtained within present microscopic approaches.

We investigated contributions of two- phonon terms to mass operators, which enter the system of equations for the single- particle quantum Green functions in non-magic nuclei. These mass operators determine the excitation energies of odd- mass nuclei with pairing. Two necessary types of the above- mentioned terms have been considered, namely, the terms corresponding to the so- called "rainbow" Feynman diagrams (self-energy ones) and the cross diagrams, which give corrections to the quasiparticle- phonon vertex. Especial attention has been paid to specificity of nuclei with pairing (non- magic nuclei), i.e. to new terms in anomalous mass operators and an improved description of nuclear pairing, the latter is discussed in detail in Ref.[1]. Our main assumption is the linearized g^2 approximation where g is the phonon creation amplitude, but a more general case has been analysed within a nonlinear three- level model too.

The formulae obtained were analysed within schematic one- and three- level models. The results are given in [2,3]. In particular, we have shown that the above- mentioned specificity of non- magic nuclei is important, at least numerically. For the cases where the g^2 approximation is invalid (nuclei with pairing in both neutron and proton systems) it is necessary to take into account both types of diagrams.

The main formal difficulties of the g^2 approximation under consideration are unphysical second order poles. To avoid them, a more general approach has been formulated which does not contain these poles. In this sense the approach developed is similar to the quasiparticle- phonon model [3] for odd- mass nuclei. However, it includes ground state correlations and the improved pairing theory, numerical contribution of which should be noticeable and measured in modern experiments. An analysis of the approach is in progress now.

References

1. A.V.Avdeenkov, S.P.Kamerdzhiev, JETP Lett. 69(1999)715
A.V.Avdeenkov, S.P.Kamerdzhiev, Phys.Lett. B459(1999)423
1. A.V.Avdeenkov, Microscopic description of single- particle characteristics in non- magic nuclei, Candidate dissertation, IPPE, 1999.
2. I.V.Bundin, Microscopic description of low- lying excitations in odd-mass nuclei with pairing, Diploma work, OINPE, 1999
3. V.G. Soloviev, Theory of atomic nuclei: Quasiparticles and Phonons, Energoatomizdat, 1989

Random Phase Approximation for Odd Nuclei and Its Application to the Description of the Giant Dipole Resonance in ^{17}O

S.P.Kamerdzhev, R.J.Liotta¹⁾, V.I.Tselyaev²⁾

¹⁾*Royal Institute of Technology, Stockholm, Sweden*

²⁾*Institute of Physics, St. Petersburg State University, Russia*

It is well known that the straightforward application of the standard random phase approximation (RPA) to the description of odd nuclei excitations comes across difficulties connected with the fact that the ground state of an odd nucleus is degenerate and is not particle-hole phonon vacuum. There are several approaches within which this problem is solved using various approximations (see for example Refs [1-4]). But neither of them can be considered as an adequate extension of the RPA to odd nuclei. As a rule, excitations of different kinds are described by different models. In particular the standard variant of the theory of finite Fermi systems [1] treats the ground state of an odd nucleus only on the average. As a result, it enables one to calculate the envelope of a giant resonance but another model is necessary for description of the multiplets splitting [4].

Here we suggest a model which is a consistent generalization of the RPA for odd nuclei. The formula for the response function for an external field acting on the odd nucleus is derived. Our derivation is based on the Green function method with the use of the equation for the 3-particle Green function. Within the obtained model (we enote it as ORPA), all contributions of the first order in the effective interaction are taken into account completely. The higher order contributions are incorporated to the necessary extent. In this sense the ORPA is analogous to the standard RPA for even-even nuclei. The ORPA enables one to describe on the common basis both the single-particle and collective parts of the excitation spectrum including giant resonances in the continuum and splitting of discrete collective states (*particle (hole) \otimes phonon* multiplets). The sum rules in the ORPA are deduced. In the framework of the ORPA the E1 photoabsorption cross section in ^{17}O is calculated. In these calculations the single-particle continuum is taken into account exactly. The results obtained are compared with the experiment.

This work was supported partly by the grant of the Swedish Institute within The Visby Programme.

References

1. A.B.Migdal. Theory of Finite Fermi Systems and Applications to Atomic Nuclei. New-York: Wiley, 1967.
2. V.G.Soloviev. Theory of Atomic Nuclei: Quasiparticles and Phonons. Bristol and Philadelphia: Institute of Physics, 1992.
3. I.Hamamoto // Phys. Rep., 1974. V.10. P.63.
4. V.A.Khodel, E.E.Saperstein // Phys. Rep., 1982. V.92. P.183.

Microscopic Analysis of the Breathing Mode in ^{40}Ca and ^{58}Ni

S. Kamedzhiev, J. Speth¹⁾, G. Tertychny

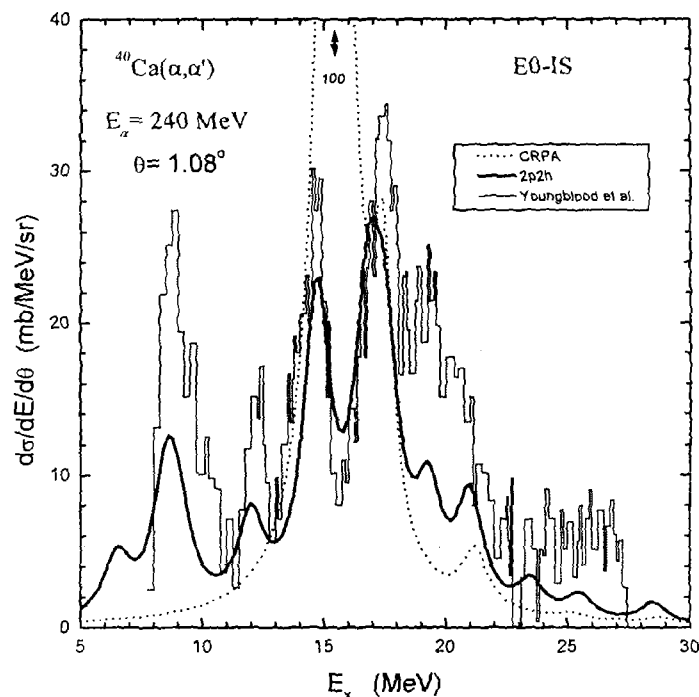
¹⁾Institute für Kernphysik, Forschungszentrum Jülich, 5228 Jülich, Germany

Recent experimental studies of the giant electric resonance region in ^{40}Ca [1] and ^{58}Ni [2,3] with inelastically scattered α -particles at energy $E_\alpha = 240$ MeV are analyzed within a microscopic nuclear structure model (e.g. see [1]).

The model includes the continuum RPA and more complex $1p1h \times \text{phonon}$ configurations, which correspond to all three known mechanisms of resonance formation in a finite nucleus, i.e. an analog of Landau damping, an escape width and a spreading width. By superimposing the contributions of different multipoles up to $L=4$ we obtain good agreement with the newest (reanalyzed) data [3] for the isoscalar monopole strength and for the total (α, α') reaction cross section in ^{58}Ni .

We emphasize the necessity of using microscopic transition densities and discuss consequences for the analyses of such experiments in light and medium mass nuclei.

As can be seen in Fig.1 our full calculations for ^{40}Ca reproduce the experimental gross structure reasonably well, but there is a difference at low and high energies. We see that the gross structure of the isoscalar monopole resonance in ^{40}Ca is caused by $1p1h \times \text{phonon}$ configurations.



References

1. D.H.Youngblood, Y.-W.Lui, H.L.Clark, *Phys. Rev. C* 55 (1997) 2811.
2. D.H.Youngblood, H.L.Clark, Y.-W.Lui, *Phys. Rev. Lett.* 76 (1996) 1426.
3. Y.-W. Lui, H.L. Clark, and D.H. Youngblood, Preprint, submitted to *Phys. Rev. C*.
4. S.Kamedzhiev, J.Speth, G.Tertychny, *Nucl. Phys. A* 624 (1997) 328.

Microscopic Theory of Giant Resonances in Non-Magic Nuclei

S.P. Kamerdzhev, E.V. Litvinova¹⁾, D. Zawischa²⁾

¹⁾Institute of Nuclear Power Engineering, Obninsk, Russia

²⁾Institut fuer Theoretische Physik, Universitat Hannover, Germany

A general microscopic approach to describe properties of excited states in non-magic nuclei is formulated. It is based on the consistent use of the Green function method in Fermi systems with Cooper pairing. The main attention is paid to even-even nuclei, but for odd nuclei with pairing some important relations are obtained too. The quasiparticle-phonon interaction which is introduced acts also in the particle-particle channel and gives a quasiparticle-phonon contribution to pairing [1]. When applied to the theory of giant multipole resonances, the approach includes all known sources of resonance width, i.e. QRPA configurations (which correspond to Landau damping in magic nuclei), the single-particle continuum (escape width) and more complex configurations (spreading width). The use of the Green function method makes it possible to include consistently the ground state correlations induced by the more complex configurations. In the approximation of the collective phonon creation amplitude squared, which is considered in detail here, these are the ground state correlations caused by two-quasiparticle-phonon configurations; effects of these correlations have been found earlier to be noticeable for magic nuclei. Such a unified approach will give a reasonable description of the giant resonances' integral characteristics including their widths and of some more delicate properties like fine structure and decay characteristics. Physical arguments and earlier results of a similar approach for magic nuclei (e.g. see [2]) allow to use the known parameters of the Landau-Migdal non-separable interaction for all non-magic nuclei (except the light ones). This means that the theory developed is suitable for realistic predictions of the properties of unknown nuclei including unstable ones. The inclusion of the single-particle continuum allows to consider also nuclei with separation energy near zero.

References

1. A.V.Avdeenkov, S.P.Kamerdzhev, JETP Lett. 69 (1999) 715.
2. S.Kamerdzhev, J.Speth, G.Tertychny, Nucl.Phys. A624 (1997) 328.

2.3 NUCLEAR DATA

New Evaluations of Gamma-Ray Production Cross Sections for Lead and Bismuth

*A.V. Ignatyuk, A.I. Blokhin, V.N. Manokhin, V.P. Lunev,
G.Ya. Tertychnyi, K.I. Zolotarev*

The development of accelerator-driven systems with the heavy metal liquid coolant requires a rather accurate data on the neutron and gamma-ray production cross sections for lead and bismuth. Discrepancies between the evaluated data of ENDF/B-VI, JENDL-3.2 and BROND-2 for these elements amount to 40-50% in many cases. To improve an accuracy of data new evaluations of the neutron induced reaction cross sections and gamma-ray yields performed at the IPPE are discussed. The evaluations are recommended for the new version of BROND-3 library that is under formation in the Russian Nuclear Data Center. This paper is a short version of the report, presented to International Conference on Radiation Shielding (October 1999, Tsukuba, Japan) [1].

For theoretical description of cross sections of the neutron induced reactions the traditional optical-statistical approach was used that takes into account consistently the contribution of the direct, preequilibrium and statistical equilibrium processes into different reaction channels. The practical calculations were made on the basis of the GNASH [2] code.

The important component of the statistical cross section description is a choice of the optical model parameters used for calculations of the transmission coefficients. In the present work the calculation of transmission coefficients was made on the basis of the generalized optical model with the potential recommended for $^{205,206}\text{Pb}$ in Ref. [3] and for $^{207,208}\text{Pb}$ in Ref. [4]. The generalized optical model permits also to estimate the cross sections for the direct excitations of collective low-lying levels.

For the consistent description of the level excitation functions and the corresponding gamma-ray yields the real schemes of low-lying levels and the branching ratios of possible gamma-ray transitions should be taken into consideration. To construct such schemes the recent compilations of low-lying levels [5] were used and unknown branching ratios were estimated on the basis of statistical calculations of the possible E1, E2 and M1 gamma-ray transitions. Intensities of such transitions were calculated in accordance with the radiation strength functions recommended in Ref. [6].

The energy dependence of secondary neutron spectra and the partial reaction cross sections in the continuum depend strongly on the level density of residual nuclei. For the level density description the back-shifted Fermi-gas model, composite Gilbert-Cameron approach and generalized superfluid model are used most frequently. These models give approximately the same description of the spectra and integral reaction cross sections if the corresponding model parameters are determined consistently from the analysis of the neutron resonance spacing and low-lying level densities. Sets of such parameters are compiled in Ref. [6]. However for many nuclei there are no such experimental data and the model parameters should be estimated on the basis of the corresponding level density systematics.

For the description of hard parts of neutron and gamma-ray spectra, as well as a high energy region of the neutron excitation functions the preequilibrium particle evaporation

plays a crucial role. The exciton model relations used by the GNASH codes are similar to great extent and the main differences between them are connected mainly with the energy dependence parameterisation of the intranuclear transition matrix element $\langle M2 \rangle$. For any parameterisation the corresponding coefficients were determined from the optimal description of experimental data on the secondary neutron spectra.

For the incident neutron energies below 7 MeV the inelastic scattering channels are dominant in all isotopes considered. So as the discrete level schemes were taken into account in the present calculations up to excitations of 3.5-4.0 MeV, this energy region can be used to test the consistency of the optical model parameters chosen and branching coefficients constructed. For neutron energies above 7 MeV the transition probability to continuum is much higher than to the low-lying levels, and the neutron cross section description depends essentially on the level density model applied.

The dominant contribution to the gamma-ray production cross sections in this energy region gives the (n,2n) reaction. For isotopes of ^{207}Pb , ^{208}Pb and ^{209}Bi a good agreement with experimental data can be reached only using the superfluid model for the level density description. This result reflects the important role of shell effects, which are included consistently into this model, but not taken into account in the Fermi-gas and Gilbert-Cameron models.

The calculated gamma-ray production cross sections are shown in Fig. 1. A good agreement of the calculated excitation functions of discrete levels, all threshold reaction cross sections, as well as the differential and integral gamma-ray yields allows us to consider the calculated curves as the optimal ones and to use them to compile the complete files of evaluated neutron data for bismuth and separated lead isotopes.

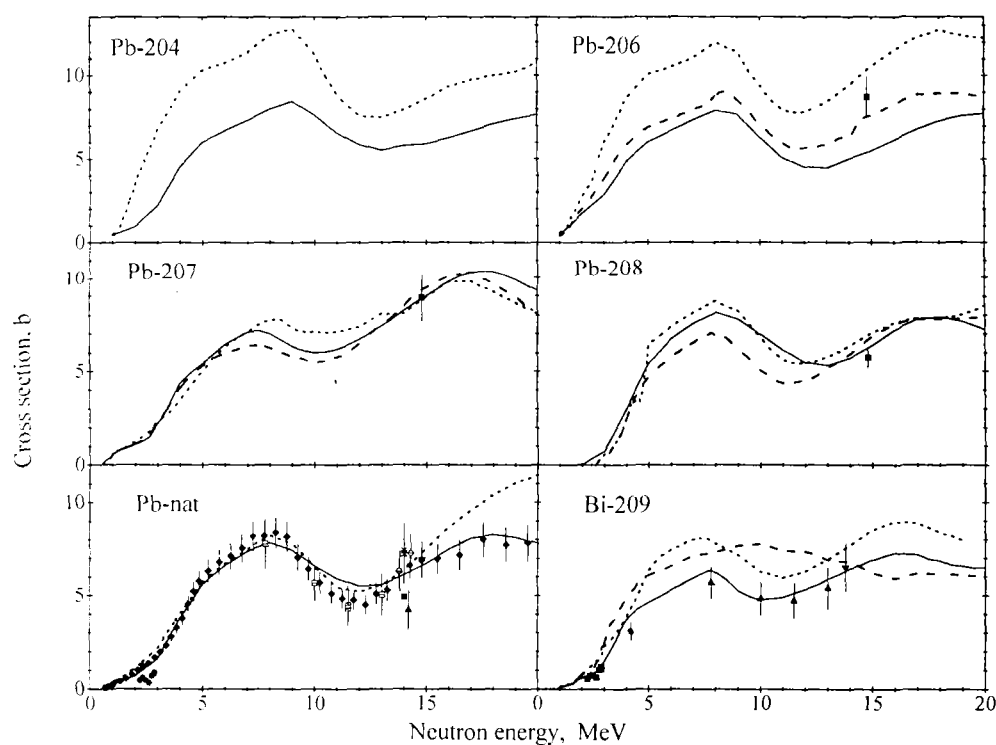


Fig. 1. Recommended total gamma-ray production cross sections (solid curves) in comparison with experimental data and the evaluations of ENDF/B-VI (dashed curves) and JENDL-3.2 (dotted curves)

References

1. Ignatyuk, A.V., Blokhin, A.I., Manokhin, V.N., Lunev, V.P., Tertychnyi, G.Ya., Zolotarev K.I., Int. Conf. on Radiation Shielding (15-19 October 1999, Tsukuba, Japan).
2. Young P.G., Arthur E.D., Chadwick M.B. Nuclear Reaction Data and Nuclear Reactors (Trieste, 1996). Ed. A.Gandini, G.Reffo, World Sci., Singapore, 1998, v. 1, p. 227.
3. Finlay R.W. et al. Phys. Rev, C30, 796 (1984).
4. Vonach H. et al. Phys. Rev. C50, 1952 (1994).
5. Firestone R.B. ed. Table of Isotopes, Eighth edition, NY: J. Wiley and Sons Inc., 1995.
6. Handbook for Calculation of Nuclear Reaction Data - Reference Input Parameter Library, TECDOC-1034, Vienna: IAEA, 1998.

Evaluations of Neutron Cross Sections for Cm-242, -243, -244

*A.I. Blokhin, A.S. Badikov, A.V. Ignatyuk, V.P. Lunev, V.N. Manokhin,
G.Ya. Tertychny, K.I. Zolotarev*

The work is devoted to the analysis of available experimental and evaluated data on the neutron cross sections for Cm-242, Cm-243, Cm-244 [1,2]. A comparison of experimental data with the results of theoretical calculations and the evaluations of the most important cross sections were performed. As a result the new version of complete files of evaluated neutron cross sections for Cm-242, Cm-243, Cm-244 were formed. These files were included into the BROND-3 library the formations of which is under development in Russian Nuclear Data Center.

The available experimental fission cross section data for Cm-243 are shown in Fig. 1 together with different cross section evaluations. The IPPE approximation curve was obtained by statistical analysis of the correlated experimental data on the basis of nonlinear regression model using rational functions.

Our results of the optical-statistical calculation of the inelastic scattering and (n,2n) reaction cross sections consistent with the evaluated fission cross section are strongly differ from the cross sections adopted in other evaluations. For high neutron energies these differences are due to not only the differences in the fission cross sections but to the discrepancies in the neutron absorption cross sections as well. The Minsk's group used for curium isotopes as well as for americium ones the optical potential resulting in lower absorption cross sections than the observed fission cross section for the light curium isotopes at the neutron energy of 14 MeV.

The experimental data available for the Cm-244 fission cross sections are shown in Fig. 2 together with different evaluations. The discrepancies of the experimental data for Cm-244 are not so considerable as for the Cm-243 however the integral fission cross section, calculated for the fast critical assembly with our evaluated data, is noticeably above the measured integral cross section [1]. The calculated integral fission cross section remains approximately the same at the use of the ENDF/B-VI and Minsk' group evaluations. At present we do not see any explanation of this contradiction between the microscopic and integral data and the problem of fission cross section validation in the energy region below 1 MeV for Cm-244 remains open.

Our results of the optical-statistical calculations of the inelastic scattering and (n,3n) reaction cross sections consistent with our Cm-244 fission cross section evaluation differs greatly from other evaluations. The discrepancies in the (n,2n) reaction cross sections are also very considerable and obviously due to the discrepancies in the neutron fission and absorption cross section evaluations.

For Cm-242 there is only one measurement of the fission cross sections in the subthreshold region, which is not sufficient to evaluate reliably the fission cross section in the region of the first "plateau". Therefore in the Cm-242 previous evaluations the empirical fission cross section systematics were used combined with the theoretical calculations and results of the fissility analysis of curium isotopes in the charged particle induced reactions.

The great concern is caused however by the contradiction of the experimental data on cross sections of the curium isotope fission by neutrons with the results of the analysis of the same isotopes fissility in direct reactions induced by charged particles.

This contradiction in the data was noted early, and we have no explanation of it up to now.

The results of the optical-statistical calculations of the fission, inelastic scattering and (n,2n) reaction cross sections consistent with the evaluations made above for fission cross sections of Cm-242 at the first plateau and 14 MeV are given in Fig. 3 together with previous evaluations of these cross sections. The discrepancies of the evaluations are considerable and the task of the testing of evaluated data remains.

On the basis of the evaluations considered above the modified files of evaluated neutron cross sections were formed for the BROND-3 library. For Cm-242 and Cm-244 the neutron cross sections for the resolved and unresolved resonance regions as well as the neutron angular distributions and neutron spectra were taken from the previous BROND-2 evaluations. For Cm-243 the relevant evaluations of Minsk group were used for this purpose.

References

1. Final Technical Report on Project ISTC 304-95, Obninsk, 1997.
2. A.I.Blokhin, A.S.Badikov, A.V.Ignatyuk, V.P.Lunev, V.N.Manokhin, G.Ya.Tertychny, K.I.Zolotarev. Evaluations of Neutron Cross Sections for Cm-242, -243, -244. In: Voprosy Atomnoi Nauki i Tekhniki, ser. Yadernye Konstanty, 2,1999.

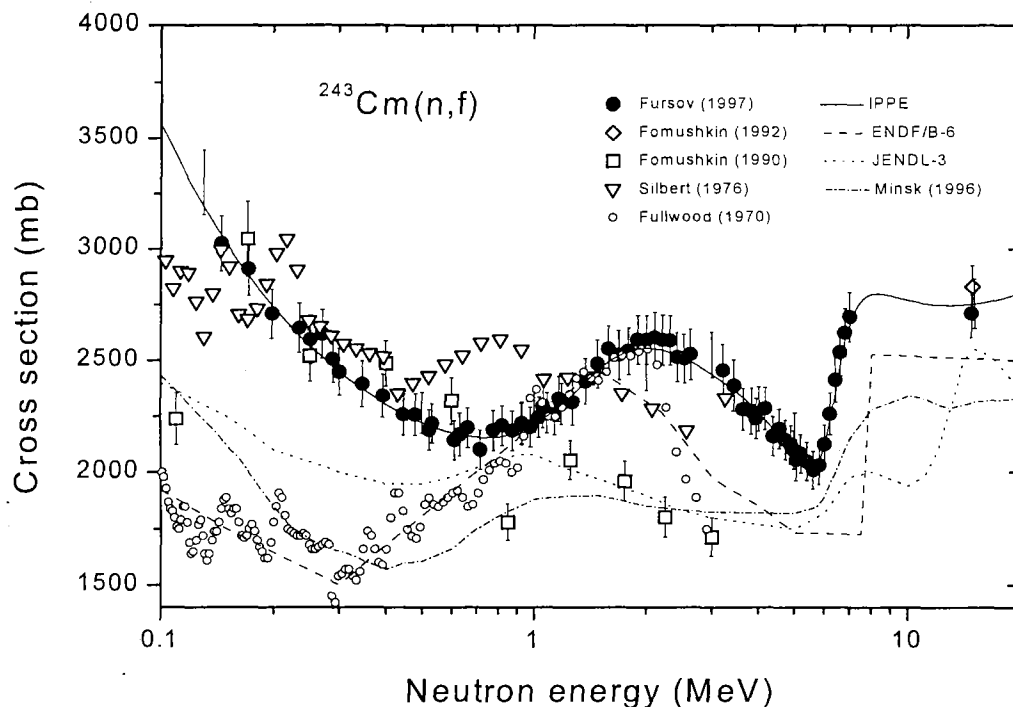


Fig. 1. Comparison of the evaluated fission cross sections for ^{243}Cm with experimental data

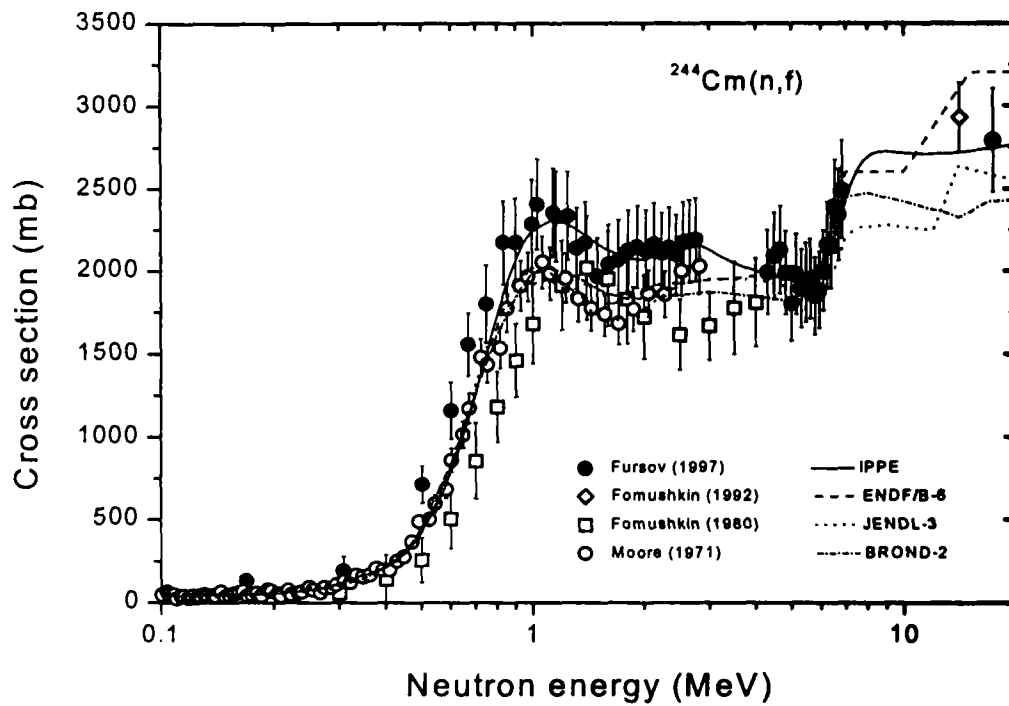


Fig. 2. Comparison of the evaluated fission cross sections for ^{244}Cm with experimental data

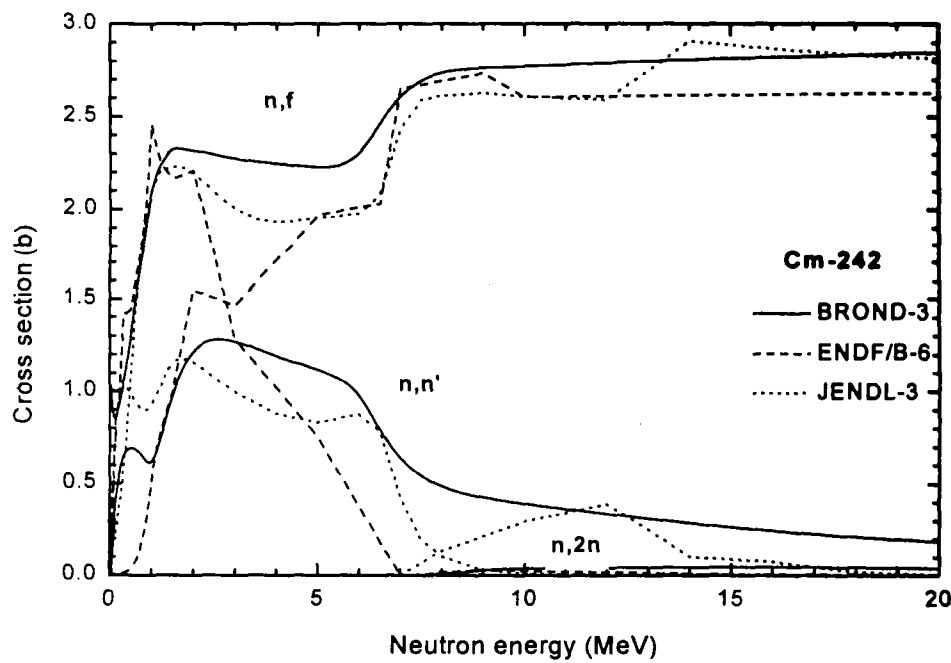


Fig. 3. Comparison of the evaluated fission, inelastic and (n,2n) reaction cross sections for ^{242}Cm

Experimental Studies of the Average Half-lives of Delayed Neutron Precursors from Fast Neutron Induced Fission of Uranium Isotopes

V.M. Piksaikin, L.E. Kazakov, S.G. Isaev

Experimental investigations of the delayed neutron characteristics for various fissioning systems have shown the systematic behavior of the average half-life of delayed neutron precursors as well as the correlation between the average half-life of delayed neutron precursors and the total delayed neutron yields. It was found that the average half-life of delayed neutron precursors $\langle T \rangle$ for isotopes of one element can be represented by the exponential dependence on the fissility parameter of the fissioning system (Z,A) : $\langle T \rangle = a \cdot \exp[b \cdot (Z^2/A)]$ [1]. It was found also that the absolute total delayed neutron yields ν_d for isotopes of one element are related to the average half-life values by the expression $\nu_d = c \cdot (\langle T \rangle)^d$ where a, b, c, d – the constants for definite element and excitation energy of the fissioning system. The systematics of the average half-life on fissility parameter is shown on Fig. 1.

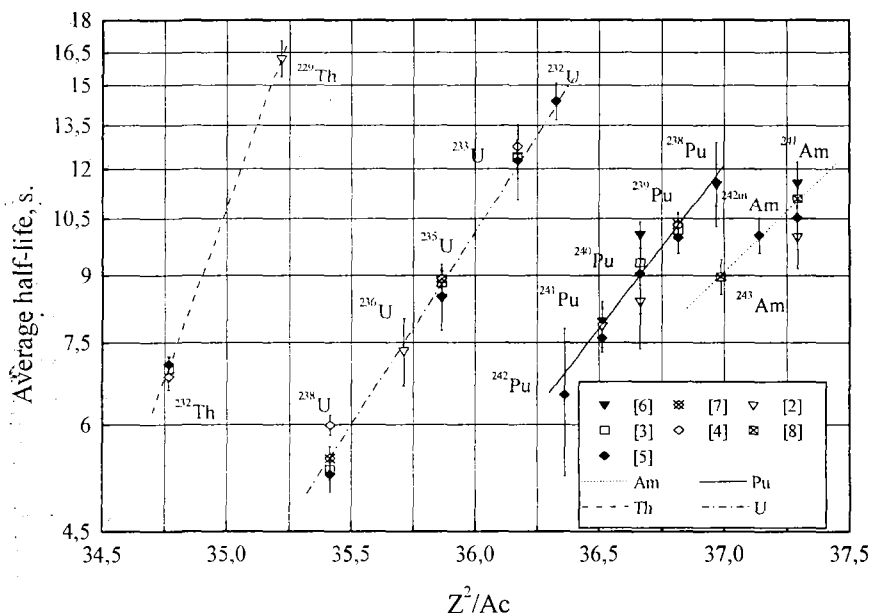


Fig. 1. Dependence of average half-lives on parameter Z^2/A_c for thorium, uranium, plutonium and americium isotopes.

The experiments have been made to verify the systematics of the average half-lives of delayed neutron precursors for the fast neutron induced fission of uranium isotopes - ^{233}U , ^{235}U , ^{236}U , and ^{238}U . The measurements of the delayed neutron relative abundance and periods of their precursors were made at the electrostatic accelerator KG-2.5 of IPPE. Monoenergetic neutron beams were generated with the aid of the reactions $T(p,n)^3\text{He}$ and $D(d,n)^3\text{He}$. The time of sample transportation from the irradiation position to the neutron detector was about 150 ms. The duration of sample irradiation was 15, 180 and 300 s. The counting time of delayed neutron activity was 424.5 and 724.5 s. The experimental results for the 1.01 MeV incident neutrons is shown on Fig. 2.

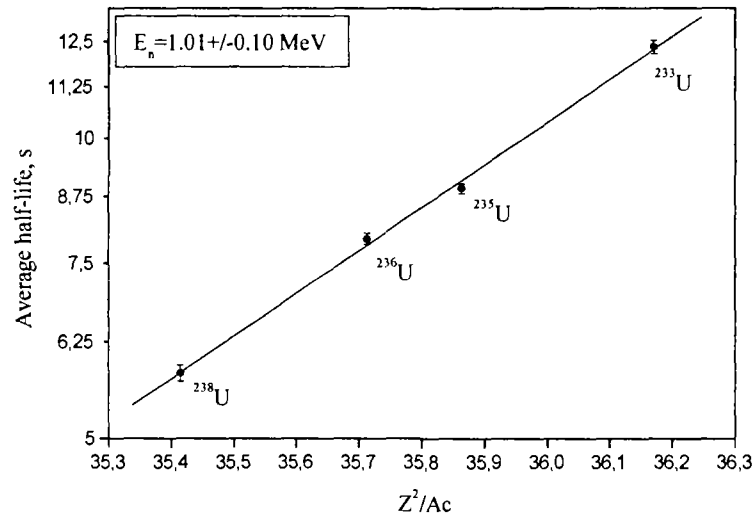


Fig. 2. Dependence of average half-lives on parameter Z^2/A_c for the 1.01 MeV incident neutrons.

The obtained results on the average half-life of delayed neutron precursors from neutron induced fission of the uranium isotopes confirm the systematics $\langle T \rangle = a \exp[b \cdot (Z^2/A)]$ with high accuracy.

References

1. V.M. Piksaikin, S.G. Isaev. Correlation properties of delayed neutrons from fast neutron induced fission. Report INDC(CCP)-415, IAEA, Vienna, Austria.
2. А.Н. Гудков, А.Б. Колдобский, С.В. Кривашеев, Н.А. Лебедев, В.А. Пчелин, "Выходы групп запаздывающих нейтронов при делении ^{229}Th тепловыми нейтронами", Ядерная физика, 49, No. 6, с.960 (1989);
3. А.Н. Гудков и др., "Измерения выходов запаздывающих нейтронов при делении ^{233}U , ^{236}U , ^{237}Np , ^{240}Pu и ^{241}Pu нейтронами спектра быстрого реактора", Атомная энергия, 66, No. 2, с.100 (1989);
4. А.Н. Гудков, С. В. Кривашеев, А. Б. Колдобский, Е. Ю. Бобков, Ю.Ф. Колеганов, А.В. Звонарев и В.Б. Павлович, "Определение выходов групп запаздывающих нейтронов при ^{235}U и ^{241}Am быстрыми нейтронами", Атомная энергия, 67, No. 3, с.702 (1989).
5. G.R. Keepin, T.F. Wimett, and R.K. Zeigler, "Delayed Neutrons from Fissionable Isotopes of Uranium, Plutonium and Thorium", Physical Review, 107, 4, p.1044 (Aug. 15,1957).
6. H. Rose and R.D. Smith, "Delayed Neutron Investigations with the ZEPHYR Fast Reactor, Part II— The Delayed Neutrons Arising from Fast Fission in ^{235}U , ^{233}U , ^{238}U , ^{239}Pu and ^{232}Th ", J. Nucl. Energy, 4, p.133 (1957).
7. R.W. Waldo, R.A. Karam, R.A. Meyer, "Delayed Neutron Yields: Time Dependent Measurements and a Predictive Model", Phys. Rev. C, 23, No.3, p.1113 (March, 1981).
8. G. Benedetti, A. Cesana, V. Sangiust and M. Terrani, "Delayed Neutron Yields from Fission of Uranium-233, Neptunium-237, Plutonium-238, -240, -241, and Americium-241", Nucl. Sci. Eng., 80, p.379 (1982).
9. C.B. Besant, P.J. Challen, M.H. McTaggart, P. Tavoularidis, J.G. Williams, "Absolute Yields and Group Constants of Delayed Neutrons in Fast Fission of ^{235}U , ^{238}U and ^{239}Pu ", J. Br. Nucl. Energy Soc., 16, p.161 (1977).
10. H.H. Saleh, T.A. Parish, S. Raman, and N. Shinohara, "Measurements of Delayed-Neutron Decay Constants and Fission Yields from ^{235}U , ^{237}Np , ^{241}Am and ^{243}Am ", Nucl. Sci. Eng., 125, p.51 (1997).

Systematics of the Delayed Neutron Characteristics and Validation of the Delayed Neutron Data Base Obtained in the Microscopic Approach

S.G. Isaev, V.M. Piksaikin, L.E. Kazakov

The microscopic approach is widely used for deriving such delayed neutron parameters as the absolute total delayed neutron yields, relative abundance and decay constants of separate delayed neutron groups for any fissioning system with known fission product yields data [2]. Namely this approach was applied in the creation of the delayed neutron base contained in the ENDF/B-VI library. The direct comparison of the absolute total delayed yields obtained in such approach with appropriate experimental data serves as a test of reliability of input data – neutron emission probability and cumulative fission product yields. In the present work the validation of the delayed neutron data base obtained by the summation technique (microscopic approach) was made on the basis of the new systematics of delayed neutron characteristics developed at IPPE [1]. It was shown that the delayed neutron data contained in the ENDF/B-VI library systematically deviates from appropriate data obtained in the macroscopic approach (aggregate data measurements). Especially it concerns the delayed neutron data determining their time behavior (relative abundances and decay constants) for plutonium and americium isotopes. The comparison of the average half-lives obtained by the summation technique [2] and on the basis of the new systematics [1] for plutonium and americium are shown on Fig. 1. and Fig. 2. respectively.

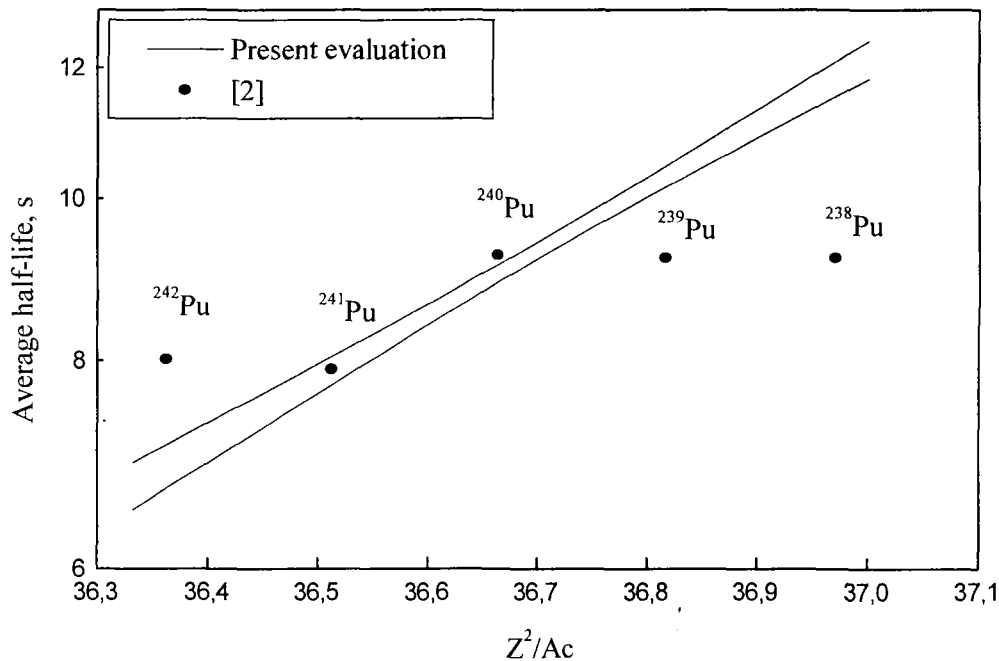


Fig. 1. Average half-lives of DN precursors for plutonium isotopes

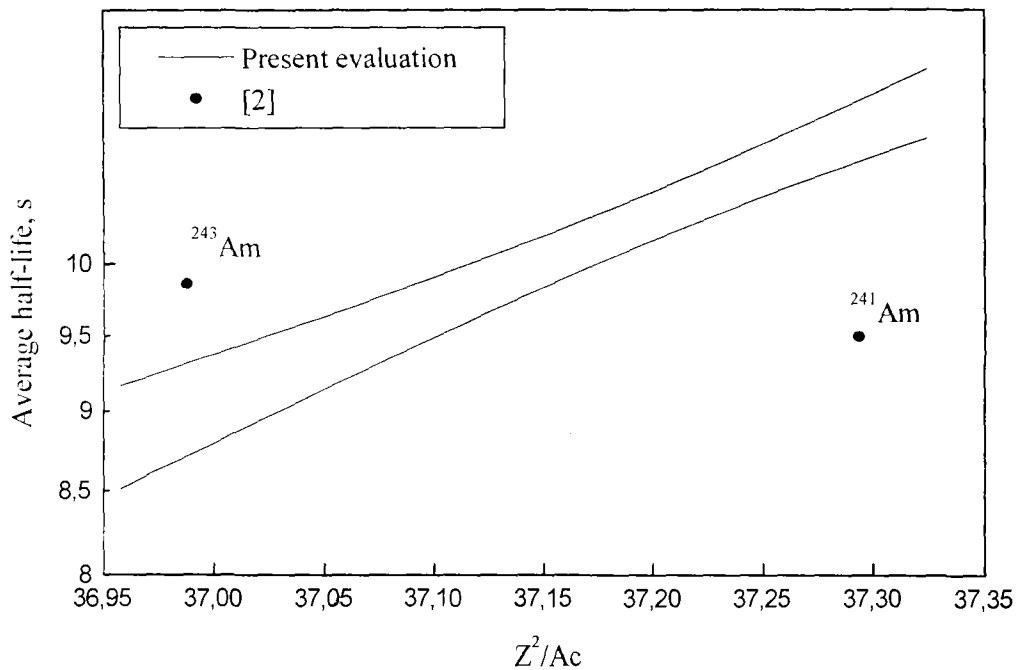


Fig. 2. Average half-lives of DN precursors for americium isotopes.

The comparison of DN data obtained by summation technique [2] and data obtained from systematics of the experimental data [1] shows large discrepancy. One of the possible source of this discrepancy may be related to the erroneous values of independent yields of fission products that used as input data in the summation method.

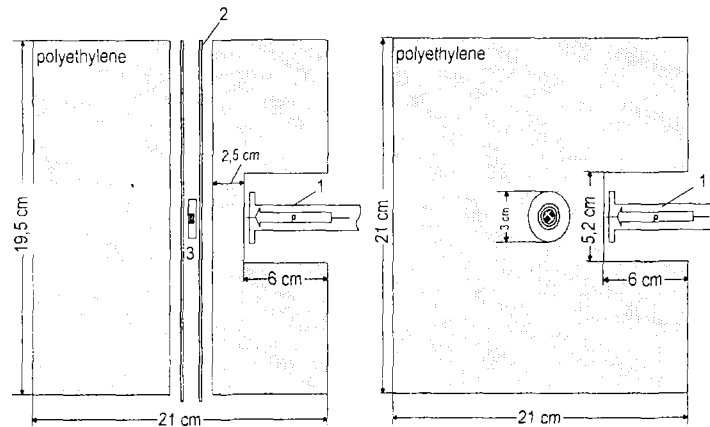
References

1. V.M. Piksaikin, S.G. Isaev. Correlation properties of delayed neutrons from fast neutron induced fission. Report INDC(CCP)-415, IAEA, Vienna, Austria.
2. M.C. Brady and T.R. England, "Delayed Neutron Data and Group Parameters for 43 Fissioning Systems", Nucl. Sci. and Engineering, 103, p.129 (1989).

Relative Abundance and Periods of Delayed Neutrons from Epithermal Neutron Induced Fission of ^{233}U , ^{235}U and ^{239}Pu

*V.M. Piksaikin, L.E. Kazakov, G.G. Korolev, S.G. Isaev,
R.G. Tertychnyi, V.A. Roshenko*

Measurements of relative abundance and periods of delayed neutrons (DN) from thermal neutron induced fission of heavy nucleus have been made on experimental set-up installed at electrostatic accelerator CG-2.5. Thermal neutrons are obtained within an 20 cm cubic polyethylene block. A schematic diagram of the experimental set-up for thermal neutron irradiations is shown in Fig. 1.



1 - target assembly, 2 - tube of sample transfer system, 3 - fissionable sample

Fig.1. Experimental set-up for thermal neutron irradiations

The calculation of incident neutron energy distribution was made by software based on Monte-Carlo technique. The results of calculations shown that average value of incident neutron energy was $2.85 \cdot 10^{-6}$ MeV. The incident neutron energy distribution is presented on Fig. 2.

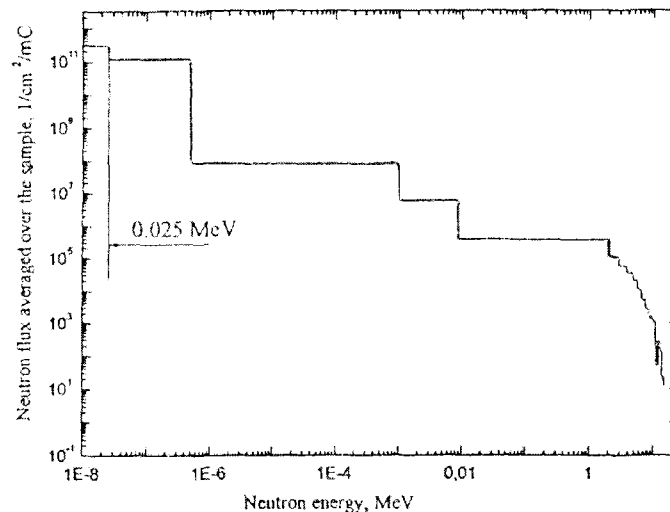


Fig.2. The incident neutron energy distribution.

Approximately forty cycles of irradiation and delayed neutron counting were made. In the present work two types of experimental data were measured. For the first type the sample irradiation time was 300 s and the delayed neutron counting time was 724.5 s. The second one is characterized by 15 s sample irradiation and 424.5 s neutron counting. The transportation time of the sample from irradiation position to the neutron detector was 0.15-0.2 s.

The relative abundance and periods of DN were obtained in the analysis of two types of decay curves by the iterative least-squares method [1]. In the analysis the matrix of correlation coefficients for each DN group parameters set was obtained. For each isotope the five sets of group parameters were considered. The average values of group parameters for epithermal neutron induced fission of ^{233}U , ^{235}U and ^{239}Pu were obtained by new averaging procedure. This procedure allows to take into account the correlation between the DN parameters.

The average half-life for epithermal neutron induced fission of ^{233}U , ^{235}U and ^{239}Pu were obtained using formula :

$$\langle T \rangle = \sum_{i=1}^6 a_i \cdot T_i ,$$

where a_i and T_i are the relative abundance and period of the i -th DN group.

The average half-life values for epithermal neutron induced fission are the following: 12.69 ± 0.11 for ^{233}U , 8.98 ± 0.11 for ^{235}U , 10.61 ± 0.19 for ^{239}Pu .

Reference

1. Piksaikin V.M., Balakshev Yu.F., Isaev S.G. e.a., "Measurements of periods, relative abundances and absolute total yields of delayed neutrons from fast neutron induced fission of ^{235}U and ^{237}Np .", Proc. Int. Conf. Nucl. Data for Sci. and Technol., Triest (19-24' May 1997) P.485.

New Data on the Proton Elastic Scattering Cross Section for Silicon

A.F.Gurbich, M.J.F.Healy¹⁾

¹⁾Cranfield University, Department of Materials and Medical Sciences, Swindon, UK

Silicon is one of the most important elements for semiconductor industry. Silicon samples are consequently often investigated by IBA methods, proton backscattering included. The proton elastic scattering cross section from silicon needed for computer simulation of backscattering spectra is non-Rutherford in the energy range of interest. So it cannot be calculated by a simple formula. Several experimental results for this cross section were reported. All the experimental data available have been recently reviewed and evaluated in the framework of the theoretical approach [1]. The significant discrepancy is observed at energies lower than ~ 1.2 MeV between the theoretical prediction of work [1] and the only experimental data set [2] available in this energy region. A new measurement was so undertaken to resolve the discrepancy.

A thin natural silicon layer was sputtered on to a polished vitreous carbon substrate to prepare a target. Low beam currents and a pile up rejection system were used to

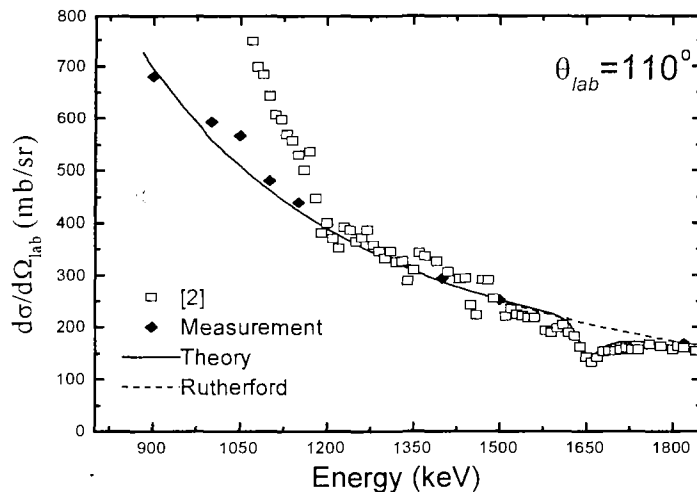


Fig.1. The measured cross sections, other available experimental data and the evaluated excitation function for proton elastic scattering from silicon at $\theta_{lab}=110^\circ$.

minimise background whilst counting Si(p,p)Si elastic scattering events at angles of 110° and 170° . The results obtained are in a fair agreement with the theoretical calculations (Fig.1). The conclusion may be consequently made that the evaluation of the work [1] provides reliable cross sections in the whole investigated energy region. Thus the power of the theoretical approach to cross section data handling is confirmed by the performed measurements.

References

1. A.F.Gurbich, Nucl. Instr. and Meth. B145 (1998) 578.
2. R.Amirikas, D.N.Jamieson, S.P.Dooley, Nucl. Instr. and Meth. B77 (1993) 110.

Evaluation of the Cross Sections for Elastic Scattering of ^4He from Carbon

A.F.Gurbich

The differential cross sections for elastic scattering of ^4He ions from light nuclei are among the most important data for IBA. So the evaluation of these cross sections which consists in producing on the base of available experimental points and appropriate theoretical models the most reliable continuous curves $d\sigma(E)/d\Omega$ at any backward angle is a necessary step towards establishing a firm basis for the analytical work performed by means of IBA.

The available experimental information on the ^4He scattering from carbon was compiled and the recommended differential cross sections in a wide region of the incident energy and scattering angles were produced in the frameworks of a theoretical approach (Fig. 1). Evaluation methodology employed was the same as has been developed for proton elastic scattering [1]. The evaluation consisted in a critical compilation and analysis of available experimental data followed by theoretical calculations.

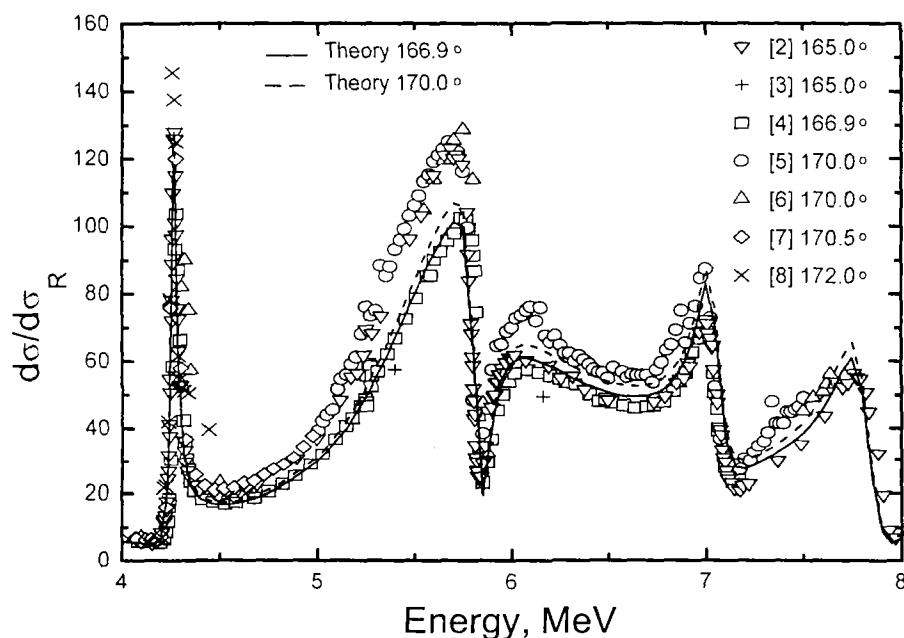


Fig.1. The available experimental data and the evaluated excitation function for ^4He elastic scattering from carbon in the energy range from 4.0 to 8.0 MeV.

The original publications were used for the analysis of the revealed discrepancies, taking into account the applied experimental technique and the possible error sources. The theoretical model [1] utilized for calculations of proton elastic scattering cross sections was further developed to involve the relevant physics in the case of the scattering of complex particles. The interaction between the impinging ion and the target nucleus was treated, in the center of mass of the equivalent single particle problem, as

scattering from a real potential well. The compound nucleus levels contribution was taken into account by addition of Breit-Wigner resonance terms to the amplitudes obtained by resolving Schrödinger equations for partial waves. Model calculations with comparison and fitting to experimental data were used for parametrization of the available experimental data.

Above 4.0 MeV the theoretical curve is very close to the data from the classical work [4] (see Fig. 1). The experimental points from [5] and [6] are systematically higher by ~20% being in a good agreement with each other. If renormalized these points appear to be in close agreement with Ref. [4] and with the calculated curve. Therefore all the difference originates from the normalization of the original experiments.. The experimental points from Ref. [2] are close to the data from Refs. [5] and [6] up to approximately 6.0 MeV and consequently they disagree with the theory. At higher energies the data from Ref. [2] are close to the data from [4] and to the evaluated curve. Such a behaviour of the excitation function is rather strange and the suspicion consequently arise that some unaccounted error influenced the results of Ref. [2]. As compared with evaluated cross sections the points derived in Ref. [3] from the thick target yield at 5.4 and 6.16 MeV are underestimated by 14% and 17%, respectively.

Except for normalization a fair agreement is in general observed between the available sets of experimental data (excluding the data of Ref. [2]) in a wide energy range. An additional calibration experiment is needed to resolve the discrepancy of the normalization. Now that the differential cross sections for $^{12}\text{C}(^4\text{He}, ^4\text{He})^{12}\text{C}$ scattering has been evaluated the required excitation functions for analytical applications may be calculated in the energy range from Coulomb scattering up to 8 MeV at any scattering angle with reliability exceeding that for individual measurement. The full text of the paper can be found in Ref. [9].

References

1. A.F.Gurbich, Nucl. Instr. and Meth., B129 (1997) 311; B136-138 (1998) 60; B145 (1998) 578.
2. Y.Feng, Z.Zhou, C.Zhou, G.Zhao, Nucl. Instr. and Meth., B86 (1994) 225.
3. C.R.Gosset, Nucl. Instr. and Meth., B40/41 (1989) 813.
4. J.W.Bittner, R.D. Moffat, Phys. Rev., 96 (1954) 374.
5. H.-S.Cheng, H.Shen, J.Tang, F.Yang, Acta Physica Sinica, 43 (1994) 1569.
6. J.A.Davies, F.J.D.Almeida, H.K.Haugen, R.Siegele, J.S.Forster, T.E.Jackman, Nucl. Instr. and Meth., B85 (1994) 28.
7. J.A.Leavitt, J.C.McIntyre, Jr., P.Stoss, J.G.Oder, M.D.Ashbaugh, B.Dezfouly-Arjomandy, Z.-M.Yang, Z.Lin, Nucl. Instr. and Meth., B40/41 (1989) 776.
8. R.Somatri, J.F.Chailan, A.Chevarier, N.Chevarier, G.Ferro, Y.Monteil, H.Vincent, J.Bouix, Nucl. Instr. and Meth., B113 (1996) 284.
9. A.F.Gurbich, Nucl. Instr. and Meth., B161-163 (2000) 124.

Differential Cross Sections of U(n,xn) Reaction at 14.3 MeV Neutron Energy

B.V. Devkin, M.G. Kobozev, S.P. Simakov, A.A. Lychagin, V.A. Talalaev

Uranium is the one of the basic elements for the nuclear reactors and may be used in fusion technology as a neutron multiplier. This requires the knowledge of the double differential neutron emission cross sections with accuracy 10 -- 15%.

In the paper we reported the results of the measurements of double differential neutron emission cross sections from U(n,xn) reaction at 14.3 ± 0.1 MeV incident neutron energy. The measurements have been made by time-of-flight technique at pulsed neutron generator KG- 0.3 of IPPE [1]. The ^{238}U sample was a hollow cylinder ($\varnothing 4.52 \times \varnothing 3.98 \times 4.87$ cm). The neutron detector consisted of the liquid scintillator NE – 218 and XP – 2041 photomultiplier. The measurements were carried out in the angle range 30° to 150° in 30° step. Corrections for the neutron multiple scattering and attenuation in the sample were estimated by the Monte – Carlo technique. The spectra of the inelastic scattering were obtained after subtraction of the elastically scattered neutrons.

The measured data are compared with the results of other experimental works in Figs. 1 and 2. They show good agreement with the data of the work [2] and essential discrepancies with [3] at forward angles. The comparison of the experimental data with data from ENDF–B6 and ENDL–85 libraries has revealed the discrepancies up to 30% in energy distribution of secondary neutrons and absence of angular anisotropy in ENDL-85.

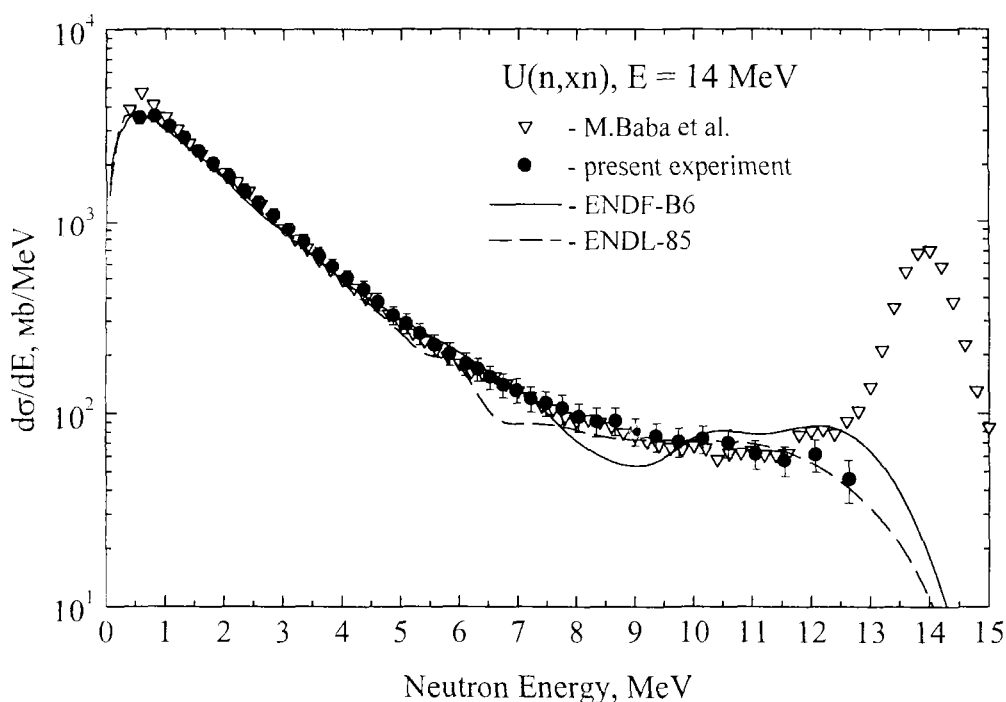


Fig. 1. The comparison of angle-integrated cross section of U(n,xn) reaction. Experiment: ● - present work, ▽ - [2]. Evaluation: — ENDF-B6, - - - ENDL-85.

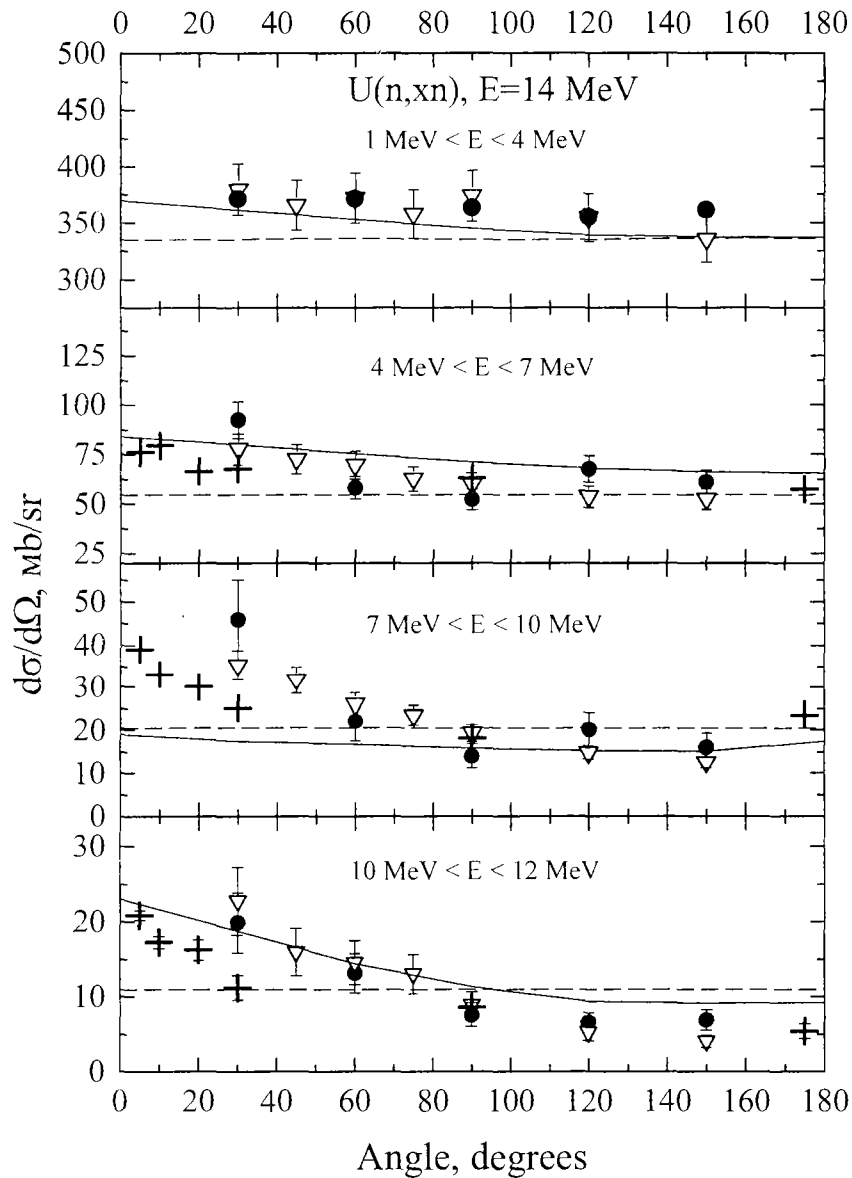


Fig. 2. The comparison of energy-integrated cross sections of U(n,xn) reaction. Experiment: ● - present, ▽ - [2], + - [3]. Evaluation: — - ENDF-B6, - - - - ENDL-85.

References

1. A.B. Anufrienko, B.V. Devkin et al., Problemy Atomnoy Nauki i Tekhniki, Seriya Reaktorostroenie, 5, 34, Obninsk (1977)
2. M. Baba, H. Wakabayshi et al. Report INDC(JPN)-129, IAEA, Vienna, 1989
3. A.P. Degtyarev et al.. Sov. Journ. of Nucl. Phys., 1981, v. 34, p. 299

Benchmarking of Evaluated Nuclear Data for Bismuth by Spherical Shell Transmission Experiments with Central T(d,n) and Cf-252 Neutron Sources

*S.P. Simakov, B.V. Devkin, M.G. Kobozev, V.A. Talalaev, U. von Möllendorff**

**Forschungszentrum Karlsruhe, Institut für Kern- und Energietechnik,
Karlsruhe, Germany*

The fusion neutron transport and multiplication properties of bulk bismuth may be expected to resemble those of lead, that is used as a neutron multiplier in the fusion reactor blanket designs, because either element has a relatively large cross section of the (n,2n) reaction for 14 MeV neutrons and very small cross sections for neutron absorption reactions. On the thermal hydraulics side, there is considerable experience with liquid lead-bismuth alloy as a coolant in fission reactors. Therefore, bismuth may be interesting also for fusion applications, and it appears worthwhile to validate or 'benchmark' the existing files of evaluated nuclear data for bismuth by integral neutron transport experiments.

Apparently, our group was the first to measure the neutron leakage spectrum from a metallic bismuth shell with 9 cm wall thickness with a T(d,n) source in 1992 [1]. Later, after modifications of the experimental arrangement, we remeasured these data and supplemented them by measurements with a Cf-252 spontaneous-fission neutron source. This was the first spherical nuclear data benchmark experiment performed with both T(d,n) and Cf-252. In the experiment reported here, the spherical bismuth shell having wall thickness 9.0 cm (1.4λ) was used. The leakage spectra measurements with the T(d,n) neutron source were made by the time-of-flight (TOF) technique from 14 MeV down to 100 keV at the pulsed neutron generator KG-0.3 of IPPE, Obninsk [2].

The neutron detector consisted of a 5 cm dia. by 5 cm length paraterphenyl crystal optically coupled to an FEU-143 photomultiplier [3]. Its anode pulses were fed to a constant fraction discriminator and pulse shape discriminator to yield start pulses for the TOF registration as well as identification pulses to distinguish neutrons from γ -rays.

A review of the relevant literature shows that the energy spectra of neutrons in the energy range above 100 keV leaking from bulk assemblies with Cf-252 spontaneous-fission neutron sources have generally been measured by proton-recoil pulse height spectrometry using hydrogenous scintillation detectors. In such experiments the source of neutrons was a capsule filled with Cf-252. To obtain the energy distribution of the detected neutrons, the apparatus pulse height spectrum was numerically unfolded using the detector response function, which had to be precisely determined. It is well known that such a procedure results in additional uncertainties. In 1988 we proposed the TOF technique for neutron spectrometry in spherical benchmarks with Cf-252 neutrons [4], using a neutron source which is simultaneously a fast ionisation chamber detecting the fission products and thus giving a time mark at neutron emission. This method has two advantages: (i) there is no need to measure the detector response function and to unfold a pulse height spectrum, (ii) the efficiency of the detector is measured in the same experiment employing the Cf-252 fission neutron spectrum with the sample sphere removed. This results in elimination of part of the experimental uncertainties.

The experimental setup for the measurements of neutron leakage spectra from the Bi shell with the ^{252}Cf neutron source (fast ionization chamber) at its center is similar to the

14 MeV neutron experiment, except for the neutron source and detector shield. This was the first spherical nuclear data benchmark experiment performed with both T(d,n) and ^{252}Cf neutron sources in otherwise identical conditions at the same facility.

Neutron transport calculations have been made using the MCNP-4 code with the ENDF/B-VI, EFF-2.4 and JENDL-FF evaluated data files. The comparison of the experimental results with transport calculations (the energy distributions of leaking neutrons) are shown in Fig. 1. The calculations with different libraries differ from each other very significantly, however, for all three libraries, the calculated neutron leakage deviates significantly from the measured one in case of the T(d,n) source, whereas for the Cf-252 source good agreement is found. We conclude that the quality of the evaluated data (first of all, the energy distribution of the secondary neutrons) decreases dramatically with neutron energy increasing from 2.1 MeV (the mean energy of Cf-252 fission neutrons) to 14 MeV. This is confirmed by comparison of the evaluated energy differential data with available experimental data, Fig. 2. For applications in fusion technology, we conclude that none of the tested files of evaluated data for bismuth is satisfactory. Especially, the ENDF/B-VI and the JENDL-FF bismuth data need to be improved.

The authors are grateful to Dr. Ulrich Fischer for his continuous advice and help concerning as well nuclear data files as Monte Carlo calculations. The work has benefited from support towards travel and staying expenses obtained on the basis of the Agreement on Scientific-Technological Cooperation in the Peaceful Utilisation of Nuclear Energy between the Federal Ministry of Education, Science, Research and Technology of the Federal Republic of Germany and the Ministry of Atomic Energy of the Russian Federation. The work of the Karlsruhe co-author was performed within the Projekt Kernfusion of Forschungszentrum Karlsruhe.

References

1. S.P. Simakov, A.A. Androsenko et al., in: Fusion Technology 1992, C. Ferro et al. (eds.), Elsevier (1993) p. 1489
2. A.B. Anufrienko, B.V. Devkin et al., Problemy Atomnoy Nauki i Tekhniki, Seriya Reaktorostroenie, 5, 34, Obninsk (1977)
3. V.A. Talalaev, S.P. Simakov et al., Acta Universitatis Debreceniensis, Debrecen, Hungary, p. 13 (1991)
4. S.P. Simakov, A.A. Androsenko et al., in report ZfK-646, Zentralinstitut fuer Kernforschung, Rossendorf (1988) p. 111
5. S.P. Simakov, B.V. Devkin et al., report INDC(CCP)-315/L, IAEA, Vienna (1990), EXFOR 41331
6. S.P. Simakov, G.N. Lovchikova et al., report INDC(NDS)-272, p. 147, IAEA, Vienna (1993), EXFOR 41155

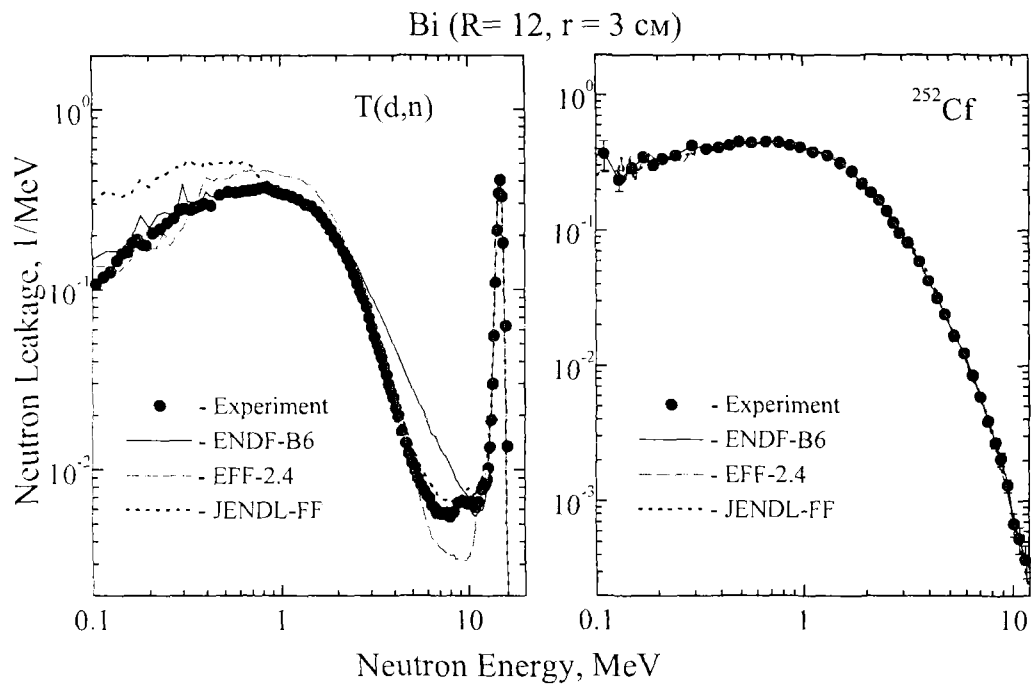


Fig.1. Neutron leakage spectra from Bi sphere with T(d,n) (left) and Cf-252 (right) neutron sources. Points: present experiment, curves: MCNP calculations with ENDF/B-VI (solid), EFF-2.4 (dashed) and JENDL-FF (dotted)

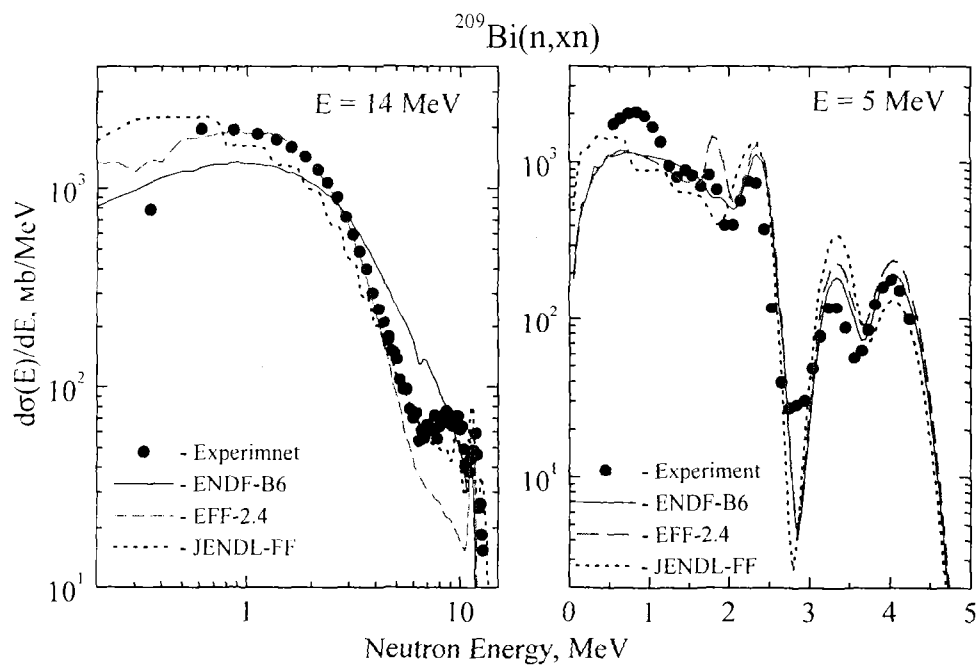


Fig.2. Energy-differential (angle integrated) neutron emission cross section of $^{209}\text{Bi}(n,xn)$ reaction at 14 MeV (left) and 5 MeV (right) incident energy. Points - experimental data [5, 6]. Calculations: solid curve ENDF/B-VI, dashed EFF-2.4, dotted JENDL-FF

Cross Sections for Discrete γ Ray Production in Interactions of 14.6 MeV Neutrons with Light and Medium Heavy Nuclei

S. Hlavac*, M. Benovic*, E. Betak*, L. Dostal*, I. Turzo*, S.P. Simakov

*Institute of Physics SAS, Bratislava, Slovakia

The cross section of prompt discrete γ ray transitions produced in 14.6 MeV neutron interactions with ^{23}Na , ^{27}Al , ^{28}Si , ^{31}P , ^{39}K , ^{51}V , ^{55}Mn and Mo have been measured. The selection of measured nuclei was to a great extent influenced by requests for experimental data included in WRENDA [1] and careful review of status experimental and evaluated data in the compilation [2]. The measurements were performed at the 14 MeV neutron source of the Institute of Physics, Bratislava. The setup, shown in Fig. 1, consists of a neutron source with an associated particle detector, neutron shielding, 244 cm³ HPGe photon detector and a CAMAC based data acquisition system. In order to reduce uncertainties we measured cross sections relative to well known cross sections.

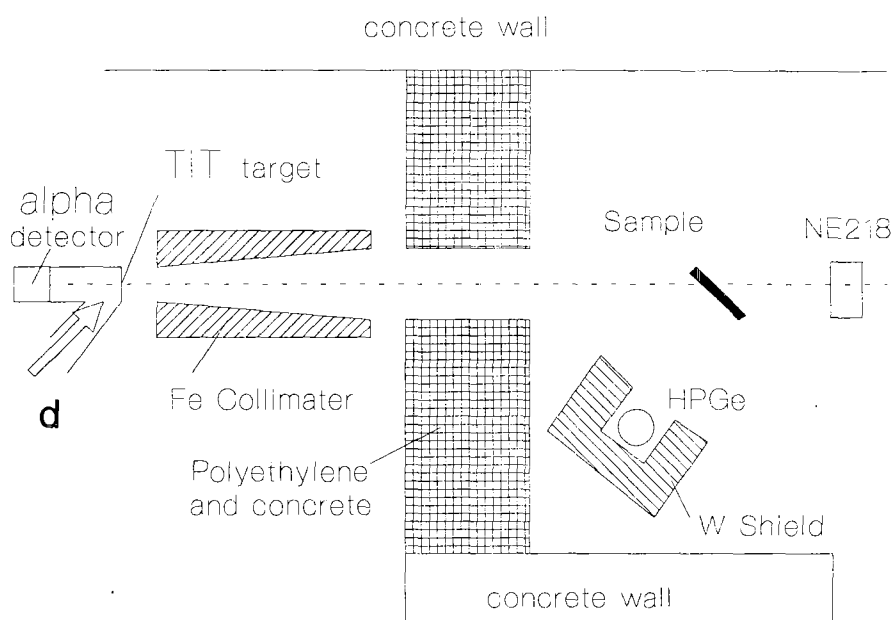


Fig.1. Schematic drawing of the experimental set-up

The discrete γ -ray transitions in $^{28}\text{Si}(n,n'\text{p})^{27}\text{Al}$, the majority of transitions in $^{55}\text{Mn}+n$ and all transitions in Mo+n reactions were observed for the first time. For some reactions the experimental results were compared with statistical model predictions, calculated with the advanced code GNASH [4] and DEGAS [5]. For example, in the Table 1 the experimental and calculated data are presented for Mo(n,xn) reaction. The agreement is generally acceptable, in some cases within a factor of two, which shows the limits of the present calculation methods.

The general situation of photon cross section measurements presented here shows that situation is far from being satisfactory.

Table 1. Experimental and theoretical cross sections of discrete γ transitions observed in Mo(n,xn) reaction.

E_{γ} , keV	Reaction	Transition initial \rightarrow final state	σ , mb		
			Experim.	GNASH	DEGAS
204	Mo(n,x γ) ⁹⁵ Mo	204(3/2 ⁺) \rightarrow 0(5/2 ⁺)	11.7 \pm 1.7	42	84
481	Mo(n,x γ) ⁹⁷ Mo	481(3/2 ⁺) \rightarrow 0(5/2 ⁺)	54 \pm 6	38	74
536	Mo(n,x γ) ¹⁰⁰ Mo	536(2 ⁺) \rightarrow 0(0 ⁺)	46 \pm 5	12	16
658	Mo(n,x γ) ⁹⁷ Mo	658(7/2 ⁺) \rightarrow 0(5/2 ⁺)	80 \pm 9	115	41
703	Mo(n,x γ) ⁹⁴ Mo	1574(4 ⁺) \rightarrow 871(2 ⁻)	148 \pm 16	198	63
720	Mo(n,x γ) ⁹⁷ Mo	720(5/2 ⁺) \rightarrow 0(5/2 ⁺)	40 \pm 5	16	32
721	Mo(n,x γ) ⁹⁷ Mo	721(3/2 ⁺) \rightarrow 0(5/2 ⁺)	24 \pm 4	14	42
735	Mo(n,x γ) ⁹⁸ Mo	735(2 ⁺) \rightarrow 0(0 ⁺)	43 \pm 5		
766	Mo(n,x γ) ⁹⁵ Mo	766(1/2 ⁺) \rightarrow 0(5/2 ⁺)	41 \pm 5	66	22
773	Mo(n,x γ) ⁹² Mo	2283(4 ⁺) \rightarrow 1510(2 ⁺)	53 \pm 6	75	43
778	Mo(n,x γ) ⁹⁶ Mo	778(2 ⁺) \rightarrow 0(0 ⁺)	192 \pm 16	174	156
787	Mo(n,x γ) ⁹⁸ Mo	787(2 ⁺) \rightarrow 0(0 ⁺)	88 \pm 8	32	42
813	Mo(n,x γ) ⁹⁶ Mo	? 2438(5 ⁺) \rightarrow 1626(2 ⁺)	28 \pm 4	28	
850	Mo(n,x γ) ⁹⁶ Mo	1628(2 ⁺), 1626 \rightarrow 778(2 ⁺)	140 \pm 16	98	6
871	Mo(n,x γ) ⁹⁴ Mo	871(2 ⁺) \rightarrow 0(0 ⁺)	241 \pm 26	266	226
943	Mo(n,x γ) ⁹³ Mo	943(1/2 ⁺) \rightarrow 0(5/2 ⁺)	14 \pm 2	4	12
948	Mo(n,x γ) ⁹⁵ Mo	948(9/2 ⁺) \rightarrow 0(5/2 ⁺)	95 \pm 11	95	11
1025	Mo(n,x γ) ⁹⁷ Mo	1025(7/2 ⁻) \rightarrow 0(5/2 ⁺)	40 \pm 5	21	20
1074	Mo(n,x γ) ⁹⁵ Mo	1074(7/2 ⁺) \rightarrow 0(5/2 ⁺)	28 \pm 4	14	11
1083	Mo(n,x γ) ⁹¹ Nb	1187(5/2 ⁻) \rightarrow 105(1/2 ⁻)	3 \pm 1	7	32
1108	Mo(n,x γ) ⁹¹ Nb	1313(5/2 ⁻) \rightarrow 105(1/2 ⁻)	8 \pm 2	4	19
1117	Mo(n,x γ) ⁹⁷ Mo	1117(9/2 ⁺) \rightarrow 0(5/2 ⁺)	81 \pm 9	92	13
1477	Mo(n,x γ) ⁹³ Mo	1477(9/2 ⁺) \rightarrow 0(5/2 ⁻)	47 \pm 6	27	4
1510	Mo(n,x γ) ⁹² Mo	1510(2 ⁺) \rightarrow 0(0 ⁺)	88 \pm 10	99	77

References

1. N. Kocherov, P.K. McLaughlin, eds., WRENDA 93/94, Report INDC(SEC)-104, IAEA, 1993
2. S.P. Simakov, A. Pavlik, H. Vonach and S. Hlavac. Status of experimental and evaluated discrete γ ray production at E=14.5 MeV. Report INDC(CCP)-413, IAEA, 1998
3. S. Hlavac and P. Oblozinsky. Nucl. Instr. and Meth., 1983, v. 206, p. 127
4. P.G. Young, E.D Arthur et al. Report LAS-12343-MS, Los Alamos 1992
5. E. Betak, P. Oblozinsky. Report INDC(SLK)-001, IAEA, Vienna, 1993

2.4 TRANSMUTATION

Isotopically Tailored Lead Target with Reduced Polonium and Bismuth Radiowastes

G.I. Khorasanov, A.Yu. Konobeyev, V.P. Lunev, A.I. Blokhin*

**Institute of Nuclear Power Engineering, Obninsk*

Presently, lead is considered as one of candidate materials for a target of Accelerator Driven Systems (ADS). Lead is a low cost material, it is a good liquid coolant and proton-to-neutron converter. Meanwhile, when lead natural (Pb-nat) with isotopic composition: %, Pb-208/Pb-207/Pb-206/Pb-204=52.35/22.08/24.14/1.42 is irradiated with fast protons a few hazardous long-lived nuclides are produced [1]. The purpose of this communication is in discussing the low activation material construction possibility for future ADSs.

Calculation for lead target activity was performed using CASCADE/SNT code developed in JINR/INPE/IPPE. In this calculations the neutron flux was taken as approximately $2 \cdot 10^{15}$ n/cm²/sec, irradiation time was fixed at 1 year, proton and neutron spectra were corresponded to dissipation of a 0.8 GeV, 30 mA proton beam in a 0.5 m diameter and 1.0 m length lead target.

Many types of nuclides are produced in a such target due to spallation, fission, (n, γ), (n,xn) and other nuclear reactions. The alpha- and hard gamma-active long-lived nuclides are the most hazardous among them. A clearance level of 10^4 Bq/kg was established for activity of these radiotoxic isotopes. Materials with activity above this clearance level must be kept under radiation control. The alpha-active polonium isotopes, Po-210,209,208, and hard gamma emitting bismuth isotopes, Bi-208,207,206,205, are known as very hazardous and relatively long-lived radiowaste. Calculated residual activity of these nuclides produced in a target of the full-scaled ADS is represented in Figs. 1 and 2. It can be seen that activity of the Pb-nat-based target exceeds the clearance level by many orders of magnitude. The main contribution to this target radiotoxicity brings bismuth isotope, Bi-207. Its activity is of $5 \cdot 10^9$ Bq/kg during 100 years of decay time, its mean energy of gamma and X-rays is hard enough, about 1.5 MeV, and the equivalent dose rate is above the remote recycling level (10 mSv/h) up to 10^3 years of decay time. It seems that in a hard proton spectrum the main channel for Bi-207 producing is the $^{208}\text{Pb}(p,2n)^{207}\text{Bi}$ reaction. This conclusion can be confirmed by calculation results given in Fig. 3. Activity induced by summarized proton and neutron interaction with nuclei and activity induced by neutron-nuclei interaction only are represented in this figure. These values of activity differ by two orders of magnitude indicating that the (p,2n) reaction is the main mechanism for Bi-207 production in the Pb-nat target. In order to reduce accumulation of Bi-207 in lead a new forthcoming technique of isotopic tailoring can be used. It is clear from Fig. 2 that activity of Bi-207 arising from lead isotope, Pb-206, used as a target, decreases to the level of 10^5 Bq/kg under the same irradiation conditions as from Pb-nat.

Correspondingly, activity of other heavy hazardous nuclides, such as Po-210, Po-209, Po-208, can be suppressed essentially when Pb-206 is used instead of Pb-nat in ADS targets. As it follows from Fig. 1, in this case production of radiotoxic alpha-active isotopes of polonium can be practically excluded.

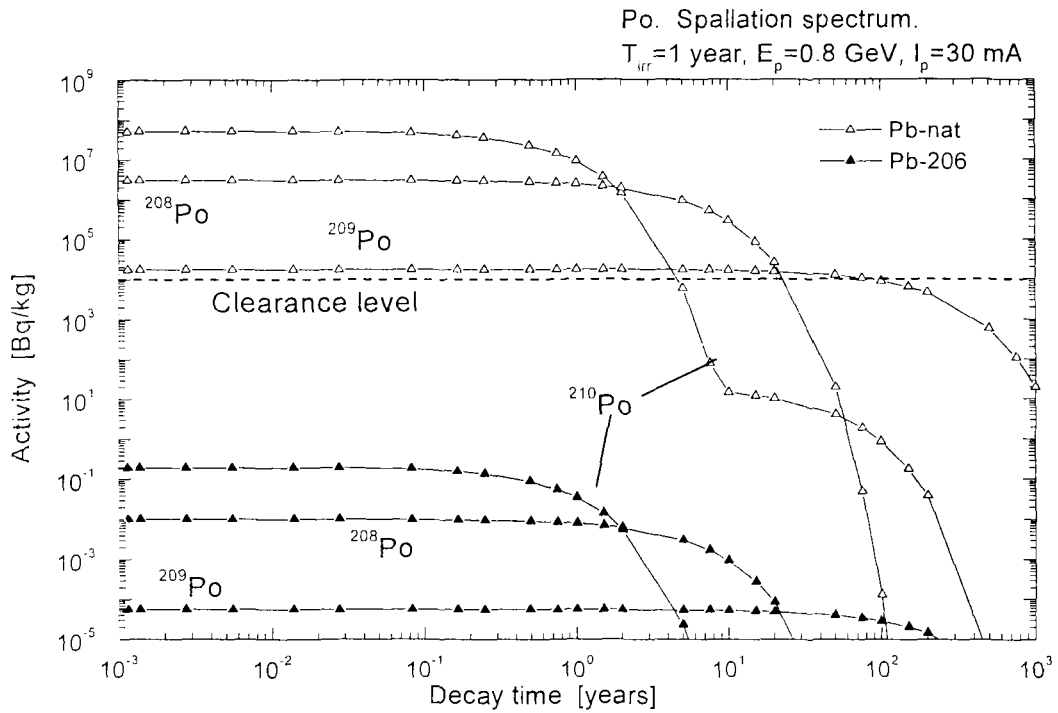


Fig. 1. Residual activity of Po-210, Po-209 and Po-208 produced in Pb-nat and Pb-206 after irradiation with proton beam $E_p=0.8$ GeV, $I_p=30$ mA, and $T_{irr}=1$ year.

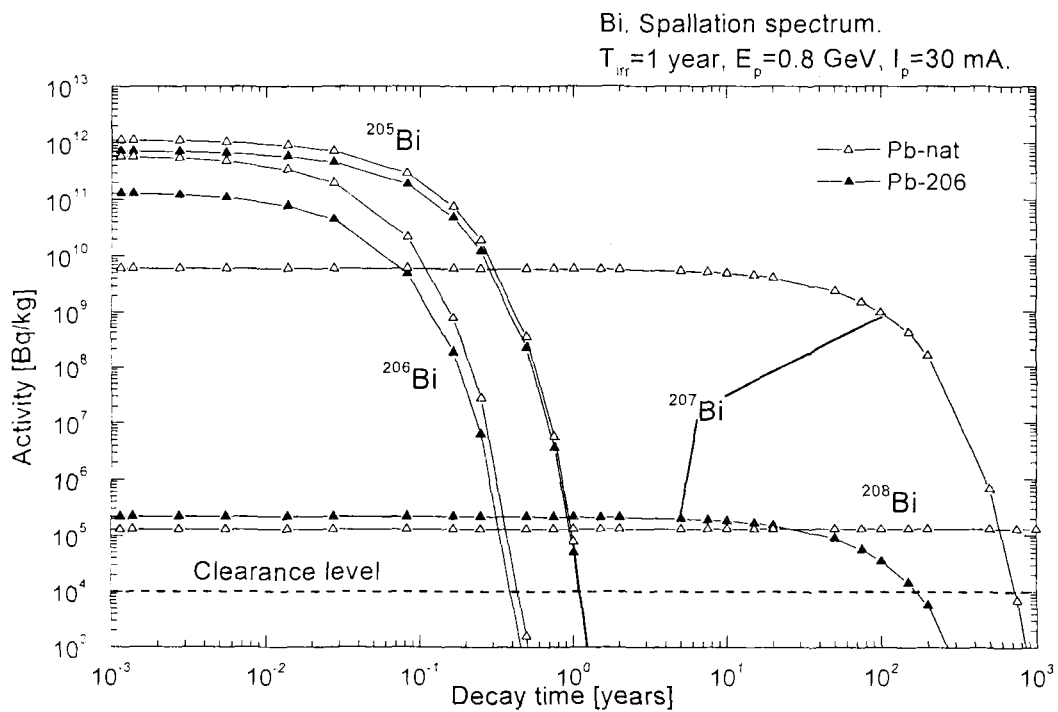


Fig. 2. Residual activity of Bi-208, Bi-207, Bi-206 and Bi-205 produced in Pb-nat and Pb-206 after irradiation with proton beam $E_p=0.8$ GeV, $I_p=30$ mA, and $T_{irr}=1$ year.

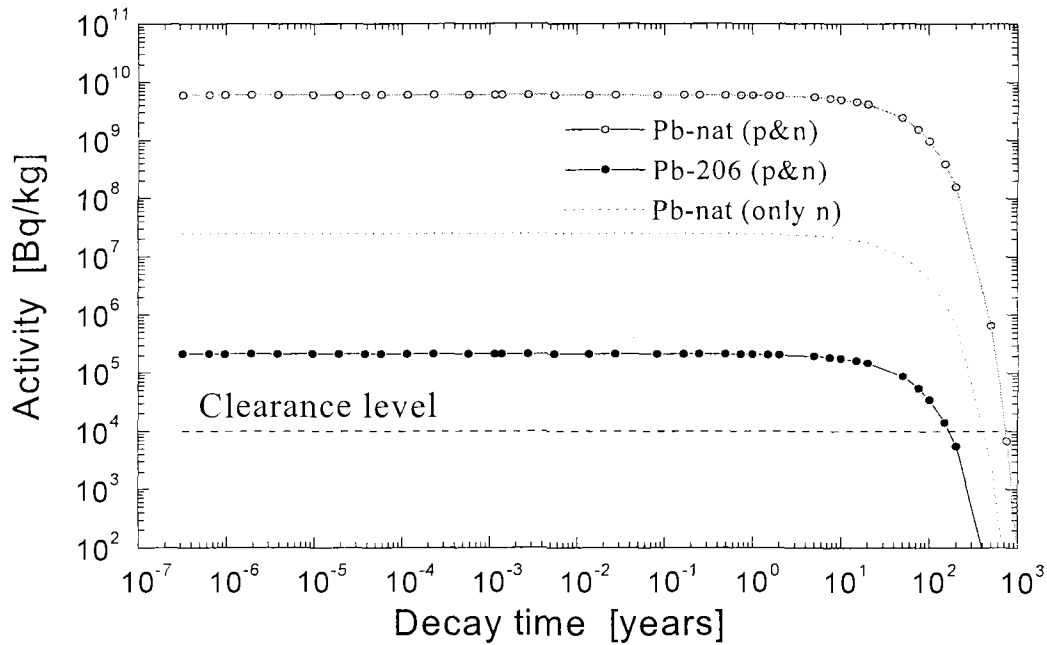


Fig. 3. Activity of Bi-207 produced in Pb-nat and Pb-206 after irradiation with proton beam $E_p=0.8$ GeV, $I_p=30$ mA, and $T_{irr}=1$ year.

It must be pointed that in using lead isotope, Pb-206, the situation with producing lighter fragments of spallation and fission reactions does not change essentially, while generation of the heavier nuclides, such as isotopes of Po and Bi, decreases to a great extent.

Thus, although isotopic tailoring option requires tremendous technical efforts, it is still the attractive option, which provides a low-activation target material for future ADSs.

References

1. G.L.Khorasanov, A.P.Ivanov, A.I.Blokhin, A.Yu. Konobeyev, M.V.Mikhailyukova, A.A.Glazkov, A.D.Koljaskin. Bi-207 Accumulation Problem in Lead Targets for ADS. In: Proc. of the Intern. Conf. on Sub-Critical Accelerator Driven Systems. Moscow, October 11-15, 1999, Edition of ITEPh, 1999, p.200-203.

Isotopically Tailored Lead Coolants for Dedicated Fast Reactors

*G.L. Khorasanov, A.P. Ivanov, V.V. Korobeinikov, A.I. Blokhin, A.N. Shmelev⁺,
A.A. Glazkov⁺, A.D. Koljaskin⁺*

Moscow State Engineering Physics Institute

Last time, a new type of safe fast reactor (FR) with molten lead coolant was proposed in Russia [1]. One of the advantages of lead as a FR coolant is in providing a significantly less positive void coefficient due to weaker moderating ability of lead in comparison with sodium.

Natural lead (Pb-nat) is a mixture of lead isotopes which consists of 52.35% Pb-208, 22.08% Pb-207, 24.14% Pb-206, and 1.42% Pb-204. Lead isotope, Pb-208, is a double magic nucleus and is characterized by unique nuclear properties. It has a high threshold for neutron inelastic scattering, $E_{\text{thresh}}=2.61$ MeV. So, lead enriched with Pb-208 seems to be a good coolant for the reactor-burner of minor actinides (MAs). Indeed, besides the advantage concerning void coefficient, the application of Pb-208 to a FR provides attaining negative magnitude of coolant temperature effect [2] and increasing MA incineration. Actually, incineration of a few nuclides such as Np-237, Pu-240, Pu-242, and Am-243 runs effectively in a hard neutron spectrum. Calculation performed by Monte-Carlo code [3] has showed that going from Pb-nat to Pb-208 as a coolant material results in hardening a neutron spectrum and increasing incineration of MA from 20 to 30 percent. As a number of required burners is rather small, they can be considered as dedicated facilities, in which it is quite possible to use such exotic coolant material like lead isotope, Pb-208.

Presently, Pb-208 is produced by lead isotopes separation in a gaseous centrifuge, and a cost of lead enrichment is high enough. The cost of Pb-208 can be decreased if a fabrication waste, which is a mixture of Pb-207, Pb-206, and Pb-204, is used for another dedicated facility. It can be for example small self-contained fast reactors for submarines or ice-cutters, which require low-activation materials. The matter is that in Pb-nat a few hazardous radiotoxic nuclides can be generated via (n,γ) and (n,xn) reactions with Pb-208 and Bi-209 nuclei [4,5]. Stable bismuth, Bi-209, is accumulating in Pb-nat with the rate of 0.1 g/kg Pb/y as it was calculated by FISPACT-3 code. Production of Bi-209 in lead irradiated in the BOR-60 FR is represented in Fig. 1. The dependencies of Po-210 and Bi-207 activity induced in lead are given in Figs. 2 and 3 as a function of cooling time. It can be seen that activity of Po-210 induced in Pb-nat runs to clearance level in 100 years of cooling, while hazardous activity of another nuclide, Bi-207, is more long-lived and its cooling time is equal to 400 years. But if lead isotopes, Pb-207, Pb-206, and Pb-204, are used as a coolant material, the corresponding cooling time required to release from regulatory control is essentially shortened.

Thus, lead coolant enriched with Pb-208 improves fast reactor safety and hardens a neutron spectrum. A waste of Pb-208 fabrication, a mixture of Pb-207, Pb-206, and Pb-204 is a low activation coolant. Both isotopically tailored coolants can be used in dedicated fast reactors.

Research performed is supported by the Russian Foundation for Basic Research, grant No 98-02-17368-a.

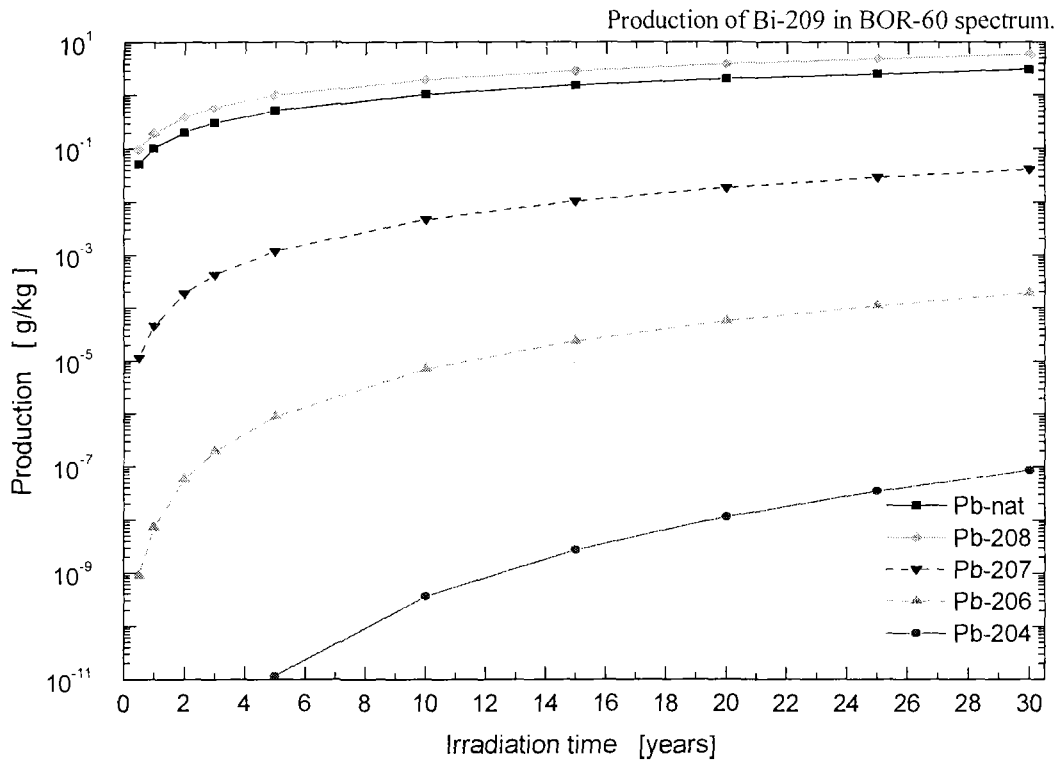


Fig. 1. Production of stable bismuth, Bi-209, in lead placed in the FR BOR-60 core

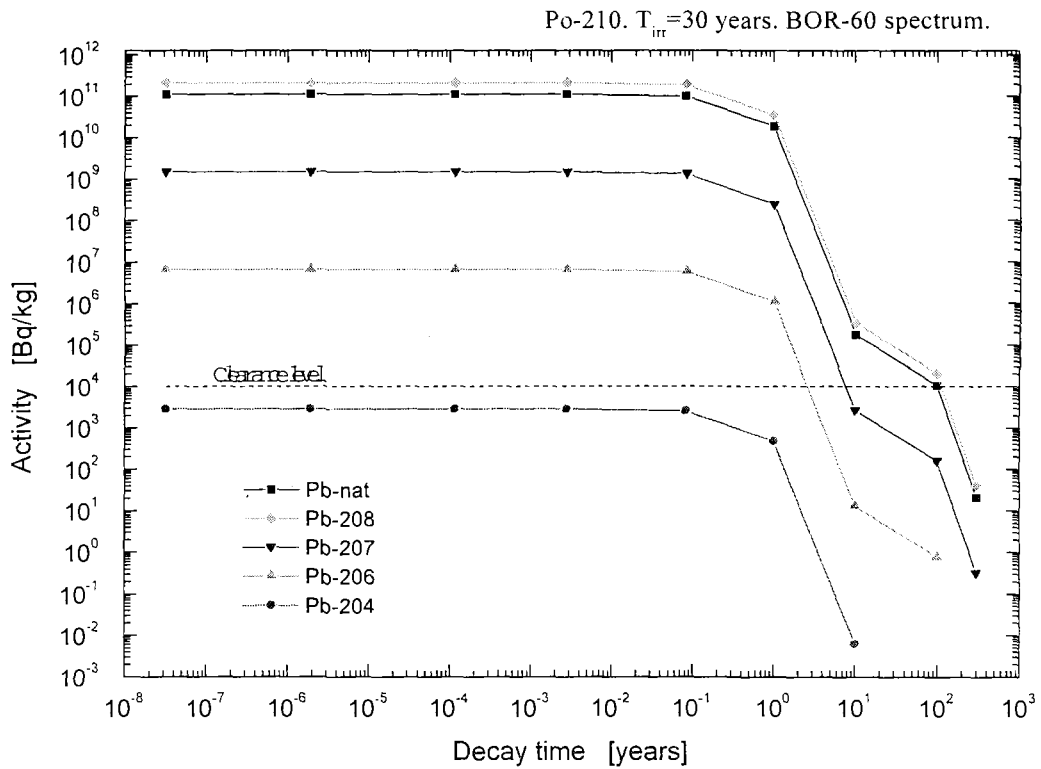


Fig. 2. Residual activity of Po-210 induced in lead

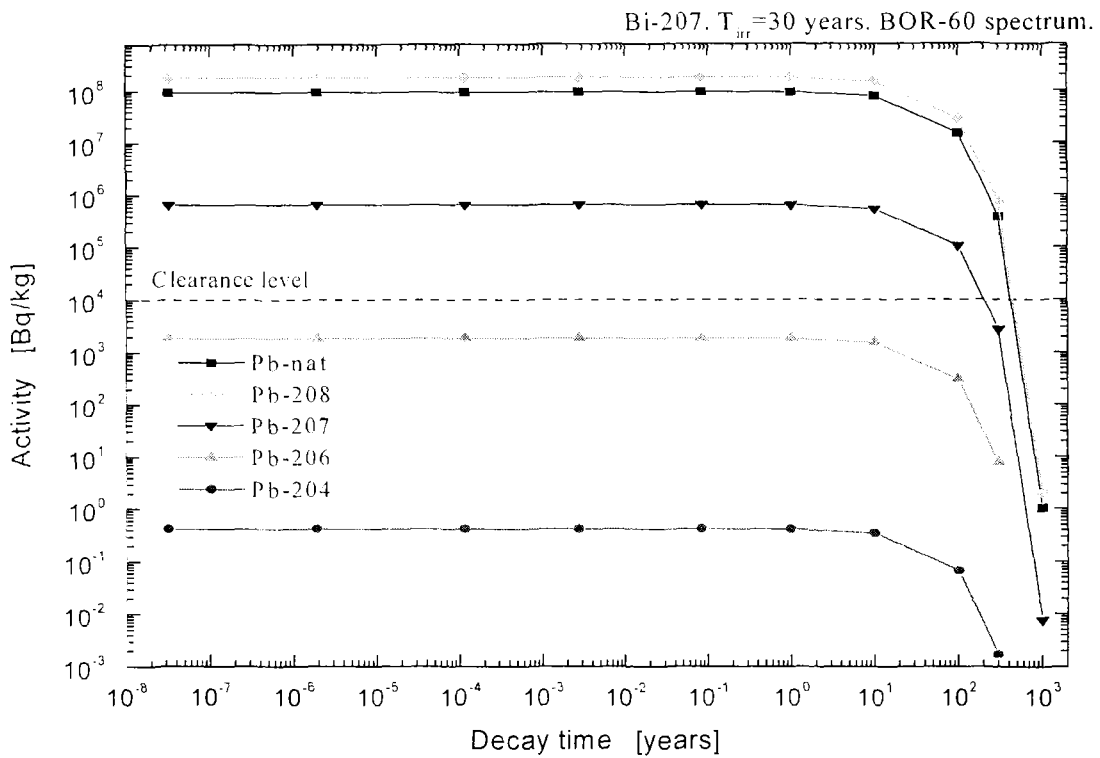


Fig. 3. Residual activity of Bi-207 induced in lead

References

1. V.V.Orlov. "Nuclear power of the next stage: profitable U-Pu breeding, safety, radwastes, nonproliferation". *Yadernaya Energetica*, N 5, p.57-59, 1997.
2. A.N.Shmelev et al. Radiowastes transmutation in nuclear reactors. In : IAEA-TECDOC-693, Vienna, IAEA, p.77-86, 1993.
3. G.L.Khorasanov, A.P.Ivanov, V.V.Korobeinikov, A.I.Blokhin, A.L.Shimkevich. "Lead coolant for fast reactor-burner with hard neutron spectrum". *Yadernaya Energetica*, N 1, p.80-84, 1999.
4. G.L.Khorasanov, A.P.Ivanov, A.I.Blokhin, A.L.Shimkevich, M.V.Mikhailyukova et al. Low-activation materials with isotopic tailoring for future NPPs. In: CD-ROM Proceedings of the Int. Conf. on Future Nucl. Systems, GLOBAL 99, Wyoming, USA, Aug.29-Sept.3, 1999.
5. G.L.Khorasanov, A.P.Ivanov, A.I.Blokhin, M.V.Mikhailyukova et al. Molten lead enriched with isotope Pb-206 as a low-activation coolant for emerging nuclear power systems. In: Proc. of the 4-th All-Russian (International) Conf. "Physical Chemical Processes at Selection of Atoms and Molecules". Moscow, TSNIATOMINFORM, p.262-267, 1999.

2.5 CONDENSED MATTER PHYSICS

The Association between Temperature Dependence of Liquid ^4He Scattering Law and the Phenomena of the Bose Condensation

I.V. Bogoyavlenskii¹, A.V. Puchkov, A. Skomorokhov

¹ *Institute of Physics and Technology, 310108, Kharkov, Ukraine*

The dynamics in liquid ^4He at low temperatures has already been a subject of interest for many years because helium behaves in a unique way. So excitation in superfluid helium in contrast to the other “simple” liquids remain extremely sharp at wave vectors up to 3.5 \AA^{-1} . Are the sharp excitations then a “signature” of the superfluid phase, connected in some way to the existence of Bose condensate in superfluid helium, or is ^4He just an extremely cold liquid?

The Density-Quasiparticle picture in the frame of the Field Theory and Dielectric function Formulation provides [1] a good description of the temperature dependence of neutron scattering data. In this picture, Bose condensate plays an explicit role, and the excitations at the phonon-maxon range of the dispersion curve is interpreted as a joint density/quasiparticle mode strongly coupled via the condensate. Within this description, the phonon at low Q is interpreted as a collective excitation of the Zero Sound mode (ZS-mode) which is not sensitive to the existence of the Bose-condensate. The sharp maxon peak is interpreted as a quasiparticle excitation of the Single Particle mode (SP-mode) which observed in $S(Q,\omega)$ only bellow T_λ . So the sharp maxon peak is a unique feature of the condensate and could not be observed in $S(Q,\omega)$ without one [1].

In this paper we report the results of the recent investigations [2] carried by inelastic neutron scattering to assess this relationship. Measurements were performed on the time-of-flight direct geometry DIN-2PI spectrometer at the Joint Institute for Nuclear Research in Dubna. Initial neutron energy was set about 2 meV and multi-detectors system at angle scattering range $6.3\text{-}71^\circ$ allow us to cover Q range from 0.2 up to 1.15 \AA^{-1} in one measurements. The Q -dependent resolution widths varied between 0.05 and 0.1 meV (FWHM).

The scattering function of ^4He was measured at eleven different temperatures in the range 0.44-2.22 K at SVP. The spectra were corrected for background, detector efficiency, and interpolated from constant \mathcal{G} to constant Q . To obtain the one-phonon parameters we used simple subtraction model (SSM) [3]. The multiphonon part of $S(Q,\omega)$ was determined at lowest experimental temperature and subtracted then from experimental spectra at higher temperatures. The damped harmonic oscillator function (DHO function) was fitted to the resulting one-phonon peak taking into account the instrumental resolution.

In results we obtain data on temperature dependence of $S(Q,\omega)$ which agree in main with previous detailed study [4]. One-phonon peak is anomalously independent of temperature at the Q less than 0.3 \AA^{-1} . Width of the peak slowly increases with temperature; position and intensity remain constant. We could not find any manifestations of the superfluid phase transition in the temperature dependence of the one-phonon parameters at this Q -region. At $0.3 < Q < 0.725 \text{ \AA}^{-1}$ one-phonon parameters demonstrate the essential temperature dependence which is most marked at temperatures near T_λ . All one-phonon parameters have jump near T_λ . Intensity and width of peak increase smoothly with temperature up to T_λ and change set of increasing after T_λ .

Position of the peak have a small dip at $T=1.9$ K and increases just below T_λ . Changes of the one-phonon peak become more marked with Q increasing. And temperature dependence of $S(Q,\omega)$ at $Q=1.15 \text{ \AA}^{-1}$ is quite different from that at the phonon region. Intensity and width of the peak increase with temperature also. Position of the peak remains constant up to 1.6 K, decreases after one and there are no indications of its rise at T_λ .

We suppose that temperature dependence of peak position at $0.3 < Q < 0.725 \text{ \AA}^{-1}$ with a dip bellow T_λ can be viewed as indication of strong hybridization between ZS and SP modes (If suppose that ZS energy for normal ^4He lies above SP energy for superfluid ^4He). Note, we find peculiarity in $S(Q,\omega)$ in this Q range [5] that can be treated as indication ZS - SP hybridization also according prediction Glyde-Griffin model [6]. Temperature independence of one phonon peak at $Q < 0.3 \text{ \AA}^{-1}$ and its smooth dependence up to T_λ at $Q=1.15 \text{ \AA}^{-1}$ indicate that there are no evidence SP -mode at $Q < 0.3 \text{ \AA}^{-1}$ and ZS -mode at $Q=1.15 \text{ \AA}^{-1}$. Wave vector range $0.3 < Q < 0.725 \text{ \AA}^{-1}$ is probably a range where SP and ZS modes exist simultaneously. Note that previous detailed study of $S(Q,\omega)$ identify dip in $\omega(Q,T)$ just bellow T_λ at all $Q < 1.4 \text{ \AA}^{-1}$, that not agree with our data completely. This disappointment may be caused by some arbitrariness of determination of the multiphonon part of $S(Q,\omega)$.

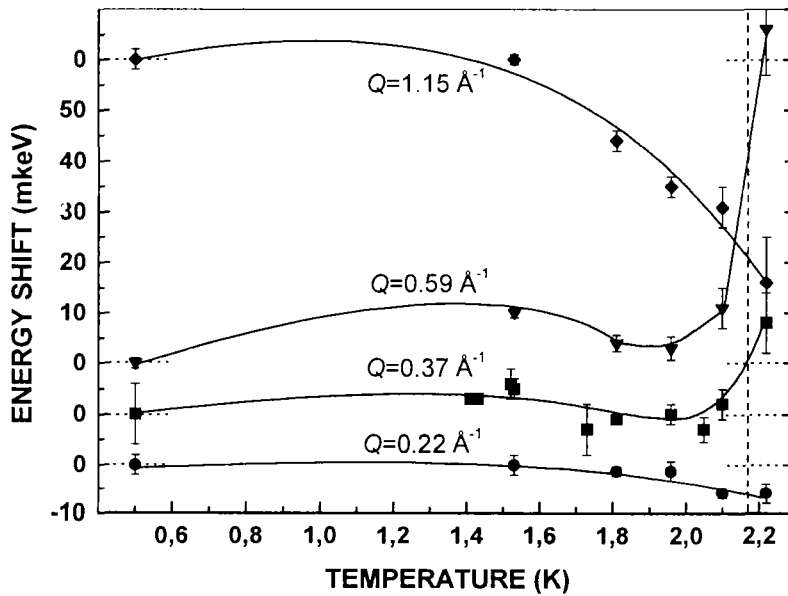


Fig.1. Energy shifts of the one-phonon peak position at SVP and various Q . Curves are simply guides to the eye

References

1. H.Glyde, Journal of Low Temperature Physics, 93(1993)862.
2. I.V.Bogoyavlenskii, A.V.Puchkov and A.Skomorokhov, Annual report 1998, FLNP JINR, p.72.
3. A.Miller, D.Pines and P.Noziers Phys. Rev., 127(1962)1452.
4. K.H.Andersen, W.G.Srtiling, J.Phys. Condens Matter, 6(1994)5805.
5. I.V.Bogoyavlenskii, A.V.Puchkov and A.Skomorokhov, Physica B, in press.
6. A.Griffin and E.C.Svensson, Physica, B165&166(1990)487.

On Diffusion of Big Ions in Aqueous Solutions

A.G. Novikov, M.N. Rodnikova¹, O.V. Sobolev²

*¹Kurnakov Institute of General and Inorganic Chemistry,
Russian Academy of Sciences, Moscow,*

²Frank Laboratory of Neutron Physics, Joint Institute for Nuclear Research, Dubna, Russia

In our previous inelastic neutron scattering experiments on aqueous solutions we have investigated effects of hydrophobic hydration, using as model particles tetraalkylammonium (TAA) ions Me_4N^+ , Bu_4N^+ and tetraphenylphosphonium (TPP) ion Ph_4P^+ [1-2]. In the course of the analysis of the experiments mentioned the main attention was paid to the dynamics of water molecules, incorporated in the hydration shells of these big ions. They contain a remarkable number of protons and contribute a sizeable portion in common neutron scattering by solutions. To separate water and ion effects supplementary experiments with heavy water solutions were performed. Now we shall use results of these experiments to infer an information concerning with the diffusion of big ions mentioned.

Due to the small contribution, introduced by water in the common neutron scattering of heavy water solutions (see fig. 4 in [1]), we can neglect with hydration effects in these solutions and consider the difference between neutron scattering by solution and water as one related to an ion:

$$S_{\text{sol}} - S_{\text{D}_2\text{O}} = S_{\text{ion}} \quad (1)$$

Then the quasielastic component of S_{ion} was extracted (detail see in [3]) and analysed in two steps. The first one was done under assumption the quasielastic scattering function to be the superposition of two Lorentzians, corresponding to the translation and rotation components of ion diffusion mobility:

$$S_{\text{qel}}^{\text{exp}}(q, \varepsilon) = \{ \sum_{1,2} A_i(q) * \Delta E_i(q) / [\varepsilon^2 + \Delta E_i^2(q)] \} \oplus R(q, \varepsilon), \quad (2)$$

where A_i and ΔE_i – are weights and half-widths of partial curves, $R(q, \varepsilon)$ – resolution function of spectrometer, q and ε - neutron wave number and energy transfer. The results of two-Lorentzian decomposition of experimental curves according exp. (2) are presented on fig. 1. It is seen, that both components if any have similar half-widths, and neither of weights behaves like it could be expected for reorientation diffusion. This is why we have preferred the one-Lorentzian representation of experimental quasielastic scattering functions:

$$S_{\text{qel}}^{\text{exp}}(q, \varepsilon) = \{ A(q) * \Delta E(q) / [\varepsilon^2 + \Delta E^2(q)] \} \oplus R(q, \varepsilon) \quad (3)$$

The reasonable description of experimental curves by exp.(3) and straight – line q^2 -dependence of intrinsic quasielastic scattering half-widths for three ions studied (fig. 2) indicate, that we deal with continuous translation diffusion, for which:

$$\Delta E(q) = 2\hbar q^2 D \quad (4)$$

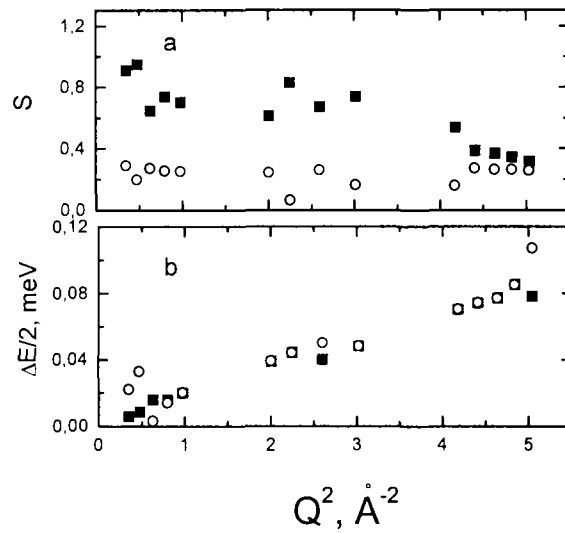


Fig. 1. The result of two-Lorentzian decomposition of quasielastic scattering functions according to exp. (2): a) intrinsic half-width of partial curves; b) weight of partial curves

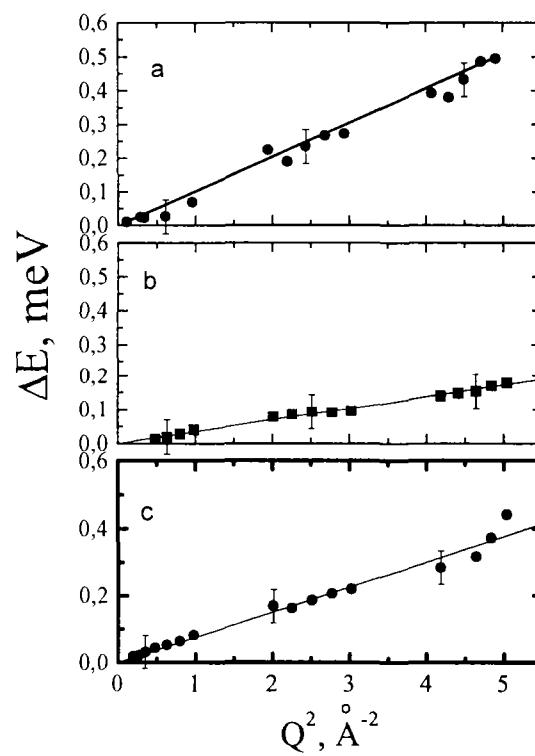


Fig. 2. Intrinsic half-width of quasielastic scattering functions for one-Lorentzian representation of experimental curves (exp. (3)): a) Me_4N^+ ion; b) Bu_4N^+ ion; c) Ph_4P^+ ion.

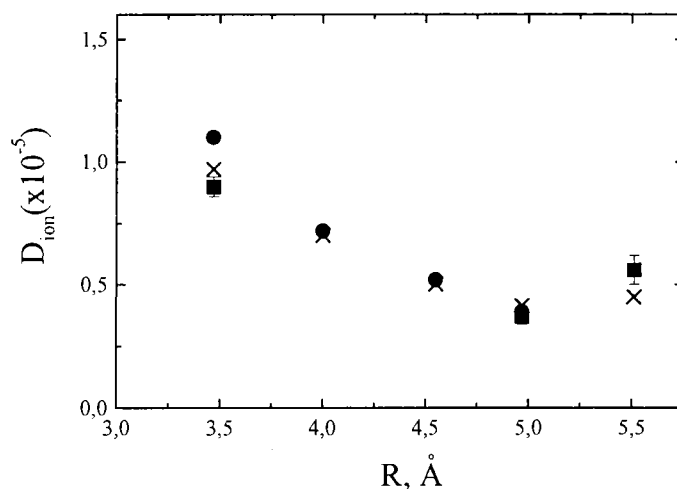


Fig. 3. The diffusion coefficients of ions as function of their crystallographic radii: ■ - this work; ● - NMR results; × - conductivity results.

Fig. 3 gives the comparison of diffusion coefficients in heavy water at 25C° for infinite dilution, obtained from our results (Fig. 2), NMR-data [4], and calculated on the basis of the conductivity (Me_4N^+ and Bu_4N^+ [5], Ph_4P^+ [6]). In the case of TAA-ions three experimental methods give similar results: the coefficients of diffusion are the smoothly falling functions of ion crystallographic radii (taken from [5]), but these radii do not coincide with the predictions of Einstein-Stokes law. TPP-ion (crystallographic radius is taken from [7]) does not fit in with common picture and looks like more moveable one compared with TAA-ions. It is not ruled out, that alkyl chains of TAA-ions fit into water structure and hinder diffusion mobility [8].

So, it can be concluded, that in heavy water the diffusion mobility of the big ions investigated obeys the continuous diffusion law without any visible evidence of reorientation.

References

1. A.Novikov, M.Rodnikova, J.Barthel, O.Sobolev. *J.Mol.Liquids*, 79(1999)203.
2. A.Novikov, M.Rodnikova, O.Sobolev. *Rus. J. Inorg. Chem.* 1999 (in press).
3. A.Novikov, M.Rodnikova, O.Sobolev. *J.Mol.Liquids*, 82(1999)83.
4. H.Hertz, B.Lindman, V.Siepe. *Ber.Bunsenges. Phys.Chem.*, 73(1969)542.
5. R.Kay, D.Evans. *J. Phys. Chem.*, 69(1965)4216.
6. M.Perie, J.Perie. *J. Sol. Chem.*, 18(1989)45.
7. J.Richardson, J.Ball, P.Boorman. *Acta Cryst.*, C42(1986)1271.
8. B.Krumgalz. *J. Chem. Soc., Faraday Trans. I*, 78(1982)437.

The Investigation of Hydrophobic Hydration Effects

A.G. Novikov, M.N. Rodnikova¹, O.V. Sobolev²

¹Kurnakov Institute of General and Inorganic Chemistry, Russian Academy of Sciences,

²Frank Laboratory of Neutron Physics, Joint Institute for Nuclear Research, Dubna

Neutron scattering experiments on $[\text{CH}_3]_4\text{NCl}$ (2M) $[\text{C}_4\text{H}_9]_4\text{NCl}$ (1M) and $[\text{C}_6\text{H}_5]_4\text{PCl}$ (0.3M) aqueous solutions carried out by our group with the use of DIN-2PI double time-of-flight spectrometer operating on a neutron beam of the IBR-2 pulsed reactor (Frank Laboratory of Neutron Physics, JINR, Dubna) [3].

Experiments and data handling methods were described in our previous papers [1,2,4]. We shall consider vibration-rotation motion of hydration water molecules, because inelastic neutron scattering is practically the only method to obtain the direct information on the spectrum of elementary excitations in the intermolecular interactions force field. It is useful to compare the generalised frequency distributions (GFD) for water molecules in $[\text{C}_4\text{H}_9]_4\text{NCl}$ and $[\text{C}_6\text{H}_5]_4\text{PCl}$ solutions with the results of ionic hydration previously obtained for LiCl [1] and CsCl [2] solutions.

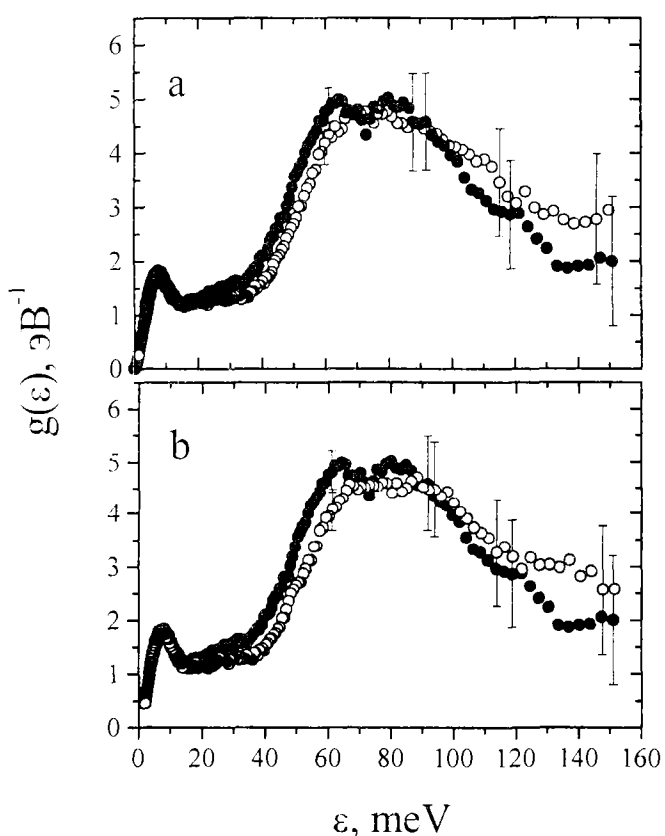


Fig. 1. Generalized frequency distributions of water molecules. Solid circles – pure water, open circles – water molecules in aqueous solutions: (a) $[\text{C}_4\text{H}_9]_4\text{NCl}$ (1M); (b) $[\text{C}_6\text{H}_5]_4\text{PCl}$ (0.3M).

The GFD of pure water molecules and GFDs of water molecules comprising the hydration shells of Cs^+ , Li^+ ions were presented in our previous papers [1,2]. Although Li^+ and Cs^+ ions belong to the different types of the ionic hydration (positive and negative), as it follows from presented data, both of these ions lead to H-B network disruption in the hydration shell. That is evidenced by decreasing of the weight of the first translation mode ($\varepsilon \approx 7$ meV) corresponding to deformation of tetrahedral angle O-O-O, which is usually regarded as the evidence of the H-B network existence [5].

The Bu_4N^+ and Ph_4P^+ ion affects molecules GFD of their hydration shell differently from ions mentioned above. It follows from Fig. 1 there are no any significant changes in the low-frequency part of spectra. This fact is indicative of the persistence of H-B network existing in the pure water in the vicinity of large hydrophobic particle. In our opinion, this result

directly correlates with the results of neutron diffraction investigations on water structure in hydration spheres of tetraalkylammonium ions [6-9]. There was shown clearly the absence of significant influence of these ions (at least, up to and including Bu_4N^+) on hydration water molecular structure, which appears as practically indistinguishable from the pure water.

It should be noted, that the study of hydrophobic effects by Raman scattering and infrared adsorption also did not show the remarkable growth of the intermolecular interactions and the space co-ordination of H-B network in the hydration water surrounding the hydrophobic particles [10].

References

1. A.G.Novikov, M.N.Rodnikova, V.V.Savostin, O.V.Sobolev, Chem. Phys. Letters. 259 (1996) 391
2. A.G.Novikov, M.N.Rodnikova, V.V.Savostin, O.V.Sobolev, Physica B. 234-236 (1997) 340.
3. User Guide. Neutron Experimental Facilities at JINR, ed. Yu.V. Taran. (Dubna, JINR Press, 1992).
4. A.Novikov, M.Rodnikova, J.Barthel, O.Sobolev, J. Mol. Phys. 79 (1999) 203-212.
5. M.Seats, S.Rice. J. Chem. Phys. 72 (1980) 3236.
6. J.Turner, A.Soper, J.Finney. Mol. Phys. 70 (1990) 679.
7. J.Turner, A.Soper, J.Finney. Mol. Phys. 77 (1992) 411.
8. J.Turner, A.Soper. J.Chem. Phys. 101 (1994) 6116.
9. J.Turner, A.Soper, J.Finney. J. Chem. Phys. 102 (1995) 5438.
10. Z.Kecki, P.Dryjnski. J. Mol.Structure 275 (1992) 135.

Collective Dynamics of Liquid Gallium Studied by Inelastic Neutron Scattering

*A. Beldiman¹, M. Ion¹, Zh.A. Kozlov², A.G. Novikov, I. Padureanu¹,
A. Radulescu¹, V.V. Savostin*

¹*Institute of Physics and Nuclear Engineering – Horia Hulubei, Romania*

²*Joint Institute for Nuclear Research, Dubna, Russia*

Atomic dynamics of liquid gallium is a matter of steady scientific interest in recent years [1–6]. Nevertheless some contradictions especial for abnormal liquids like gallium still exist. Gallium is the simple metal of the III-rd group in the periodic table of elements, but it exhibits several unexpected properties. One of them is the anomaly of the static structure factor $S(Q)$, known also for other elements such as Ge, Sn, Sb and Bi. The correlation between these features and dynamic properties is in a much less satisfactory state. The investigation of the short range order in liquid gallium [1] by means of neutron diffraction into the temperature range 290–343K ($T_m=303$ K) has shown that $S(Q)$ is a superposition of two structure factors where β -phase is present. This could explain the strange crystallisation of gallium and the physical meaning of the temperature $T^*=333$ K close to Debye temperature. It was suggested that liquid gallium exhibits a kind of «memory effect», but the inelastic neutron scattering (INS) experiment [7] has shown that the dynamic properties of α -Ga do not depend on thermal history. It was also stated [4] that dynamic structure factor $S_c(Q, \omega)$ obtained from INS experiments shows sound wave peak at $\hbar\omega \approx 5-6$ meV and $Q = 1.6-1.7 \text{ \AA}^{-1}$. These collective modes could be correlated with the second structure observed on the high- Q side of $S(Q)$ main peak.

In this connection a new INS experiment was carried out at temperature 373 K aiming to get new data about the microdynamics of α -Ga. Measurements were performed with the DIN-2PI time-of-flight neutron spectrometer of the direct geometry set up at one of the neutron beams from the IBR-2 pulsed reactor (Frank Laboratory of Neutron Physics, JINR, Dubna). The incident neutron energy was 4 meV with the resolution of 4%. The wide interval of scattering angles from 6° up 134° was used within the range of $Q_0 = 0.2 - 2.8 \text{ \AA}^{-1}$. The sample container consists of twenty quartz tubes whose height is 12 cm, the inner diameter 3 mm and wall thickness 0.2 mm.

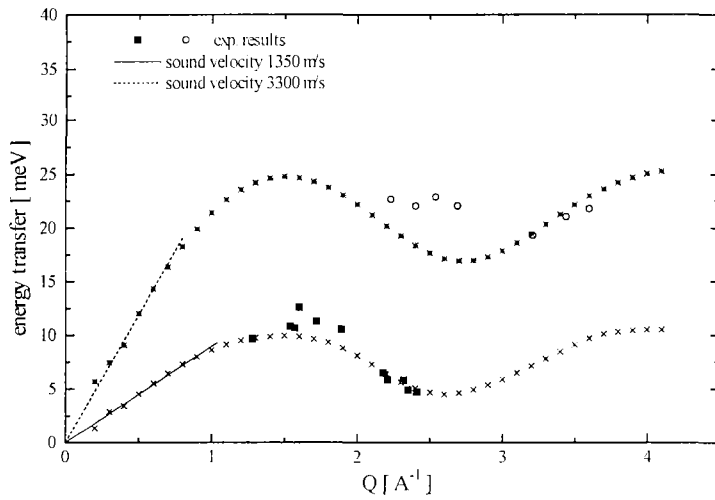
All the corrections involving the background from the empty sample holder, the attenuation factor into the sample, the detector efficiency have been applied to experimental data. As a result, the scattering function $S(Q, \omega)$ was extracted. $S(Q, \omega)$ is expressed as weighted sum:

$$S(Q, \omega) = \frac{\sigma_c}{\sigma_b} S_c(Q, \omega) + \frac{\sigma_i}{\sigma_b} S_i(Q, \omega)$$

where σ_c , σ_i σ_b stand for the coherent, incoherent and bound scattering cross section respectively. $S_i(Q, \omega)$ was evaluated from a theoretical model [8]. $S_c(Q, \omega)$ was transformed by an interpolation procedure from fixed scattering angle spectra into the representation at constant Q . The features appearing are interpreted as the evidence of the existence of propagating collective modes.

Liquid gallium is not a simple metal and quite different from alkaline metals. The calculations [9] performed with pair interaction potentials also within viscoelastic theory confirm the idea that the hardness of the repulsive part is a major factor and it depends

slowly on temperature. The problem is more complicated for α -Ga at temperatures as 373 K not far from melting point where superposition of two structures exists. This feature is reflected by both the $S(Q)$ and the derived potential. Therefore both structures may have some influence on the collective excitations. Unlike molten alkali and other simple metals, the damping effect is higher for α -Ga, but the idea [3,4] that α -Ga cannot sustain finite-frequency excitations because of relatively high longitudinal viscosity is a questionable problem. From the analysis of $S_c(Q, \omega)$ we have build the dispersion relations (Fig. 1). The positions of the inelastic peaks plotted against corresponding Q reveal the existence of two dispersion relations which seem to be the consequence of anomalies observed in $S(Q)$ and pair interaction potential. The solid line depicts the dispersion of hydrodynamic sound velocity of 1350 m/s and the dashed line corresponds to a hydrodynamic dispersion $\omega_Q = cQ$, with $c = 3300$ m/s. We think that the lower frequency curve lying close to spectral moment $\langle \omega_0^2 \rangle^{1/2}$ is related to the main structure of the $S(Q)$ for α -Ga, while the higher frequency component is a consequence of the second structure observed in $S(Q)$, close to $\langle \omega_l^2 \rangle^{1/2}$. The shape and characteristic of the low frequency dispersion curve are in agreement with the results obtained in [6] from first principles molecular dynamics simulations for α -Ga at $T = 702$ K and 982 K. It is worth to



mention here that the propagation of hypersonic waves in α -Ga was studied by Brillouin scattering of light [10]. The measured frequencies follow a hydrodynamic dispersion with an anomalous high velocity, $v=3700$ m/s, which is quite near to the one derived from the high frequency dispersion curve in our results.

Fig. 1. The dispersion curves for α -Ga at 373 K. The empty circles and full squares represent the experimental points. The crosses and the asterisks depict $\langle \omega_0^2 \rangle^{1/2}$ and $\langle \omega_l^2 \rangle^{1/2}$

References

1. S.N. Rapeanu and I.Padureanu, Physica Scripta T 57 (1995) 18.
2. I.Padureanu and S.N.Rapeanu, Balkan Phys. Lett. 3 (1995) 218.
3. I.Padureanu et al, Rom. J. Phys. 36 (1993) 579.
4. F.J.Bermejo et al, Phys. Rev. E 49 (1994) 3133.
5. J.M.Holender et al, Phys. Rev. B 52 (1995) 967.
6. F.J.Bermejo et al, Phys. Rev. E 56 (1997) 3358.
7. W.Luzny et al, Phys. Stat. Sol (a) 116 (1989) K25.
8. S.W.Lovesey, J. Phys. C 6 (1973) 1856.
9. I.Padureanu, A.Beldiman and A.Radulescu, Rom. J. Phys. (in press).
10. J.G.Dill and E.M.Brody, Phys.Rev. B14 (1976) 5218.

SANS Spectrometer for 1MW NUR reactor at URGN, Algeria

*S. Danilkin, V. Konstantinov¹⁾, A. Novikov, A. Puchkov, B. Solovjev¹⁾,
Sh. Zeinalov¹⁾, A. Wiedenmann²⁾*

¹⁾ Joint Institute for Nuclear Research, Dubna, Russia

²⁾ Hahn-Meitner Institute, Berlin, Germany

The small angle neutron scattering spectrometers (SANS) have received nowadays wide acceptance due to very rich possibilities, which they open for investigations of the structural peculiarities of density and concentration fluctuations on a length scale of 10-1000 Å. Due to the large scattering cross sections at low angles SANS can be used on the low flux neutron sources. We present a new SANS spectrometer which has been designed and manufactured in IPPE and JINR for the 1 MW NUR research reactor at Unité de Recherche en Génie Nucléaire (URGN), Draria, Algeria.

The design of the particular SANS instrument was governed by the rather low neutron flux of the NUR reactor. The scheme of the instrument composed by in-pile collimators, evacuated beam tube, cooled Be-Bi filter, velocity monochromator, argon filled detector chamber and set of linear position sensitive detectors is shown in Fig. 1.

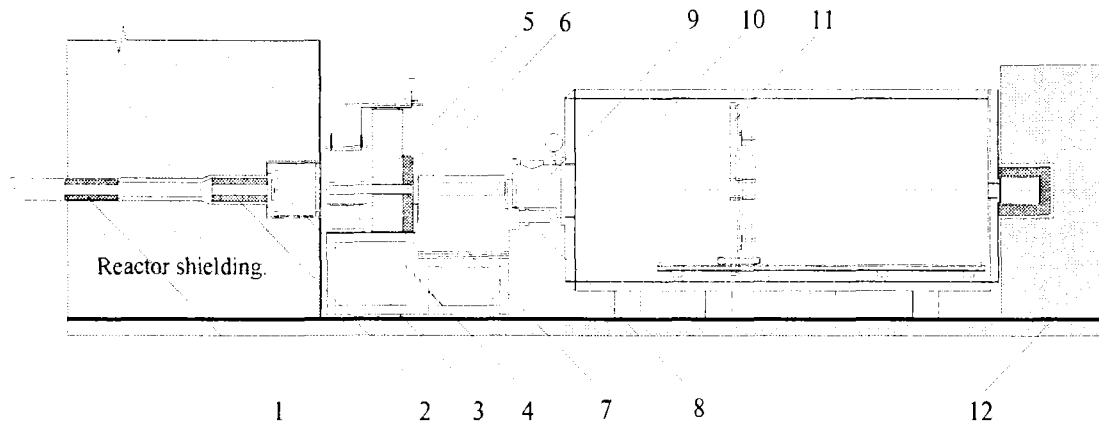


Fig. 1. The layout of SANS spectrometer installed at the NUR reactor of Draria, Algeria. 1,2-steel in-pile collimators; 3-beam shutter; 4-cryostat with Be-Bi filter; 5-shielding blocks; 6-evacuated beam tube; 7-mechanical monochromator, rotating in vacuum jacket; 8-changeable collimators; 9-evacuated sample chamber with adjustable sample table; 10-argon filled detector chamber; 11-movable position sensitive detector; 12-beam stop.

Velocity selector. A new type of mechanical monochromator with high transmission (more than 90%) and wavelength resolution of $\Delta\lambda/\lambda \sim 14\%$ was designed allowing the neutron wavelength to be selected between 4 Å and 10 Å. The selector is an aluminium cylinder of 600 mm length rotating in a vacuum jacket around the horizontal axis. The selector slits of helical shape are 60 mm high and 7.5 mm wide. They are formed by absorbing plates with a thickness of 0.5 mm and made of a Gd (10%)-Al alloy. The helical angle is equal to 0.295 rad. The center of the slits is at 200 mm from the axe. The results of the selector calibration by the time-of-flight method are shown in Fig. 2.

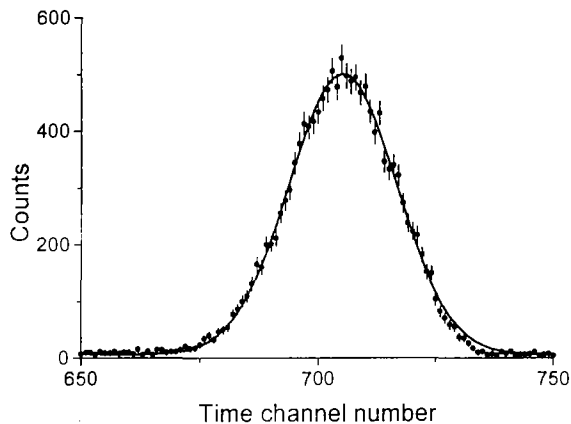


Fig.2. Wavelength calibration of selector by time-of-flight method. Solid line – Fit to a Gaussian function. Rotation speed $\nu=3500\text{rpm}$, $L=3\text{m}$, $\lambda=5\text{\AA}$, $\Delta\lambda/\lambda\approx 14\%$;

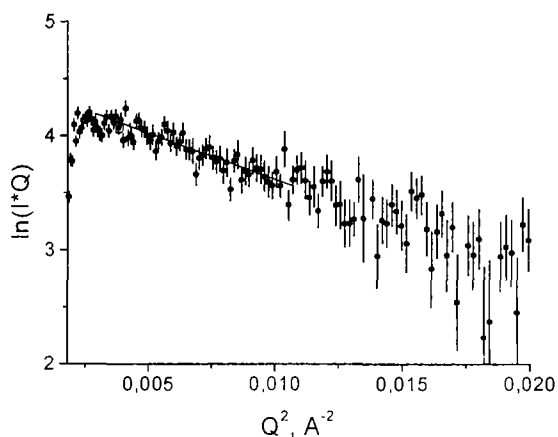


Fig. 3. Guinier-plot of intensity obtained for 1M solution of TDMAO in D_2O , which after correction by solvent reproduces scattering for particles with gyration radius of 13\AA

Detector. Four linear position sensitive neutron counters are assembled in radial direction relative to the neutron beam axis forming a star-shaped detector (Fig. 1). Such a composition of counters provides the enlarged solid angle for detection of scattered neutrons. If desirable, the number of counters can be doubled. Counters with a diameter of 32 mm and an active length of 600 mm are filled with a ^3He (4 atm) and Ar (2 atm) provide the spatial resolution of 10mm and an efficiency of 90% for neutrons with $\lambda=5\text{\AA}$. The detectors is mounted on a movable platform allowing the “sample-detector” distance to be changed between 2.5 m and 4 m. This makes possible to change the solid angle of detection and to expand the range of scattering angles. The detector chamber is filled by argon in order to diminish the losses of intensity. Long-term tests have been performed which proved the overall stability of the spectrometer components including mechanical monochromator, detectors and electronics. Calibration measurements of the instrument showed that the wavelength range and resolution, range of momentum transfer and spatial resolution of detectors are in good agreement with the expected values. From measurements of the incoherent scattering of a light water standard the monochromatic neutron flux intensity at the sample position was estimated to $10^5\text{ n/cm}^2\text{s}$ for neutrons with $\lambda=5\text{\AA}$.

As a final spectrometer test a small-angle scattering experiment was performed with tetradecyldimethylamine oxide (TDMAO). The cross sections on 1M solution of TDMAO in D_2O were measured and analysed in terms of Guinier-plot (Fig. 3), leading to a gyration radius of 13\AA , which is close to the value, known in literature [1].

Acknowledgement

We would like to thank director URGN Dr. M.Moulay, head of the SANS group URGN Dr. B.Meftah and the staff of reactor department for help and the fruitful cooperation during installation and commissioning of spectrometer. We are grateful to Dr. N.Gorski for putting in our disposal the sample of TDMAO.

Reference

1. N.I.Gorski, J.Kalus, J.Phys.Chem., 101(1997)4393.

Effect of Cr Content on the Crystal Structure and Lattice Dynamics of FCC Fe-Cr-Ni-N Austenitic Alloys

A. Beskrovni¹, S. Danilkin, H. Fuess², E. Jadrowski¹, M. Neova-Baeva³, T. Wieder²

¹ Joint Institute for Nuclear Research, Dubna, Russia

² University of Technology Darmstadt, Darmstadt, Germany

³ Institute of Solid State Physics, Sofia, Bulgaria

The high nitrogen austenitic steels are of high strength and corrosion resistance and offer the structure stability at low temperature and during cold working. The steel properties depend on the interstitial (N) and substitution (Cr, Ni, Mn) atom content. In paper [1] the effect of Cr content on the crystal structure and interatomic bonding was studied in Fe-xCr-11Ni-0.5N (x=15; 20; 25; 29 wt. %) alloys. The diffraction measurements were carry out with Philips-Micro III x-ray diffractometer and with neutron diffractometer DN-2. The inelastic neutron scattering spectra were measured with DIN-2PI spectrometer.

The diffraction measurements show the FCC structure for all steels studied. The neutron diffraction discloses the small contamination of the BCC α -phase in all samples. The amount of the α -phase does not exceed 3% according to the results of the Rietveld refinement. The linear dependence of the lattice parameter a (Å) on Cr content x (wt. %) was observed: a (Å) = $(3.572 \pm 0.004) + (0.0015 \pm 0.0002) x_{Cr}$ (wt. %) in case of powdered material, and a (Å) = $(3.5704 \pm 0.002) + (0.0013 \pm 0.0001) x_{Cr}$ (wt. %) in case of bulk material. The difference in a (Å) for both material classes may result from macroscopic residual stresses within the bulk samples, which have been relaxed, in the powdered samples. The atomic Goldschmidt radius (reduced to the FCC co-ordination number 12) of Cr is bigger than of Fe and Ni that could explain the lattice dilatation with chromium content increase.

The INS measurements show that frequency spectrum of the metal atoms depends on the Cr content only slightly, showing the softening of the spectra at low frequencies. From a fit of the Debye spectrum to the low-energy part of the experimental frequency distributions the decrease of Θ_D was observed with increasing Cr content: Θ_D (K) = $(404 \pm 7) - (0.6 \pm 0.3) \cdot x_{Cr}$ (wt. %). The second moment of the frequency distribution of the metal atoms $\langle \varepsilon_{Me}^2 \rangle$ was found to be independent on Cr content within experimental errors. Similar observations concerning the Cr effect on interatomic bonding are reported in paper [2] where the elastic constants of Fe-Cr-Ni-Mn polycrystalline alloys were measured using an ultrasonic method. Cr slightly increases the bulk modulus and G changes in opposite direction. This observation contradicts the Eshelby model predictions. A volume change should produce the same sign for $\Delta B/B$ and $\Delta G/G$.

The different dependencies of B and G on the Cr content could be connected with contribution of the bond-bending forces to elastic moduli, which have the opposite sign. The bond-bending forces $\varphi'(r_1)/r_1$ for the first neighbours typically have a negative sign, therefore if $|\varphi'(r_1)/r_1|$ is increased with increasing Cr content, the decrease of the shear modulus and the increase of the bulk modulus can take place simultaneously. The influence of the Me-N interaction on the elastic moduli changes can be omitted because our experiments show small change of the nitrogen vibrational frequency with increasing Cr content in the studied steels and nitrogen content in steels was the same.

Chromium also causes changes in the localized vibrations of nitrogen. The small increase of the nitrogen frequency observed with Cr content contradicts with the lattice

dilation caused by Cr atoms. The decrease of the nitrogen peak width with Cr content is also untypical (Fig. 1). Such behavior is possibly connected with changes in the electron screening and in the stress-induced interaction caused by the different Cr content. These effects could cause the ordering of the nitrogen atoms with increase of Cr content that manifests itself as a decreasing of the nitrogen peak width. This assumption is confirmed by computer simulation of the ordering in the Fe-40Ni-35Cr-xN alloys. As it was demonstrated by Owen [3], the nitrogen atoms preferentially occupy the octahedral sites where they have a large excess of Cr over Ni atoms in the first coordination shell.

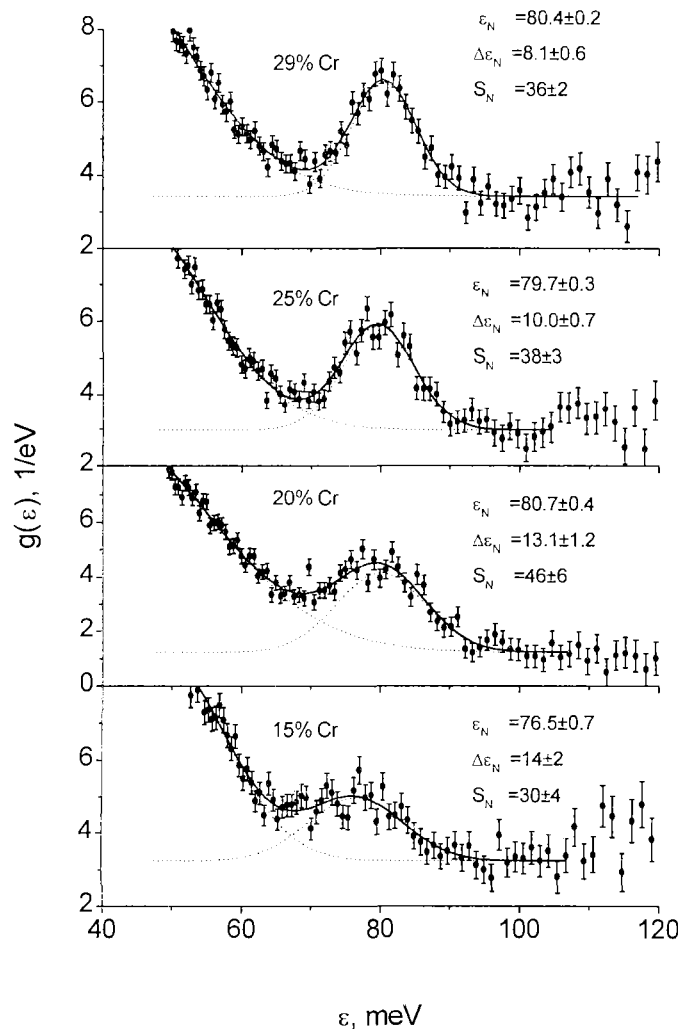


Fig. 1. Nitrogen peaks in frequency spectra of Fe-xCr-11Ni-0.5N alloys
 ϵ_N , $\Delta\epsilon_N$ and S_N – nitrogen peak frequency, width and area.

References

1. A.Beskrovni, S.Danilkin, H.Fuess, E.Jadrowski, M.Neova-Baeva, T.Wieder: Effect of Cr Content on the Crystal Structure and Lattice Dynamics of FCC Fe-Cr-Ni-N Austenitic Alloys, J. of Alloys and Compounds, 1999, v. 291, p. 262.
2. S.Kim, H.Ledbetter, Y.Y.Li: Elastic constants of four Fe-Cr-Ni-Mn alloys, Journal of Materials Science 1994, vol. 29, p. 5462
3. M.Grujicic, W.Owen: Nitrogen induced ordering in face-centred cubic Fe-Ni-Cr-N solid-solution alloys, Proc. of 3rd Intern. Conf. HNS'93, part I, Eds. V. Gavriljuk and V.Nadutov, Kiev (1993), p.686.

Nitrogen Effect on Lattice Dynamics of FCC Fe-Cr-Mn (Ni) Austenitic Alloys

S. Danilkin¹, A. Beskrovni², E. Jadrowski²

¹ *Institute of Physics and Power Engineering, Obninsk, Russia*

² *Joint Institute for Nuclear Research, Dubna, Russia*

In paper [1] the nitrogen effect on the crystal structure and vibrational frequency distribution of the Fe-18Cr-19Mn- x N ($x = 0.38; 0.56; 0.76; 0.93$ wt. %) alloy was studied with neutron scattering method. The diffraction measurements were performed with the neutron diffractometer DN-2 [5] [2]. The inelastic neutron scattering spectra were measured with DIN-2PI spectrometer [2].

The neutron diffraction measurements show that these alloys are the FCC solid solutions and the nitrogen atoms cause the lattice dilatation: $a(\text{\AA}) = 3.600 + 0.034 x_{N+C}$ (wt. %).

Vibrational frequency spectrum of the metal atoms. The metal atom frequencies depend only slightly on the nitrogen content. The second moment of frequency distribution, which is proportional to the mean atomic force constant in the crystal, $\langle \varepsilon^2_{Me} \rangle$, do not depend on the nitrogen content within the experimental errors (less then ≈ 1 %). However Debye temperature determined from the low energy part of spectrum decreases from $\Theta_D = 416 \pm 5$ K at 0.38 % N to $\Theta_D = 407 \pm 5$ K at 0.93 % N, that gives $\Delta\Theta_D/\Theta_D \approx -2\%$. This correlate with behaviour of the elastic constants of these alloys studied by the ultrasonic method in paper [3]. Nitrogen atoms cause the decrease of the shear modulus, G , and increase of the bulk modulus B . Whereas the decrease in the shear modulus agree with the model based on volume changes that predicts decrease of G , the change of B is inconsistent with volume increase.

Using data for longitudinal and transverse velocities v_l and v_t from paper [4] we obtain that $\Delta\Theta_D/\Theta_D$ is -1.7 %, that agrees with INS experiment. The changes of the shear modulus are related with variation of Debye temperature, Θ_D , therefore changes in shear modulus arise from the softening of the low energy part of the frequency distribution determined mainly by the transverse vibrations.

To explain the small nitrogen effect on the $\langle \varepsilon^2_{Me} \rangle$ we should notice that B is related to $\langle \varepsilon^2_{Me} \rangle$, therefore for both $\langle \varepsilon^2_{Me} \rangle$ and B other factors then volume changes should be taken into consideration. Effect of nitrogen - metal atom interaction is among the first. The contribution of Me-N bonds could be significant even at low nitrogen content because the interatomic Me-N constants are in 4 ÷ 5 times higher then Me-Me forces. The analysis in frame of the model of lattice dynamics for disordered interstitial alloy shows that the effect of the additional Me - N bonding is comparable with changes produced by the lattice dilation. The calculations using Fe-Fe potential of Johnson give the following values for the second moment of the metal frequency spectrum: $\langle \varepsilon^2_{Me} \rangle = 636$ meV² for $x=0.38$ wt. % N and $\langle \varepsilon^2_{Me} \rangle = 659$ meV² for 0.93 wt. % N, which is in agreement with observed increase of B .

Thus, changes in the elastic moduli caused by nitrogen could be connected with complicated modification of the vibrational frequency distribution. At low energies the $\delta G(\varepsilon, x)$ is negative showing the softening of frequency distribution with increasing nitrogen content. At the same time at high frequencies the increase frequency of the

spectrum boundary takes place that keeps the second moment of the frequency distribution $\langle \varepsilon_{Me}^2 \rangle$ constant.

Nitrogen vibrations. Nitrogen frequencies for all studied at present alloys were plotted against the lattice parameter (Fig.1). In spite of rather large errors in experimental data, the decrease of nitrogen frequency with increasing lattice parameter is clearly seen. The least-squares analysis gives the following dependence: ε_N (meV) = $(380 \pm 50) - (84 \pm 14) a$ (Å). The relative change of nitrogen frequency is described by the following equation: $\Delta\varepsilon/\varepsilon = (0.008 \pm 0.005) - (1.56 \pm 0.20) (\Delta V/V)$. In this equation the coefficient $k_V = 1.56$ is close to Gruneisen parameter $\gamma = 1.98$ for these steels.

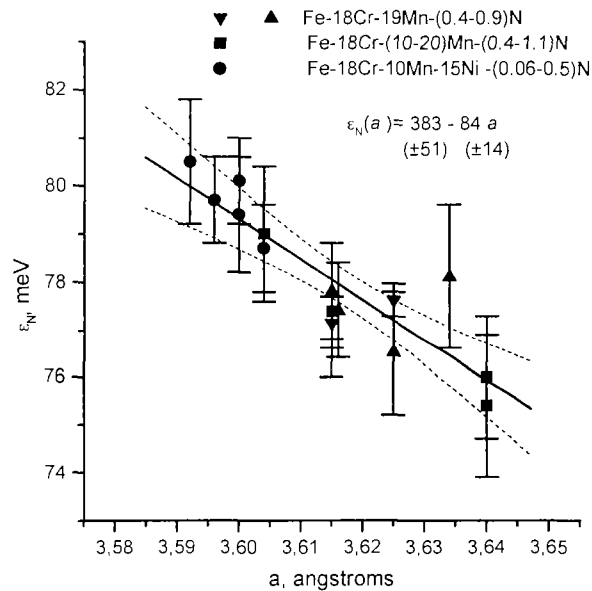


Fig. 1. Nitrogen atom frequency vs. lattice parameter

References

1. S.Danilkin, A.Beskrovni, E.Jadrowski: Nitrogen Effect on the Lattice Dynamics of FCC Fe-Cr-Mn(Ni) Austenitic Alloys, Materials Science Forum, 1999, v. 318-320, p. 19-24.
2. Neutron Experimental Facilities at JINR, User Guide, Frank laboratory of Neutron Physics, Joint Institute for Nuclear Research, Dubna, 1992.
3. S.Lin, H.Ledbetter Materials Science and Engineering, 1993, v. A161, p. 81.

Low-Frequency Excitations in Zirconium Hydrides

*A.Radulescu**, *I.Padureanu**, *S.N.Rapeanu**, *A.Beldiman**, *Zh.A.Kozlov***,
V.A.Semenov

** National Institute of Physics and Nuclear Engineering - Horia Hulubei,
PO Box MG-6, 76900 Bucharest (Magurele), Romania*

*** Joint Institute of Nuclear Research, 141980 Dubna, Russia*

The inelastic neutron scattering investigations were carried out on ZrH_x systems with $x= 0.38, 0.52$ and 0.80 [1] by means of the DIN-2PI time-of-flight spectrometer installed at the IBR-2 pulsed reactor of JINR-Dubna. The samples including both the disordered solid-solution of H in α -HCP Zr and the ordered γ -hydride with a FCO Zr lattice were polycrystalline powders. The experimental $S(Q,\epsilon)$ in the range of low energies measured at scattering $\theta=32^\circ$ is shown in Fig. 1. As it is seen all the spectra exhibit a sharp feature located around 15 meV and a broader one around 25 meV. Other features whose presence becomes weaker at higher H content are also observed around 11 meV and 18 meV.

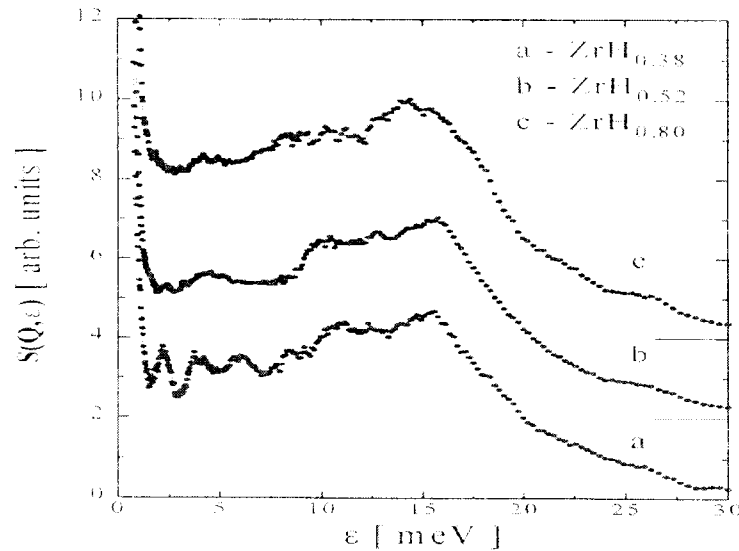


Fig. 1. The scattering function $S(Q,\epsilon)$ of ZrH_x measured at the scattering angle $\theta=32^\circ$.

In addition to the expected spectral components located in the range of acoustic vibrations of Zr atoms in various regular lattices of the samples other unexpected features are also revealed at low energies, between 2-10 meV. For $ZrH_{0.38}$ these features show a good resolved fine structure as peaks at 2.5 meV and 6 meV while for increasing H content this structure becomes much less evident. An analysis of the generalized vibrational density of states (GVDS) spectra in parallel with that of metallic Zr [2] (Fig.2) allowed to give an interpretation to the peaks located at energies higher than 10 meV. The latter one are identified as Zr acoustic vibrations both in a HCP lattice (those located at 11 and 18 meV) and in a FCO one (those located at 15 and 25 meV). The new features revealed in $S(Q,\epsilon)$ spectra at energies lower than 10 meV can not be assigned to the lattice vibrations. However, their dependence of the H content is an evidence of excitations undoubtedly related to H dynamics. A such low energy H dynamics is represented either by tunnelling or resonant modes. These are typical for H

dissolved in metals as it was theoretically shown for resonances in H-(V, Nb, Ta and Pd) systems [3] and for tunnelling effects in H(D)-(Zr, Hf) systems [4].

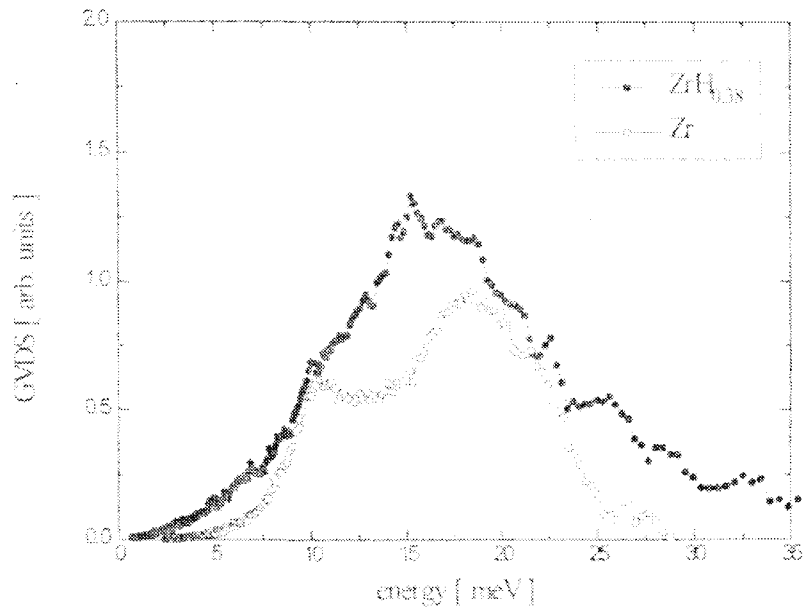


Fig. 2. GVDS for $ZrH_{0.38}$ compared with that for α -Zr.

References

1. A.Radulescu, I.Padureanu, S.N.Rapeanu, A.Beldiman, Zh.A.Kozlov, V.A.Semenov, Preprint JINR, E14-99-165.
2. A.Radulescu, I.Padureanu, S.N.Rapeanu and A.Beldiman, Phys. Stat. Sol.(b), in press (1999).
3. V.Lottner, H.R.Schober and W.J.Fitzgerald, Phys. Rev. Lett., 42(1979)1162.
4. S.L.Drechsler, G.M.Vujicic and N.M.Plakida, J. Phys. F: Met. Phys., 14(1984)L243.

Low-Frequency Collective Modes in the Superionic Phase of Lead Fluoride

A. Radulescu¹, I. Padureanu¹, S.N. Rapeanu¹, A. Beldiman¹, M. Ion¹, Zh.A. Kozlov², V.A. Semenov

¹*Institute of Physics and Nuclear Engineering-Horia Hulubei, Bucharest 76900, Romania*

²*Joint Institute of Nuclear Research, 141980 Dubna, Russia*

The dynamic structure factor $S(Q, \omega)$ for fluoride PbF_2 in the normal and the superionic states at $T = 293$ and 823 K has been investigated by cold neutron scattering [1]. A particular interest in these compounds was stimulated because some fluorite like CaF_2 , SrCl_2 , BaF_2 , SrF_2 , and $\beta\text{-PbF}_2$ exhibit fast-ionic conduction or “superionicity” above characteristic temperatures T_c much below the melting temperatures T_m . The ionic conductivity of these compounds increases exponentially with temperature from values smaller than $1 \Omega^{-1}\text{m}^{-1}$, which are typical for normal ionic solids, to a value of about $100 \Omega^{-1}\text{m}^{-1}$ comparable to those of ionic melts [2,3]. This high increase is accompanied by a fast increase in heat content, also at T_c [4,5]. It has been generally stated that the rising in the ionic conductivity and heat content are attributed to the development of a superionic phase at temperature above T_c with a thermally activated dynamic disorder in anion sublattices.

At present, according to the large volume of existing data, it seems that the conduction mechanism as well as the dynamic behaviour of anion disorder responsible for the superionic conductivity are well understood. Nevertheless, some contradictions, both in the experimental and the theoretical results exist [6].

The conduction mechanism in these materials occurs through the mobility of the ions and, at normal temperatures this is due to the anionic Frenkel disorder. It has been stated that the anionic disorder must be also responsible for the conductivity in the superionic state. Both the superionic and low-temperature disorders are of the same kind but a special mechanism for the anion dynamic at high temperatures is involved. From the majority of previous studies it was concluded that a rather small fraction of anion was displaced from their regular sites, the fraction of true Frenkel defects being smaller. The high conductivity is result of the high mobility of these defects [7-10], the most important dynamic process being the diffusive motions.

Other results obtained so far contradict this general point of view. They consider that the difference between the superionic and the low-temperature disorders is one of degree, a massive disorder of the anion sublattice above T_c being assumed [11,12]. In this respect, the dynamics of the defects looks like that of the particles in a liquid where the distinction between their residence time and their flight time disappears, a sublattice melting point of view being sometimes used in association with the fast-ionic behaviour.

We consider that the fast ionic conduction mechanism via anionic diffusion defects, is not a fully elucidated problem yet. Some ion-transport mechanism [13] have not been investigated enough. A specific behaviour of the elastic constants of lead fluoride in contrast with other of fluorite has been reported when temperature is being raised above T_c [8]. In order to give some insight into the diffusion mechanism in the wave vector and energy transfer ($\mathbf{Q}, \hbar\omega$) space, new investigations will be necessary. A direct proof of the diffusive mechanism in such disordered systems is provided by the investigation of the neutron quasielastic spectrum in the small energy transfers region.

Because of the insufficient investigation of PbF_2 in the range of \mathbf{Q} space up to 2 \AA^{-1} we performed an analysis on this compound by quasielastic cold neutron scattering at the DIN-2PI time-of-flight spectrometer set up at the IBR-2 fast-pulsed reactor from JINR-Dubna. The sample of a polycrystalline lead fluoride was analysed under normal and superionic state at $T = 823 \text{ K}$. An incident neutron wave-length of 5.358 \AA allowed us to perform measurements in a range of scattering vectors $0.2 \leq |\mathbf{Q}| \leq 2.15 \text{ \AA}^{-1}$ with a better resolution than the previous quasielastic neutron-scattering investigations of this compound. The energy resolution $\Delta E = 0.148 \text{ meV}$ (full width at half maximum) was measured by means of vanadium. Thirteen batteries of He-detectors were used to detect the neutron spectra at various angles between 9° - 134° .

For a fully coherent scatterer like PbF_2 , the double differential cross section is related to the dynamic structure factor $S(\mathbf{Q}, \omega)$ through the relation

$$\frac{d^2 \sigma}{d\Omega dE'} = N \frac{k'}{k} \frac{1}{4\pi} \sigma_c S(\mathbf{Q}, \omega) \quad (1)$$

where N is the number of particles in target systems, E' is the final energy of the neutrons, σ_c is the bound nucleus coherent scattering cross section and the c index denotes the coherent scattering process with $\hbar\mathbf{Q} = \hbar(\mathbf{k} - \mathbf{k}')$ the momentum transfer, and $\hbar\omega$ the energy transfer. The results obtained in uniform energy scale from the corrected time-of-flight spectra were interpolated at constant wave-vector transfer \mathbf{Q} as function of energy transfer $\hbar\omega$ (Fig. 1).

In the superionic state $S(\mathbf{Q}, \omega)$ at constant wave-vector transfers reveals symmetrical peaks at $\sim \pm 0.5 \text{ meV}$ in the \mathbf{Q} -space range 1.55 - 2.05 \AA^{-1} . This structure is similar to the long-wavelength collective excitations (Brillouin doublet) specific to some liquid metals. Such an observation could support the idea of liquid-like behaviour at the level of the anion sublattice in the superionic state. However, the energies of these excitations are about one order of magnitude smaller and the corresponding \mathbf{Q} values are rather high compared to those of the collective modes observed in the simple classical liquids. Therefore these excitations are of different nature from those characteristic for a classical liquid [14,15].

The results of this study lead to the conclusion that a strong correlation between the superionic transition and the low-frequency dynamics exists, raising new questions that may imply a new interest in the microscopic processes associated with the superionic transition.

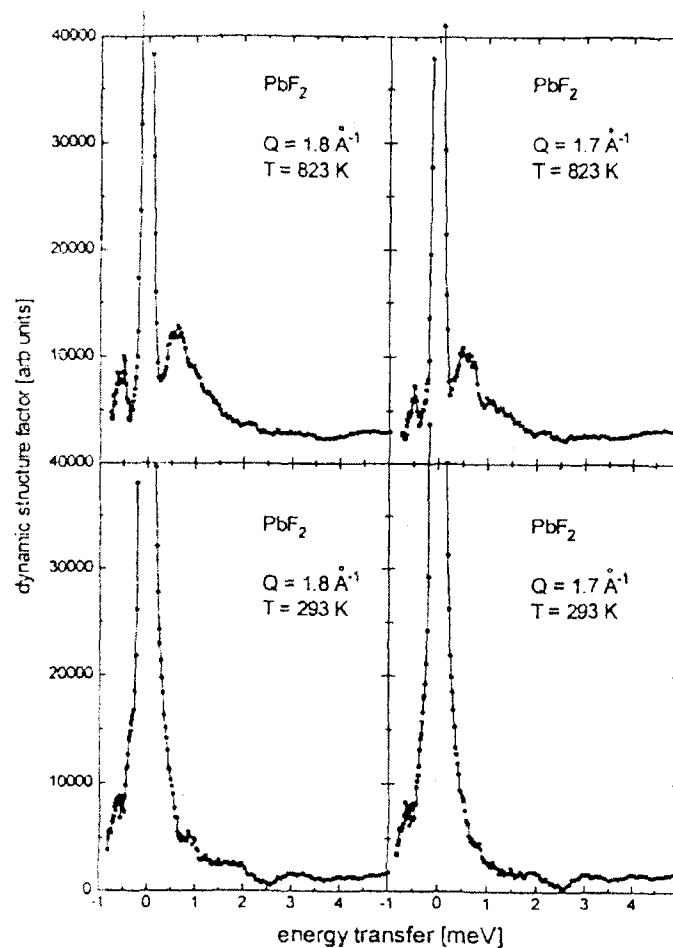


Fig. 1. Dynamic structure factor of PbF_2 at $T=823$ and 293 K as a function of the energy transfer for two values of Q .

References

1. A.Radulescu, I.Padureanu, S.N.Rapeanu, A.Beldiman, M.Ion, Zh.A.Kozlov, V.A.Semenov, Phys. Rev. B59(1999)3270.
2. C.E.Derrington and M.O'Keefe, Nature (London), Phys.Sci. 246(1973)44.
3. V.M.Carr, A.V.Chadwick, and R.Saghafian, J. Phys. C11(1978)L637.
4. C.E.Derrington, A.Navrotsky, and M.O'Keefe, Solid State Commun. 18(1976)47.
5. A.S.Dworkin and M.A.Bredig, J. Phys.Chem. 72(1968)1277.
6. M.T.Hutchings, K.Clausen, M.H.Dickens, W.Hayes, J.K.Kjems, P.G.Schnabel, and C.Smith, J. Phys. C17(1984)3903.
7. M.J.Gillan and D.D.Richardson, J. Phys. C13(1979)L61.
8. C.R.A.Catlow, J.D.Comins, F.A.Germano, R.T.Harley, and W.Hayes, J. Phys. C11(1978)3197.
9. M.H.Dickens, W.Hayes, M.T.Hutchings, and C.Smith, J. Phys. C12(1979)L97.
10. M.Dixon and M.J.Gillan, J. Phys. C11(1978)165.
11. M.O'Keefe, Comments Solid State Phys. 7(1977)163.
12. A.Rahman, J. Chem. Phys. 65(1976)4845.
13. C.R.A.Catlow, M.J.Norget and T.A.Ross, J. Phys. C10(1977)1627.
14. R.D.Copley and J.R.Rowe, Phys. Rev. A9(1974)1656.
15. I.Padureanu and S.N.Rapeanu, Rom. J. Phys. 40(1995)1047.

Local Polaritons of New Type on Interface of Girotropic Enantiomorphous Crystals

O.A.Dubovsky, A.V.Orlov

Investigation of excitons and vibrations localized on crystals defects – such as admixture, vacancy, dislocation or a boundary of crystal – attract attention in view of possibility their technological utilization in different optical devices. Corresponding wave functions of local exciton and phonon states of different types as a rule uniformly diminish with a distance from defect and a local state radius usually essentially exceeded lattice constant (Ref.1). In Ref.[2] was found local polaritons (LP) of a new type, extending along interface of clockwise and counterclockwise rotating crystals. The existence of this LP is connected with a space dispersion effect and they possess a number of unusual peculiarities in behavior of dispersion curves and parameters of space attenuation. This LP was found for crystals C_{2v} and D_{2d} classes only. A system of contacting clockwise and counterclockwise rotating 1D crystals is investigated in a given article. A real systems of that type may be girotropic polymeric and biological chains, which are investigated in a number of work (Ref.3). A LP state of a new type was found. This LP state have strongly oscillating and space decreasing wave function and local state term splitting from unlocalized states zone. It is seen from the obtained results, that LP of the same type, as in [2] and in present article, can exist not only in crystals of C_{2v} and D_{2d} crystal groups, but in crystals of other groups also.

Crystal chain of normally to axes oriented dipole oscillators is presented in inset of Fig.1. This crystal possess counterclockwise rotating in a region of cite numbers $n < 0$ and clockwise rotating in a region $n > 0$. Central oscillator, separating regions of clockwise and counterclockwise rotating, correspond $n = 0$. The following system of secular equations was found for wave functions Ψ_n of symmetric polariton states $\Psi_n = \Psi_{-n}$ with the energy $\hbar\omega$

$$\begin{aligned} (\omega^2 - \omega_0^2)\Psi_n = \frac{2\omega_0|\mathbf{P}|^2}{\hbar a^3} \sum_{m \geq 0} \left[(1 - \delta_{nm})\phi(\omega, (n - m)) + \right. \\ \left. + (1 - \delta_{m0})\phi(\omega, (n + m)) \right] \cos\left(\frac{2\pi}{3}|n - m|\right)\Psi_m ; \end{aligned} \quad (1a)$$

$$\phi(\omega, |n \pm m|) = \left[\frac{1}{|n \pm m|^3} - i \frac{((\omega/c)a)}{|n \pm m|^2} - \frac{((\omega/c)a)^2}{|n \pm m|} \right] \exp\left[i \left(\frac{\omega}{c} a \right) |n \pm m| \right]; \quad (1b)$$

$$0 \leq n \leq N.$$

In (1) ω_0 – dipole transition frequency of individual molecule, \mathbf{P} – corresponding matrix element of dipole momentum operator, a – chain constant, $2N+1$ – a number of cites. Then diagonalization of matrix, corresponding system (1), was carried out. The value of optic parameter $(\omega_0 c/a)$ was supposed to be equal to ordinary value for different crystals $(\omega_0 c/a) = 10^{-3}$. As a result polariton frequency ω'_l and attenuation ω''_l in units $V \equiv |\mathbf{P}|^2 / a^3$ was obtained. Also was obtained its wave function $\Psi_n = \Psi_{n'} + i\Psi_{n''}$.

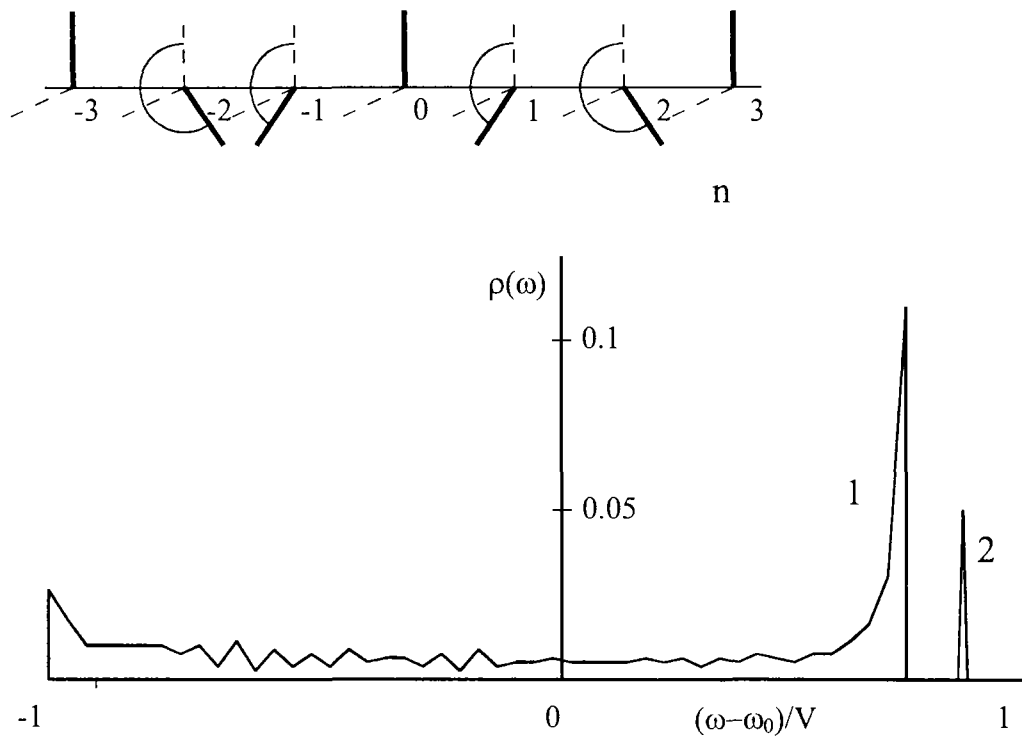


Fig.1. Polariton density of states of contacting enantiomorphous crystals

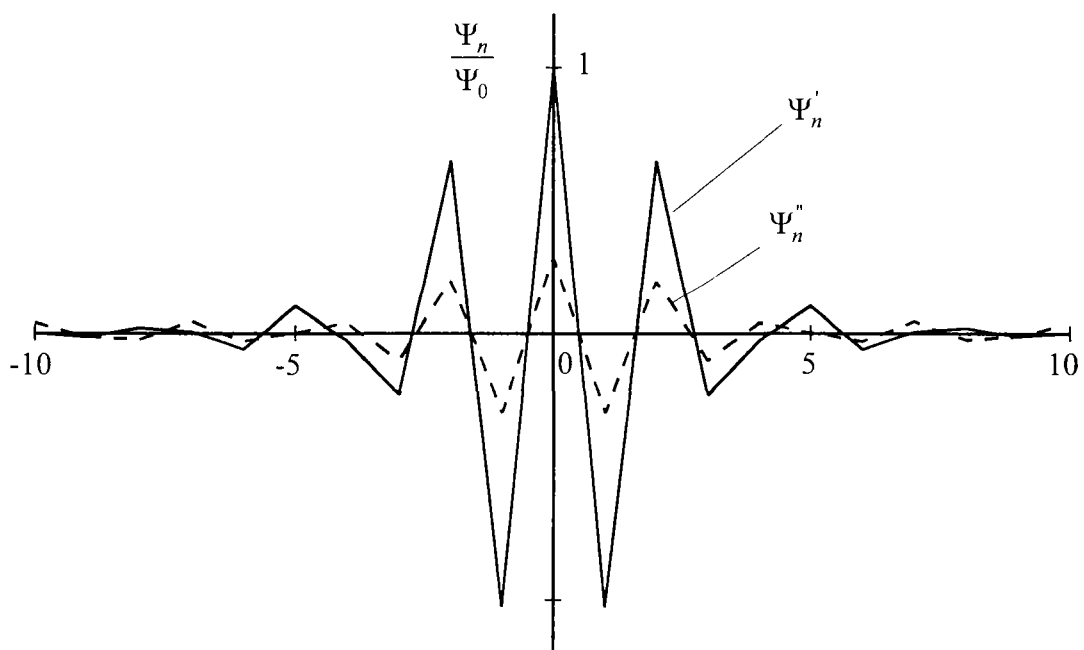


Fig.2. Space dependence of wave function of LP. Solid line – real part, shaded line – image part

Fig.1 represent plot of polariton density of states in a chain, consisting of 801 sites. Curve 1 – zone of unlocalized states. Peak 2 – term of LP. It split from upper boundary of unlocalized zone on a value $0.12|\mathbf{P}|^2/a^3$.

Fig.2 represent wave function of LP $\Psi_n^{(l)} = \Psi_n^{(l)'} + \Psi_n^{(l)''}$. It is seen, that real part $\Psi_n^{(l)'}$ (solid line) possess valuable oscillations with sign altering on the lattice constant length in the vicinity of interface, and this length increase with removing from interface. Wave function attenuates on the length $\sim 10a$. Imaginary part $\Psi_n^{(l)''}$ (shaded line) is enlarged on Fig.2 in 10^7 times and obey the same attenuation and oscillations.

References

1. V.M.Agranovich, O.A.Dubovsky. Optical Properties of Mixed Crystals. North-Holland, Amsterdam (1988). P.297.
2. V.M.Agranovich, O.A.Dubovsky. Fizika Tverdogo Tela **20**, 11, 3237 (1978).
3. W.Moffitt. J. Chem. Phys. **23**, 1, 467 (1956).

2.6 MATHEMATICAL MODELING

Numerical Benchmark for Calculation of Convective Heat Transfer During Crystal Growth by the Floating Zone Method Under the Null Gravity Conditions

V.K. Artemiev, V.P. Ginkin, T.M. Lukhanova, V.I. Folomeev

A numerical test is proposed for verification of convection heat transfer calculation codes in two-dimensional cylindrical geometry. Such geometry is typical for crystal growth by the floating zone method. Dimensions, boundary conditions and thermal characteristics used in the test correspond to real data from space experiments for Ge crystal growth. The Navier-Stokes equations are solved for velocities, pressure and energy in the melt region. A nonuniform temperature profile causing Marangoni thermal capillary convection at the free surface of the melting zone is prescribed.

The region of calculation is a finite cylinder with the diameter-to-height ratio equal to one (Fig.1).

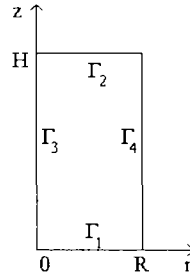


Fig.1. The region of calculation: $R=0,5$ cm, $H=1$ cm

The Navier-Stokes and energy equations are solved in the region of calculation:

$$\begin{aligned} \frac{\partial V_r}{\partial t} + V_r \frac{\partial V_r}{\partial r} + V_z \frac{\partial V_r}{\partial z} &= -\frac{1}{\rho} \frac{\partial P}{\partial r} + \nu \left(\frac{1}{r} \frac{\partial}{\partial r} r \frac{\partial V_r}{\partial r} + \frac{\partial^2 V_r}{\partial z^2} - \frac{V_r}{r^2} \right) \\ \frac{\partial V_z}{\partial t} + V_r \frac{\partial V_z}{\partial r} + V_z \frac{\partial V_z}{\partial z} &= -\frac{1}{\rho} \frac{\partial P}{\partial z} + \nu \left(\frac{1}{r} \frac{\partial}{\partial r} r \frac{\partial V_z}{\partial r} + \frac{\partial^2 V_z}{\partial z^2} \right) \\ \frac{1}{r} \frac{\partial}{\partial r} (r V_r) + \frac{\partial V_z}{\partial z} &= 0 \\ \rho c_p \left(\frac{\partial T}{\partial t} + V_r \frac{\partial T}{\partial r} + V_z \frac{\partial T}{\partial z} \right) &= \lambda \left(\frac{1}{r} \frac{\partial}{\partial r} r \frac{\partial T}{\partial r} + \frac{\partial^2 T}{\partial z^2} \right) \end{aligned}$$

The boundary conditions are as following:

$$\begin{cases} \text{on } \Gamma_1 : T = T_{\text{melt}} , & V_r = V_z = 0; \\ \text{on } \Gamma_2 : T = T_{\text{melt}} , & V_r = V_z = 0; \\ \text{on } \Gamma_3 : \frac{\partial T}{\partial r} = \frac{\partial V_r}{\partial r} = \frac{\partial V_z}{\partial r} = 0 ; \\ \text{on } \Gamma_4 : T = \Delta T \exp \left(-A \left(z - \frac{H}{2} \right)^2 \right); V_r = 0; \frac{\partial V_z}{\partial r} = \frac{\partial \sigma}{\partial T} \frac{\partial T}{\partial z} , \end{cases}$$

where ΔT – maximal temperature drop at the Γ_4 boundary; $A = - (H/2)^{-2} \ln(T_{\text{melt}} / \Delta T)$.

This model problem is similar to a real one of thermal capillary convection calculation in a facility where Ge-crystals are grown under the null gravity conditions by the floating zone method. For the sake of simplicity the melt/crystal interfaces Γ_1 and Γ_2 are chosen to be flat and parallel, however the model accounts for all principal features of the problem.

The region of calculation is divided into nonuniform meshes by lines parallel to the coordinate axes (Fig.1). The mesh nodes for temperature and pressure were located at the centres of meshes, for radial velocity V_r – at the middle of the mesh boundaries in r direction and for axial velocity V_z – at the middle of the mesh boundaries in z direction.

The model problem was solved in natural variables by two independent codes **FLUID2D** and **VT-2D** created by different authors. The **FLUID2D** code uses monotonous balance neutral finite difference schemes and the implicit method of stabilisation for solving the non-linear Navier-Stokes equations. The linearized difference equations are solved by an explicit incomplete factorization method, and a method with Chebyshev acceleration is used for solving the self-adjoint pressure equation. In more details, this numerical technique is presented in [2].

VT-2D code applies Buleev-Timukhin approximations [3]. The Seidel method and the minimal iteration method with preliminary preconditioning by N.I.Buleev's incomplete factorization method are used for solving linear equation systems.

Besides, the energy equation is solved using temperature variable in **FLUID2D** and enthalpy variable in **VT-2D**. **FLUID2D** code defines the stabilised solution using the following criterion: the input heat power coming through the free surface equals to the output power going out the butt-ends with 0.01% accuracy. The velocity field should satisfy $\left\| \operatorname{div} \vec{V} \right\|_h < \varepsilon$ where ε is a beforehand given accuracy (for dimensionless variables usually $\varepsilon \leq 5 \cdot 10^{-4}$).

To compare results of the codes **FLUID2D** and **VT-2D**, calculations were carried out on identical grids with uniform meshes in both directions of the calculation domain. The results obtained by **FLUID2D** and **VT-2D** codes show a good agreement.

After that, calculations using **FLUID2D** were made on a succession of nonuniform (corresponding to a logarithm law near the boundaries of the domain) grids with a proportional node number increase in both directions. A minimal value of the step h_{\min} near the boundaries was set, and then the grids with the logarithmic thickening were generated.

The results of the calculations are listed in Table 1 that includes the maximal absolute values of the radial $|\bar{v}_r|$ and axial $|\bar{v}_z|$ components of velocities, the maximal absolute values of the full velocity $|\bar{v}|$, and the maximal absolute values of velocity extrapolated to the side boundary of the domain $|\bar{v}|_{\text{extr}}$.

These data show that the solution is stabilized for $h_{\min} = 0.3125 \times 10^{-5} \text{ m}$. In this case the maximal absolute values of velocity is equal 4,3 cm/s. In Fig.2 the isotherm fields are presented for $\Delta T = 5^\circ$. In Fig.3 the isolines of the absolute values of velocity $v = \sqrt{v_r^2 + v_z^2}$ corresponding to this variant are plotted. The performed calculations show that it is necessary to describe elaborately the solution in the near-boundary layers of the melt to obtain this solution with an acceptable accuracy. Therefore when the finite-difference approach is used, a significant number of meshes and a strong thickening of the grids near the boundaries of the domain are required.

Table 1. Grid 100×200 (N_r=100)

$h_{min} / 10^{-5} M$	Max $ \vec{V} $ cm/s	Max $ \vec{V}_r $ r=R/2 cm/s	Max $ \vec{V}_r $ cm/s	Max $ \vec{V}_z $ cm/s	Max $ \vec{V} $ extr. cm/s
5	3.8	1.6	2.6	3.8	4.2
5	3.8	1.6	2.6	3.8	4.2
2.5	4.1	1.7	2.8	4.1	4.4
1.25	4.2	1.7	2.9	4.2	4.4
0.625	4.3	1.6	2.9	4.3	4.4
0.3125	4.3	1.6	2.8	4.3	4.3

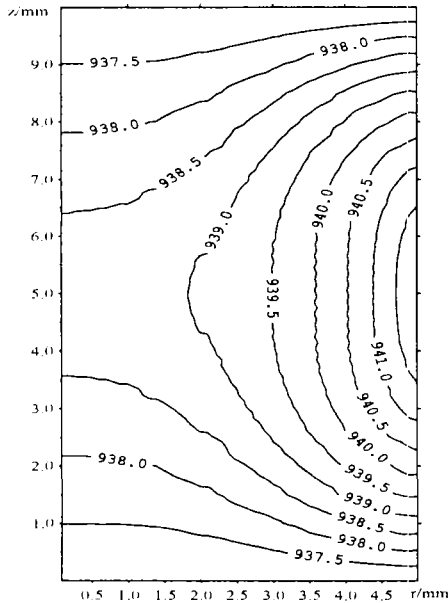


Fig. 2. The temperature distribution for $\Delta T=5^\circ$

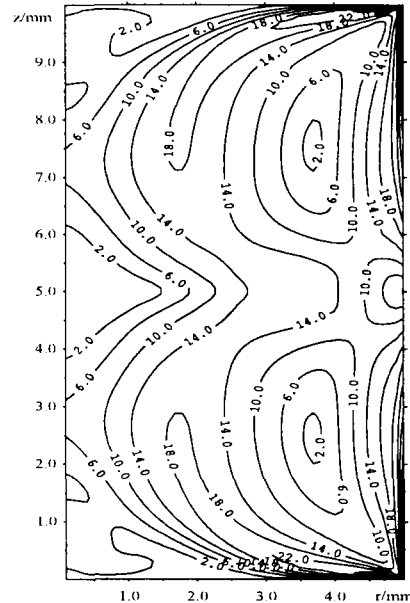


Fig. 3. The velocity distribution for $\Delta T=5^\circ$

Conclusions

The performed calculations show a satisfactory agreement in results obtained by **FLUID2D** and **VT-2D** codes. The described model problem and its solution form the first simplest test for verification of two-dimensional codes calculating convection heat transfer under the influence of Marangoni thermal capillary forces. The mathematical problem formulated is similar to the real problem of crystal growth by the floating zone method in the space. The analysis performed demonstrates that to provide an appropriate accuracy of numerical results, one has to describe thoroughly near to boundary layers in the melt. When applying a finite-difference approach, one has to carry out calculations with a large number of meshes and use a strong grid thickening at the boundaries of the calculation domain.

References

1. G.Chen, B.Roux, D.Camel, P.Tison, G.P.Garandet, J.J.Favier, A.S.Senchenkov, R.Moreau, 1994, Numerical Study of GEZON Experiment, *Microgravity Sci. Techn.*, v.7/2, pp.120-123.
2. V.K.Artemyev, 1992, An implicit method for the solution of the Navier-Stokes equations in natural variables, *Modelling in mechanics*, Novosibirsk, vol.6 (23), № 1, pp.17-22.
3. N.I.Buleev, G.I.Timukhin, 1972, On the construction of the finite difference equations for incompressible fluid flow equations, *Numerical methods in mechanics*, Novosibirsk, vol.3, №4, pp.19-26.

The Numerical and Experimental Study of the Bridgman Crystal Growth on a Model Devic

*V.K. Artemyev, V.P. Ginkin, N.V. Gusev
N.A. Verezub¹, A.Z. Mjal'dun¹, A.I. Prostromolotov¹*

¹*Institute for Problems in Mechanics RAS, Russia*

The processes of convection heat transfer in a cylindrical ampoule with NaNO₃ melt, undergoing crystallization by Bridgman method, is investigated by methods of physical and mathematical modeling. The calculations on mathematical model are carried out on the basis of previously measured temperature distributions on the borders of the ampoule. The results of measurements of the temperature field in the volume with melt are used for verification of the calculated data. It is shown that for agreement of the calculated results with the measured data, the mathematical model should take into account thermocapillar convection at the NaNO₃ open melt surface. The results can be used for improvement of the numeric methods for modeling convection processes in volumetric crystallization conditions.

The experimental data of the temperature measurements allow to formulate the problem of conjugate heat transfer in the melt and in the ampoule wall. The scheme of the calculation domain is represented. The natural convection in the melt is described on assumption that the deviations of all thermodynamic parameters from their values, corresponding to conditions of a static equilibrium, are small. In this case, it is possible to approximately represent the density variation, causing flow as a result of interaction between the gravitational volumetric force and the gradient of hydrostatic pressure, as the influence of temperature, and the density change in the equation of continuity can be neglected (Boussinesq approximation). The crystallization front and the free surface of the melt are supposed to be flat.

Governing equations in the two-dimensional (r-z) - approximation in a dimensionless form are written as:

$$\nabla \vec{V} = 0, \quad (1.1)$$

$$\frac{\partial v_r}{\partial \tau} + v_r \frac{\partial v_r}{\partial r} + v_z \frac{\partial v_r}{\partial z} = - \frac{\partial p}{\partial r} + (\nabla^2 v_r - v_r / r^2) / \text{Re} \quad (1.2)$$

$$\frac{\partial v_z}{\partial \tau} + v_r \frac{\partial v_z}{\partial r} + v_z \frac{\partial v_z}{\partial z} = - \frac{\partial p}{\partial z} + \nabla^2 v_z / \text{Re} + \text{Gr} \theta / \text{Re}^2 \quad (1.3)$$

$$\frac{\partial \theta}{\partial \tau} + \vec{V} \nabla \theta = \nabla (\lambda \nabla \theta) / (\text{Pr Re}). \quad (1.4)$$

In the quartz wall of the ampoule, the heat conduction equation is solved:

$$\frac{\partial \theta}{\partial \tau} = a \nabla^2 \theta. \quad (1.5)$$

Here $\vec{V} = (v_r, v_z)$ - the velocity vector, p - pressure, $\theta = (T - T_0) / \Delta T$ - dimensionless temperature, $\Delta T = T_w - T_m$ - temperature difference between its maximum value on the ampoule surface and the melt temperature.

On the free surface of the melt ($z = H/L$), the profile of temperature $\theta = \Theta_u(r)$ and condition $\partial v_r / \partial z = 0$ or Marangoni condition

$$\frac{\partial v_r}{\partial n} = \frac{Ma}{RePr} \frac{\partial \theta}{\partial l},$$

where $Ma = -(\partial\sigma/\partial T)\Delta TL/\rho\nu\alpha$, Marangoni number, are set.

An implicit method for solving the Navier-Stokes equations in natural variables [1] modified with reference to the equations of thermal convection is used.

In the calculation domain, a grid with a logarithmic thickenings to the crystallization front, the free surface and the wall of the ampoule was used (Fig.1b). Usually 35 nodes (30 in the melt, 5 in the wall) were set on the radius and 60-on the height, the thickening was selected such that the first step at the wall was of the order 0.001 cm. The calculations with the number of nodes 53 (45 and 8) and 60 were made, and the difference from calculations with a greater number of nodes were insignificant.

The flow stabilization time makes 402 seconds. At the top of the melt, the circulating flow intensifies, and the maximum value of velocity achieves 0.84 cm/sec. This flow takes not only near-surface layers, but also penetrates deeply into the volume of fluid. At the crystallization front a weak secondary vortex arises, the velocity here is essentially less in comparison with that at the top of the domain. It should be noted that if Marangoni convection is absent, the maximum value of velocity decreases to 0.36 cm/sec. As a result, the influx of cold masses of the fluid begins to diminish at the near-crystal zone and the fluid at the top becomes more heated. The structure of the temperature field at the bottom of the domain is similar both when accounting for and when disregarding Marangoni convection (Fig. 1a and b). At $z \geq 1.0$ cm there are differences due to the thermocapillar convection influence.

Numerical results and experimental data are in a satisfactory agreement. The above analysis has shown that the experimental data and numerical results agree best in the case of the melt height $H=4.3$ cm, thus providing the basis for a test problem (benchmark) for verification of programs simulating gravitational and thermocapillar convection during crystal growth by the vertical Bridgman method.

The experimental data and numerical results for the vertical Bridgman method have demonstrated that a steady thermal stratification is observed when the temperature distribution is not monotonic (on 1/3 of the height for the experiment considered) on the side wall of the ampoule.

The temperature differences on the free surface cause an intensive thermocapillar convection which increases the maximum flow rate, intensifies essentially the heat transfer and reduces warm-up of fluid at the top of the melt.

The above analysis has shown that the experimental data and numerical results agree best for the melt height $H=4.3$ cm, thus providing the basis for a test problem (benchmark) for verification of programs simulating gravitational and thermocapillar convection during crystal growth by the vertical Bridgman method.

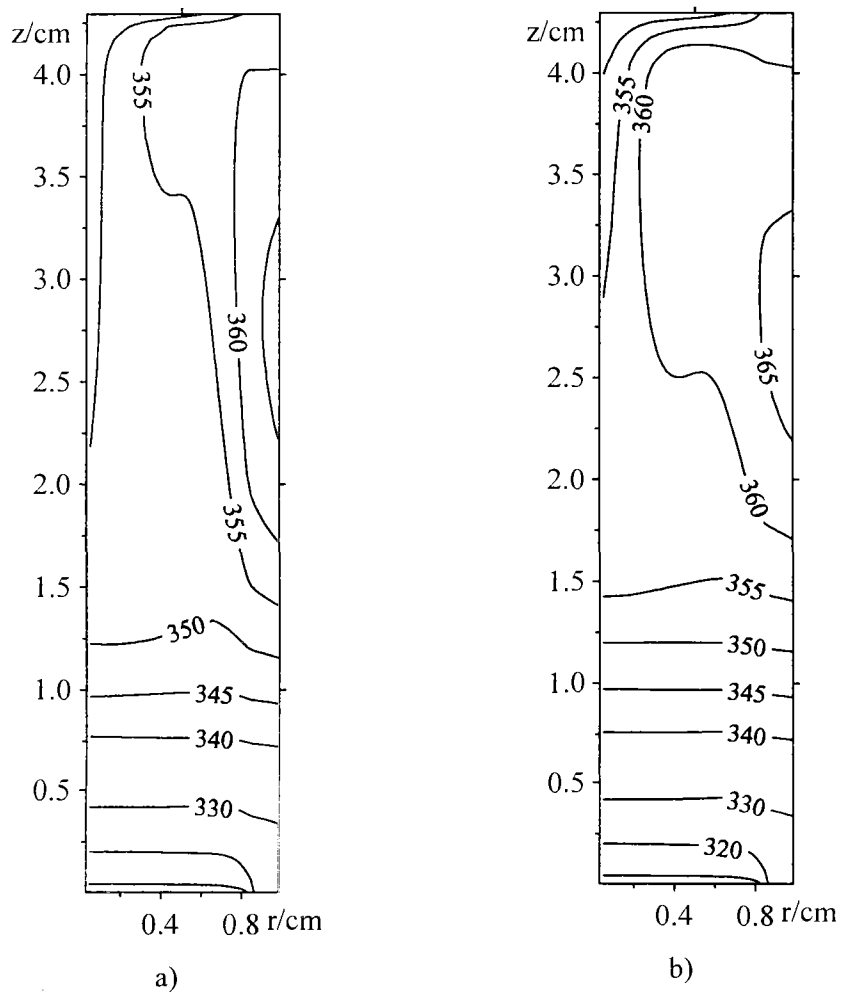


Fig.1. Temperature contours accounting for (a) and disregarding (b) Marangoni convection

Reference

1. V.K.Artemyev, 1992, An implicit method for a solution of the equations Navier-Stokes in natural variables, *Modeling in mechanics*, Novosibirsk, vol.6(23), №1, pp.17-22.

Mathematical Software Development and Numerical Investigation of Heterogeneous Effects in Fast Critical Assemblies and Reactors

A.A. Bezborodov

The aim of the work carried out [1] was: high-processed deterministic numerical methods development, mathematical software creation, numerical investigations of heterogeneous effects in fast critical assemblies and reactors, experimental data using for neutron cross-sections correction of groups constants sets and fast critical assemblies and reactors neutron-physics calculations provision by reactor codes. The main results were:

1. Macro-subgroup numerical method was developed to solve neutron transport equation by deterministic methods (DSn for integro-differential equation and first-flight collision probabilities for integral one) in heterogeneous medium. Given algorithm allows to use the traditional group method in eigenvalue problem. It takes account of resonance heterogeneous effects correctly.
2. Effective method for integral equations system solving with full or declarative consideration of arbitrary neutron subgroups amount in group energy range has been developed.
3. Using a collision probability technique (FFCP) and so called self-scattering reduction scheme (SSRS), direct solution of the above-mentioned system have been gotten. It has a fast convergence.
4. Heterogeneous corrections to wide range of the experimental data on fast critical assemblies with $K_{\infty} \approx 1$ and with complex core structures have been evaluated. This ones have been included in data base LEMEX (macroscopic experiment evaluations). It first was established that resonance heterogeneity effects in home fast critical assemblies may be great: more than 3% in K_{∞} for the KBR-11, KBR-12 fast assemblies. Until recently similar effect was in the German fast assembly SNEAK-5.
5. Numerical investigations have shown that pin's and cassette's heterogeneity has essential influence on the integral characteristics of the BN-800 reactor type model: $\sim 0.26\%$ in K_{eff} .
6. There is essential resonance boundary effect in nuclear reactor cores with reflectors consist of construction materials. The ordinary multigroup calculations may distort K_{eff} of such reactors strongly: $\sim 4.5\%$ for ZPR-III-54 fast critical assembly. Developed subgroup technique in combine with DSn and collision probability methods allows to estimate such effects with high assurance. Up date one could do it by means of Monte-Carlo method only.
7. Boundary resonance effects and resonance heterogeneity have been investigated in the BN-1600 fast reactor type model with heterogeneous core. They don't render considerable influence on main neutron-physics reactor parameters. This calculation technique enables boundary resonance effects to be evaluated with great precision. It can be done for fast reactors of different type. And considerable boundary resonance effects may be in fast reactors with soft neutron spectrum.
8. FFCP and others computer codes were developed for this computational techniques realization. Some of them were included in constant provision systems.

Reference

1. A.A.Bezborodov. Mathematical software development and numerical investigation of hetero-geneous effects in fast critical assemblies and reactors. Cand. thesis, IPPE, Obninsk, 1999.

The TAPIA3 Code Describing the Physical Processes Governing the Progression of Core Meltdown Accidents

G.A. Mjakishev, I.M. Bondarenko, A.I. Koval, A.A. Izotov, O.M. Naumenko

Following the accident at Three Mile Island Unit №2, interest in the analysis of the phenomena of severe accidents increased significantly. In early 1980, a number of industrial groups as well as national laboratories of USA were provided developmental versions of the MARCH code. Then the MELCOR code was released. The MARCH code attempts to treat a large number of complex and interrelated physical phenomena. Some of these phenomena are well understood and others are not (and may never be). In some cases the models used are simplification of the actual processes, either because experimental data are lacking to provide the level of understanding necessary to improve the model or because the priority for funding in the past did not justify the effort. In using the MARCH code for a variety of applications, a number of limitations of the code (ranging from lack of treatment of some important phenomena to unnecessary simplification, as well as some errors) have been identified; consequently, a number of ad hoc versions of the code were developed by individual users. Future efforts in this area are associated with the further development of an improved code.

The TAPIA3 code describes the response of water-cooled reactor systems to accidents which because of failures in engineered safety features, lead to core meltdown. The code performs the calculations from the time of accident initiation through the stages of coolant blow down and boil off, and core heat up and meltdown. Engineered safety features are modeled include emergency core cooling systems and spray heat exchangers. Effects of metal-water reactions are considered. The code attempts to treat a larger number of complex and interrelated physical phenomena. The all phenomena are treated in a selfconsistent manner within the assumptions and approximations inherent in the code. A major effort was undertaken to improve the transportability of the code between various computer systems. This is reflected in the use of FORTRAN-77 as well as improved modularity in the coding and the division of the major subroutines. The code consists of several major subroutines together with a large number of supporting subroutines and functions.

The Analytical Solution to the Linear System of Point Reactor Kinetics Equations when the Reactivity is an Arbitrary Function of Time

D.M. Babanakov

The paper presents the analytical solution to the linear system of point reactor kinetics equations with one group of delayed neutrons and the reactivity approximated by an arbitrary smooth function of time. The analytical solution is written as a sum of exponents according to an approach, which can be interpreted as a generalization of the full eigenvalue problem, proposed in [1]. To obtain the solution, an asymptotic series in a small parameter is constructed. Numerical results to show a fast convergence of the series are discussed. A case of the reactivity linearly dependent on time is considered. Using the quasistationary derivative method [2], the analytical solution is obtained in the form of an explicit time dependence expressed as a combination of elementary functions. The closed form of the solution can be used to make a benchmark in the field of reactor kinetics.

References

1. D.M.Babanakov, I.R.Suslov, "The analytical solution to systems of ordinary differential equations with time-dependent coefficients", the Journal of mathematical modeling, vol.9, №8, Moscow, 1997.
2. Yu.V.Rakitski i dr. "Chislennyye metody resheniya zhestkikh sistem", M., 1979.

Spatial and Time-Dependent Calculation of Fast Reactor Transients

*A.A. Bezborodov, A.V. Volkov, S.M. Ganina, V.P. Ginkin,
I.A. Kuznetsov, N.M. Troyanova, Yu.E. Shvetsov*

The GVA code complex was developed in the State Research Center - Obninsk Institute of Physics and Power Engineering for the calculation of spatial-dependent transients in fast reactors. This code complex is based on three independent codes, namely:

- GRIF-SM code for three-dimensional thermal hydraulics calculation of BN-like reactors with possibility to take into account two phases of sodium state;
- VOLNA code for three-dimensional Hex-Z calculation of reactor dynamics in multigroup diffusion quasi-static approximation;
- ARAMACO code for homogenized multigroup cross-sections preparation using typical fast reactor neutron spectrum.

The joining of these codes in one code complex allows to solve the main task - the direct numerical simulation of spatial and time-dependent behavior of reactor core parameters under accidental conditions. As primarily faults can be considered such events like the main coolant pump stopping and spontaneous movement of control rods.

Now the initial stage of accident can be only calculated by the GVA code complex when the fuel melting and destroying of reactor core do not occur. However there is no limitations to expand this approach for next stages of accident when the material replacement takes place. Moreover we suppose that the quasi-static approximation is the only acceptable and practicable for detail and complex description of accidents, which cause fuel melting and fuel assemblies destroying.

The GRIF-SM code solves the transient system of mass, impulse and energy conservation equations in the frame of porous body and the porosity, penetrability and other coefficients are the function versus spatial coordinates. Such approach permits to describe the boiling of sodium and its condensation in the upper part of reactor and to take into account the hydraulics interference of core channels. The input data of GRIF-SM are the spatial power distributions at each time moment. The output data are spatial distributions of pressure, coolant's velocity and density, temperatures of fuel, cladding, coolant and other materials.

The VOLNA code solves the spatial and time-dependent neutron transport equation in the diffusion approximation. The quasi-static approach of solution is applied in this code when the original equation is identically transformed to the system of two equations, one for spatial and time-dependent shape function $\psi(r,t)$ and another one for time-dependent only amplify factor $P(t)$. The equation for $P(t)$ is similar to point kinetics equation and the $P(t)$ factor can be interpreted as reactor power. The neutron flux is the production of shape function by amplify factor.

The important feature of quasi-static approach is the possibility to use two different time mesh steps. The shape function $\psi(r,t)$ is recalculated with big time step and the amplify factor $P(t)$ is recalculated with small time step.

The input data for VOLNA code are spatial distributions of cross-sections at each time moment and the velocities of control rods movement. These velocities are used indirectly, the code calculates the location of moving control rods ends and finds the averaged by volumes cross-sections in the cells containing these ends.

The output data of VOLNA code are the spatial power distribution in the reactor core, the group neutron flux and the group densities of precursors.

The group cross-sections for VOLNA code are calculated by ARAMACO code. The input data for ARAMACO are distributions of temperature and density of fuel, constructional materials and coolant found at each time moment by GRIF-SM code.

The initial state of reactor in GVA code complex is exact critical state. This state can be changed by change of cross-sections in any reactor cell. That means the introduction of reactivity due to any physical reason. The reactivity is calculated during solving of time-dependent diffusion equation as an integral by reactor volume of changes in cross-sections distribution and shape function and critical reactor fission neutron importance function are the weight functions.

The results of four different accidents calculations by GVA code complex are discussed. The considered accidents were as following:

- the stopping of all main coolant pumps (MCP) with simultaneous fault of control rods;
- 6 compensating rods are going up from the reactor core with the velocity 10 cm/s;
- 6 compensating rods are going up from the reactor core with the velocity 0.5 cm/s;
- 6 compensating rods are going up with the velocity 5 cm/s during 2 seconds, then they are stopped.

Resume

1. The GVA code complex is developed for the joint solving of spatial and time-dependent dynamics equation and thermal hydraulics equations in three-dimensional geometry. The GVA can be used for transient and accidental calculations of fast reactors.
2. The ULOF and TOP accidents in the BN-800 reactor were calculated by GVA. These calculations are in good agreement with the results of calculations by the GRIF-SM code. However the calculations with GVA allow to take into account the shifts of spatial power distributions caused by the movement of reactor materials during accident and by movement of control rods (up to 10-15% of initial values).
3. It is desirable to provide detail verification of the GVA code for the applying of it in the practice of reactor calculations.

An Optimal Preconditioning Procedure in the Conjugate Gradient Method for 3d Hex-Z Geometry

V.P. Ginkin, A.V. Kulik

The problem of solution of the linear algebraic equations system:

$$A y = f \tag{1}$$

with a known vector $f = \{f_i\}$ and a nondegenerate matrix A is one of the fundamental ones in the numerical mathematics. Usually it is an intermediate, but most laborious stage in the numerical solution of applied problems.

The conjugate gradient method is one of the most efficient methods for solving linear systems of algebraic equations with a symmetrical matrix of coefficients. It was shown in Ref.[1] that the incomplete factorization method by N.I.Buleev should be a good preconditioning procedure in the conjugate gradient method. The most significant factor providing a high rate of convergence of the method is the use of the so-called compensation of iterative terms. The idea of the compensation is that a diagonal matrix multiplied by the iterative parameter θ is subtracted from the iterated matrix. The entries of the diagonal matrix equal to sums of entries over the rows of the iterated matrix. This iterative scheme is called the Diagonal compensation Incomplete Factorization scheme (DIF).

In this paper, another variant of the incomplete factorization method is applied where the compensating matrix includes not only diagonal but also peripheral entries provided that the sums of entries over the rows of the iterated matrix equal to those over the corresponding rows of the compensating matrix. This scheme is called the Peripheral compensation Incomplete Factorization scheme (PIF). The compensating matrix is formed such that the first terms of the Taylor series of its row-wise expressions were equal to those of the row-wise expressions of the iterated matrix. The compensating matrix is multiplied by the iterative parameter θ as well.

The proposed variant of the incomplete factorization scheme with the peripheral compensation was analyzed for a 3D diffusion type problem in HEX-Z geometry.

The table below lists the number of iterations J performed to solve with a predetermined accuracy a complex Neuman-Dericlet problem (on one boundary the Dericlet condition is imposed, on the others - the Neuman condition) by the Conjugate Gradient method (CG) as dependent on θ and the number of calculational meshes in one direction N . The incomplete factorization schemes with diagonal (CGDIF) and peripheral (CGPIF) compensation were used as the preconditioning procedures.

The data of the table and Fig.1 indicate that the use of the PIF and DIF schemes as the preconditioning procedures in the conjugate gradient method provides a considerable acceleration of the convergence of the method, besides in case of optimal values of the iterative parameter θ and $N=64$ the number of iterations according to the CGPIF scheme is half as many as that according to the CGDIF scheme, and less than that according to the CG scheme by a factor of 8.5.

N	16		32		64	
Θ	CGDIF	CGPIF	CGDIF	CGPIF	CGDIF	CGPIF
0.00	31	31	65	65	131	131
0.30	30	29	60	60	121	121
0.50	29	27	59	55	116	112
0.60	30	26	59	53	115	108
0.80	31	24	64	47	121	92
0.90	50	22	-	41	-	79
0.95	-	20	-	37	-	69
0.96	-	21	-	35	-	65
0.97	-	22	-	34	-	62
0.99	-	26	-	31	-	53
1.00	-	39	-	74	-	156
CG	108		216		429	

The sign "-" means that the scheme is divergent.

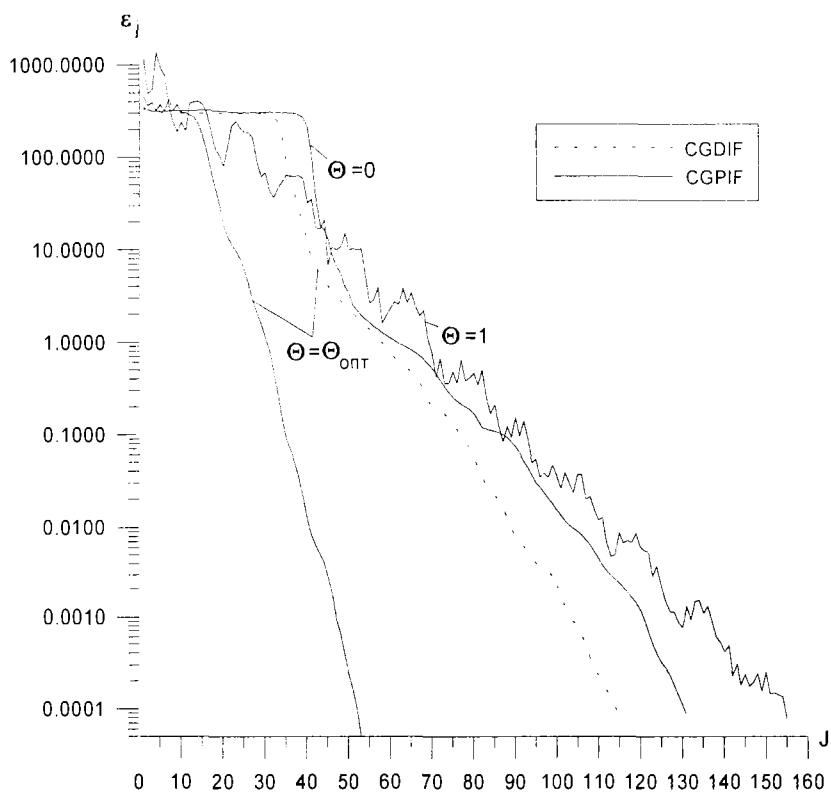


Fig.1. Decrease of the norm of the error as dependent on the number of iterations

Reference

1. V.P.II'in. Incomplete factorization methods. - Singapore: World Scientific Publishing Co., 1992.

Influence of Transversal Non-Homogeneous Parameter Distributions on Wall Friction, Heat and Mass Transfer in One and Two-Phase Flow in Vertical Annular and Subchannel Geometries

Y.Kornienko, ¹H.Ninokata

*¹Tokyo Institute of Technology, Research Laboratory for Nuclear Reactors
Tokyo, Japan*

Analysis of transient and accident regimes of nuclear reactors requires mathematical models for non-steady state one and two-phase flows in different geometry. Therewith such analyses are usually carried out using Lumped Parameter Analysis (LPA) codes. One of the greatest difficulties is associated with the establishment of the constitutive relationships for the one-dimensional annular and sub-channel flow treated by LPA codes. Usually, such codes utilize tube-type coefficients, on the basis of an equivalent diameter and of transversal homogeneous parameter distribution, for the solution of the momentum, heat and mass (substance) transfer equations. But, as a rule, for complicated conditions (when there are several physical effects in an interaction with non-homogeneous parameter distribution), the knowledge of such closure relationships leaves much to be desired.

Analytical, integral relationships are obtained from the initial three-dimensional drift flux formulation with taking into account transversal non-homogeneous distributions of such parameters as inner sources (sink) of heat, and momentum, and mass, transversal and axial substance transfer. The approach is based on the Reynolds flux, boundary layer and generalized coefficient of substance transfer. One more task has been to illustrate the validity of the «conformity principle» for the limiting cases. The method proposed is based on the similarity theory, boundary layer model, and a phenomenological description of the regularities of the substance transfer, as well as on an adequate simulation of the forms of flow structure by a generalized approach to build (an integrated in form and semi-empirical in maintenance structure) analytical relationships for wall friction, heat and mass transfer coefficients. In the one-dimensional model, a number of serious shortcomings of the conventional model have been pointed out and new formulations to eliminate them are presented. These shortcomings mainly arose due to the improper consideration of the parameters and phase distributions in transverse direction.

Analytical solutions are obtained for fully developed vertical mixed convection flows and two-phase flows with saddle-shape void fraction profiles within annular and conventional rod bundle subchannel geometry. Friction factors and Nusselt numbers are presented and fitted as function of Gr/Re^2 and of Ar/Re^2 . A modified friction factor is defined to be used in applications where only bulk-averaged fluid temperature and void fraction are available, as in the case LPA and most one-dimensional experiments. It is shown that the modified friction factor can vary significantly from the standard definition, which highlights the necessity of using the modified friction factor in analyses where the bulk density is used.

Modernization of Numerical Scheme and Calculation Algorithm for Accidental Regimes in the Code "TRAP-97"

V.K.Artemyev, Y.N.Kornienko, ¹S.I.Zaitsev

¹*OKB "Gidropress", Podolsk, Russia*

The code "TRAP-97" is aimed to analyze VVER transient thermohydraulics processes, and regimes with broken NPP equipment, including accident with loss of coolant. Now TRAP-97 calculations demand much CPU time, especially for large break LOCA accident. So, one of the central problem is the time step optimization for complicated processes with different character time constants.

The basic features in proposed modernization are: monotone, balance, neutral deference schemes. They allow to keep the important integral features of the original differential equations. Besides, it is proposed the calculation scheme for pressure and implicit stabilization method. Here we present of the monotone, balance, neutral deference scheme formulation on the base of continuity and substance φ transfer equations:

$$\frac{d\rho}{dt} + \frac{d\rho u}{dz} = 0, \quad (1)$$

$$\rho \frac{d\varphi}{dt} + u \frac{d\varphi}{dz} = \frac{d}{dz} \eta \frac{d}{dz} + f, \quad (2)$$

where variable φ is designate velocity, enthalpy, or concentration of the flow, the rest designations are common acceptable.

In the finishing form the used deference equations are presented below:

$$\xi_i^{n+1} \equiv \frac{\rho_i^{n+1} - \rho_i^n}{\Delta t} + \frac{(\rho u)_{i+1/2}^{n+1} - (\rho u)_{i+1/2}^n}{\Delta z_i} = 0, \quad (3)$$

$$\rho_i^n \frac{\varphi_i^{n+1} - \varphi_i^n}{\Delta t} - a_i \varphi_{i-1}^{n+1} - b_i \varphi_{i+1}^{n+1} q_i \varphi_i^{n+1} = f_i, \quad (4)$$

where

$$a_i = 0.5 u_{i-1/2} + \alpha_{i-1/2} \operatorname{cth} \alpha_{i-1/2} \eta_{i-1/2} / \Delta z_{i-1/2}, \quad (5)$$

$$b_i = -0.5 u_{i+1/2} + \alpha_{i+1/2} \operatorname{cth} \alpha_{i+1/2} \eta_{i+1/2} / \Delta z_{i+1/2}, \quad (6)$$

$$\alpha_{i+1/2} = \Delta Z_{i+1/2} u_{i+1/2} / 2 \eta_{i+1/2}, \quad (7)$$

$$q_i = a_i + b_i. \quad (8)$$

For function $\alpha \operatorname{cth} \alpha$ it is possible to use the simple approximation in the form $\alpha \operatorname{cth} \alpha \approx |\alpha| + 1 / (1 + |\alpha| + |\alpha|^2)$. In the proposed algorithm the equation (3) serves for construction of the three points equation for pressure. In the such iteration process the $\xi_i^{n+1} \neq 0$ value is used as convergence criterion. Here we use the implicit stabilization method for solution of the set equations and linearization on the each stabilization step.

Medium Term Forecast Calculations of Radioactive Waste Migration from Niiar Deep Injection Disposal

A. Zinin, G. Zinina

The purpose of the work is to carry out the calculations to predict migration of radioactive waste from the Disposal Site at Scientific Research Institute of Nuclear Reactions (NIIAR) for the conditions close to real geometry and real geologic structure. Special attention is focused on consideration of non-linear effects caused by density-driven convection (gravitational segregation). The results of numerical studies allow to evaluate the influence of different factors ("floating" of lighter waste, heterogeneity of permeable formations, existence of high conductivity layers, anisotropy of rock transmissivity) on the spread of waste.

The feature of NIIAR disposal site is the high salt content of the waters saturating the formations III and IV used for the waste disposal. The displacement of salt formation waters on the waste with low salt content leads to the complex alteration of natural formation water flow, density-driven convection, changes of filtration properties.

In this report the waste migration in the permeable formation IV which lies in depth 1130 - 1410 m is considered. Waters saturating formation IV are of chloride-sodium type with total salt content 200 - 220 g/L.

The base tool for modeling is the GEON-3DM code, developed in the SSC IPPE. GEON-3DM code verification was made on two test problems from the International HYDROCOIN Project and on the special test problems jointly with American specialists in the JCCEM project frame.

The results of Sr-90 migration in the formation IV are presented. Waste injection regime data until 1997 go with real data, after 1997 it's assumed that injection is conducted until 2010 with injection rate 60000 m³/year and specific activity 5*10⁻⁵ Ci/L. According to prognosed injection scenario, by 2010 total activity waste injected will reach 2.2*10⁹ MBq.

The model of migration solution includes the neutral component which determines the solution density and migrates without interaction with host rocks and several tracer components rendering no effect on solution density, however they can be affected by radioactive decay and retained by interaction with host rocks. The system of differential equations includes the pore solution mass balance equation, Darcy equation generalized for the case of variable density, the chloride-sodium mass balance equation, formulated in the terms of solution density, and, finally, radioactive component transport equation.

Numerical studies show that the base parameter defining the rate of "floating" of light waste is hydraulic conductivity anisotropy in the horizontal and vertical directions. The relation $K_{f_z} / K_{f_{xy}}$ is assumed to be equal 0.1 in the calculations made.

In this report the calculations are made for the radioactive component with half - life of nuclide about 30 years, that corresponds to isotopes Strontium-90 and Cesium-137.

Schematization of permeable formation IV is based on data of gamma logs for monitoring wells. The alternation of zones with high permeability (fractured) rocks and low permeability rocks over the thickness of formation IV causes the flow properties to be sharp heterogeneous.

According to calculations, the maximum advance of isoline 10⁻⁹ Ci/L in the south-west direction from the waste disposal site reaches 3.1 km after 100 years from the beginning of injecting, 3.5 km after 150 years, 3.9 km after 200 years, 4.2 km after 250-

300 years. Prognosis data obtained show that radioactive waste with half - life about 30 years are located within the bounds of model domain and over the period of 300 years radioactive waste with concentrations higher than established basic limits don't appear beyond the boundary of the subsurface exclusion zone.

Numerical modeling studies detected that "floating" effect is developed more stronger for the "isotropic" case ($K_{fz} / K_{fxy} = 1$). It may be observed even in the injection period. The extrusion of light salt waters leads to the forming of cone waste plume.

Conclusions

- Numerical forecast modeling studies of the radioactive waste migration in formation IV from NIIAR deep injection disposal are made. The modeling scenario assumes that operation life of NIIAR disposal site will be continued until 2010.
- Schematization of permeable formation IV is based on data of gamma logs for monitoring well P-5. The feature of this schematization is alternation of zones with high permeability (fractured) rocks and low permeability rocks over the thickness of formation IV.
- Calculations are made for the radioactive component with half - life about 30 years, that corresponds to isotopes Strontium-90 and Cesium-137.
- The agreement between modeling data and observed ones is good for the P-9 monitoring well at the values of hydrogeologic parameters taken.
- The calculations show that with disposal site operation life scheme accepted (until 2010), formation waters with the radioactive waste exceeding established basic dose limits won't appear beyond the boundary of the subsurface exclusion zone for the radionuclide group considered over the whole modeling period.
- Hydraulic conductivity anisotropy in the horizontal and vertical directions influences in a great extent on the plume shape and waste distribution over the thickness of formation IV. In particular, waste "floating" effect practically doesn't appear when $K_{fz} / K_{fxy} = 0.1$.
- Model domain schematization accepted does not allow to explain the absence of waste in some monitoring wells (P-7, P-11). Additional field studies are necessary to be done for closer definition and detailed elaboration of geofiltration properties.

References

1. A.Zinin, G.Zinina. Provedenie srednesrochnyh prognoznyh raschetov migratsii radioaktivnyh othodov ot glubinnogo zahoroneniya othodov na poligone NIIAR s ychetom anizotropii provodimosti porod. Otchet FEI, inv.№10092, s.43 (in russian)).
2. A.Rybal'chenko, M.Pimenov, P.Kostin and others. Deep Injection Disposal of Liquid Radioactive Waste in Russia. Battelle Press Columbus, Richland, 1998.

Molecular Dynamics Study of Pair-Potential Parameters Effect on Structure and Atomic Dynamic of Liquid Sodium

I.Yu. Shimkevich, A.L. Shimkevich

Results of the molecular–dynamics (MD) investigation of influence for the different approximation of pair potential on the structure and dynamic characteristics of liquid sodium near the melting point are presented. We have considered two models of local pseudopotentials which more often have been used for MD investigation of metals and given the adequate description of liquid structure and atomic dynamics of the alkaline metals. The various dielectric functions of pseudopotential models have been considered and the optimal parameters have been estimated for liquid sodium.

Ascroft pseudopotential model [1] with the dielectric functions developed by different authors during the last two decades [2-11] and Hasegawa model [12] with Ichimaru and Utsumi [13] dielectric function used the last years for alkaline metals [14] were examined for investigation the properties of liquid sodium at the temperature 373K. The various considered local field functions $G(q)$ which defines the dielectric function are presented in Table.

The field functions are connected directly with fluctuation of electron density in system. Besides that, MD calculations have been performed with different values of the potentials parameter R_c that almost define Ashcroft pseudopotential and is one of the parameter of the dielectric Ichimaru function [13].

The electron exchange-correlation correctives of dielectric functions

References on definition ν	Parameter ν in model	MДМММК [15]
J. Hubbard [2,8]	$\nu = 1$	$\nu = 1$
L. J. Sham [3,9]	$\nu = 1 + \frac{4}{\pi q_F a_0}$	$\nu = 3.6857$
A. O. E. Animalu [4,9]	$\nu = 1 + \frac{2}{\pi q_F a_0}$	$\nu = 2.3429$
[5]	$\nu = \nu_1 = \frac{2}{1 + 0.153 / \pi q_F}$	$\nu = 1.8969$
P. Nozieres, D. Pines [7,8]	$\nu = \nu_2 = \frac{2}{1 + 0.026 r_s \left(\frac{m^0}{m} \right)}$	$\nu = 1.8095$
MДМММК [15]	$\nu = 0.5 \times (\nu_1 + \nu_2)$	$\nu = 1.8532$
Kleinman [6]	$G(q) = \frac{1}{4} \left[\frac{q^2}{q^2 + \nu q_F} + \frac{q^2}{\nu q_F^2} \right]$	$\nu = 1.8532$
Vashisto, K. S. Singwi [10] (exp_AB)	$G(q) = A_\nu [1 - \exp(-B_\nu q^2 / q_F^2)]$ for Na: $A_\nu = 0.995$, $B_\nu = 0.2625$	
D. J. W. Geldard, S. H. Vosko [5,8]	$G(q) = \frac{q^2}{2(q^2 + \nu q_F^2)}$	
Ichimaru, K. Utsumi [13]	$G(q) = A Q^4 + B Q^2 + C + [A Q^4 + (B + \frac{8}{3} A) Q^2 - C] \frac{4 - Q^2}{4 Q} \ln \left \frac{2 + Q}{2 - Q} \right $, where A, B, C - parameters [13], $Q = q / q_F$.	

The selection of optimal parameters has been based on comparison with experimental data and results of other authors [11,14] such structure characteristics of liquid sodium as radial density function $4\pi r^2 \rho(r)$, the partial radial distribution functions $g(r)$, structure factors $S(q)$, and microdynamic characteristics as the velocity autocorrelation functions $Z(t)$, frequency spectra $Z(\omega)$, mean-square displacement $\langle r^2(t) \rangle$ and self-diffusion coefficients D .

The base conclusions are similar with earlier works [11, 14] that the structure of nearest power is insensitive to details of the pair potential. Considered structure characteristics for all types of potentials give the results that good agree with experimental results and others authors data.

The dynamical properties are very sensitive to the field function used and factually it is demand the potential selection for every concrete properties. For the model of Ashcroft pseudopotential it is follow to refuse from using the Hubbard corrective ($\nu=3.6857$) for liquid sodium. The value of parameter $R_c=1.90$ au is too high for the Hasegawa model with Ichimaru [13] dielectric function and the value of parameter $R_c=1.85$ au is more optimal.

Computer experiments follow to receive the potentials details that influences on the properties of liquid sodium. But the simulation of liquid sodium under others temperatures and in a mix with others compounds to demand the addition investigation.

References

1. N.W.Ashcroft, Electron-Ion Pseudopotentials in Metals // Phys. Lett. 1966, vol.23, №1, pp.48-50.
2. J.Hubbard, Proc.Roy.Soc. A240, 539, 1957, A243, 336, 1958.
3. L.J.Sham, Proc.Roy.Soc. A283, 1965, p.33.
4. A.O.E.Animalu, Phil. Mag., vol.11, 1965, p.379.
5. D.J.W.Geldard, S.H.Vosko, The Screening Function of an Interacting Electron Gas // Canad. J. Phys., 1966, vol.44, pp.2137-2171.
6. L.Kleinman, New Aproximation for Screened Exchange and the Dielectric Constant of Metals // Phys. Rev., 1967, vol.160, №3, pp.585-589.
7. P.Nozieres, D.Pines, Phys.Rev.,vol.178, 985,1969.
8. D.L.Price, K.S.Singwi, M.P.Tosi, Lattice Dynamics of Alkali Metals in the Self-Consistent Screening Theory // Phys. Rev. B, vol.2, №8, 1970, pp.2983-2999.
9. Shyu Wei-Mei, K.S.Singwi, M.P.Tosi, Many-Electron Correlation Effects on the Metallic Interionic Potential // Phys. Rev. B, 1971, vol.3, №2, pp.281-289.
10. P.Vashishto, K.S.Singwi, Electron Correlation at Metallic Densities. V // Phys. Rev. B, vol.6, №3, 1972, pp.875-887.
11. Miranda J.M. Gonzalez, V.Torra, A molecular dynamics study of liquid sodium at 373K // J. Phys. F: Met. Phys., 1983, vol.13, pp.281-289.
12. M.Hasegawa, K.Hoshino, M.Watabe and W.H.Young // J. Non-Cryst. Solids 117/118, 1990, p.300.
13. Setsuo Ichimaru, Kenichi Utsumi, Analytic expression for the dielectric screening function of strongly coupled electron liquids at metallic and lower densities // Phys. Rev. B, vol.24, №12, 1981, p.7385.
14. Shimojo, K.Hoshino, M.Watabe, Dynamical Correlation Functions and Memory Functions of Liquid Sodium - a Molecular Dynamics Simulation // Journal of Physical Society of Japan, 1994, vol.63, №1, pp.141-155.
15. И.Ю.Шимкевич, А.Л.Шимкевич, МДММК (Молекулярная динамика и метод Монте-Карло) программа для построения кристаллических и неупорядоченных систем // Препринт ГНЦ РФ ФЭИ-2524, Обнинск, 1996.

2.7 APPLIED RESEARCH

To the Question about the Mechanism of Energy Transfer under the Interaction of Accelerated Heavy Ions with Polymers

G.S. Zhdanov

One of the most amazing scientific results got in the twentieth century consisted in the discovery of the feasibility to visualize the areas of radiation damages localized along a heavy ionizing particle pathway in the substance by its subsequent physico-chemical treatment in inorganic alkali and acid solutions. The detected regularity has found a broad application mainly in two directions; as a method of recording accelerated heavy particles and as a basis for developing quite a new technology according to which precision polymeric track membranes can be produced. In order to develop both directions it is necessary to have a deep understanding of those processes which go on in the heavy ion track. In the first case the registered particle parameters (energy, mass, charge) are determined by the size of the visible track, in the second case by means of charged particles micro-holes are produced and they are rigorously calibrated by their sizes. However, the knowledge about the processes of latent track formation and evolution in polymers is insufficient. The interaction of accelerated heavy ions with the substance has its own importance for the understanding of fundamental processes in high energy chemistry.

The models of latent track formation in polymers which exist to-day (the models of 'ion explosion', of 'thermal wedge', different models related to energy losses - dE/dx , e.g. initial ionization, losses limited by radii, etc.) explain the phenomenon of track formation but do not allow many experimental results to be adequately described [1-3]. It is manifested first of all by the inconsistency between the etched track shape and calculated values of energy loss distribution along the track radius and length, and secondly by the increase in the etching rate outside the calculated latent track. From this it follows that the existing models do not take into account a number of factors which significantly influence the changes of polymer properties in the 'near-track' space.

In the theoretical models of latent track formation primarily the radiation effects are considered. The models of 'ion explosion' and 'thermal wedge' concern the processes in the track core. Actually the processes in the track halos ('penumbra') are not considered. At the same time there are numerous data which indicate a long-range mechanism of absorbed energy transfer, namely: physical and chemical changes in polymer are observed over the anomalously big distances from the heavy ion track axis [4]. Let us extendedly consider the possible mechanisms of energy transfer over big distances from the track axis. Out of all the radiation effects energy transfer due to the secondary electrons seems the most probable long-range effect. And though separate electrons (with a maximum energy) can transfer the energy over the distance of tens and hundreds nanometers, their contribution into the total absorbed dose will be too small. Out of other mechanisms (secondary processes) capable of transferring energy over bigger distances from the track area the following can be considered: a) excitation energy and charges over big distances of 200-300 nm and more; b) migration of low-molecular active particles from the track area and their subsequent reaction in the 'near-track' space. However for certain reasons their contribution into the polymer degradation is insignificant. First of all it is due to the fact that concentration of intermediate active particles and excited states in the track core and neighboring space will be so high that

annihilation of excited states and recombination of charges and free radicals will be the most probable processes. Moreover, physical and chemical transformations over big distances are observed for various types of polymers, including those for which the reaction under consideration will not result in degradation of polymer properties (e. g. polypropylene cross-linking).

The physical factors which accompany the accelerated ion movement through polymer and which are not considered in the models seem the principal contributors into degradation of polymer properties in the 'near-track' space. The heavy ion effect has a specific feature which is related to a high density of the energy being released. The period of ion-polymer interaction (10^{-13} s, during this time on the average the ion goes through the polymer film with the thickness of ~ 10 - 20 mkm) is not enough for the absorbed energy to disappear. It results in an increase in the track temperature and thus in a thermal elastic stress, high local pressure and propagation of micro-shock waves in the 'near-track' space. In case of irradiation deactivation of excited particles electromagnetic radiation is generated in the optical range of frequency, including the one which is visible. The accumulation of charged particles generated in the course of substance ionization at the moment when the multi-charged ion goes through will result in developing a local volume charge around the track and in formation of accompanying internal electric field.

So actually the polymer radiolysis in the 'near-track' space goes on with the influence of physical factors induced in polymer by an ion which goes through it. In reality none of the latent track formation models available takes these phenomena into account. It is a known fact that external mechanic and electromagnetic fields significantly influence the radiation chemical processes in polymers. Usually they refer to destabilizing factors, i. e. they increase the radiation effect. Photoradiation and pressure effects run to several hundreds percent [5,6]. The effect of electric and magnetic fields is less significant and poorly studied [7]. The essence of the effect of external physical factors under consideration consists in the change of direction of radiation chemical reactions of intermediate active particles, thus usually causing a deeper polymer damage. It can be stated a priori that when heavy ions go through polymer the induced physical factors will affect the radiation chemical processes in the track. The impact of electromagnetic fields can be evidently expected on the intermediate active particle reactions. It will cause the increase in polymer damaging effect. Photoradiation processes can result in an insignificant increase in the 'near-track' damaged space but not in its drastic expansion, as it is observed in experiments.

In our opinion, out of all the physical factors considered longitudinal micro-shock waves play a decisive role in damaging polymer in the 'near-track' space. According to various estimations the track temperature [adiabatic approximation] reaches 60000-70000 C and the induced pressure jump at the wave front is equal to 100-120 kbar. By the EPR method for orientation of peroxide macro-radicals [rigidly connected with polymeric chains] it was shown that in this case elastic longitudinal waves propagate in a radial direction from the track axis as well as in the direction of heavy ion movement [8]. They orient polymeric chains lining them up in the direction of wave propagation. It is quite reasonable to assume that with a micro-shock wave propagation in the places of polymer compression and expansion thermo-mechanical reactions can occur. These reactions can cause polymer degradation far beyond the track area. The proposed concept can explain quite a number of experimental results on polymer transformation over anomaly big distances from the track axis (up to 0,2-0,3 mkm) and does not contradict the existing models of latent track formation in polymer. Let us quote one or

two factors as an example which confirms the correction of the model concepts being developed. The experiments related to the track annealing temperature effects in polyethylene terephthalate (PET) showed that the process of latent track formation is reversible. Latent track in PET are annealed ['healed'], i.e. the damaged polymer is recovered and it could not be so if polymer damages are induced by radiation chemical reactions. In this case as the temperature rises due to a thermo-oxidation destruction the polymer damages must become even more pronounced. Another example. According to the laws of classical radiation chemistry of polymers as the temperature goes down (a negative field) the yield of all the radiation chemical processes becomes much slower. Irradiation of polymers with different properties with heavy ions at the temperature of 100-150 K causes their more significant damage as compared to their irradiation at higher temperatures (300 K) [9]. The observed phenomena can be reasonably explained from the point of view of thermo-mechanical reactions induced by shock waves.

It should be noted, that the Kharkov school of physicists made an attempt to explain the changes in the properties in the 'near-track' space by means of shock wave impact for gypsum single crystals. However, the authors were inclined to explain the observed effects by generation of shock waves from the knocked out secondary electrons. As applied to polymers this viewpoint has been expressed for the first time.

This work was supported by Russian Foundation for Basic Research and the Government of Kaluga Region (grant no. 00-03-96004).

References

1. R. L. Fleisher, P.B.Price and R.M. Walker. Nuclear Track in Solids. Principles and Application, University of California Press. Berkeley,1975.
2. S.A. Durrani, R.K.Bull. Solid State Nuclear Track Detection Principles. Methods and Application
3. (AERE,Harwell,UK,Pergamon Press,1987)
4. B.V.Mchedlishvili, G.N.Flerov. New class of microfiltration membranes in the precision separating of the colloid solutions. J. of Mendeleev All-Union Chemical Society. 1987,No.6,pp. 641-647.
5. G.S. Zhdanov et al. Structural changes in polymers treated by accelerated heavy ions. Abstr. IraP94,1994,p.95.
6. V.K.Milinchuk, E.R. Klinshpont, V.P. Kiryukhin. Effect of high pressure on the formation and rection of free radicals in the radiolysis of polymers. Radiat.Phys.Chem.1983, Vol.21,No.6, pp.519-526.
7. G.S. Zhdanov and V.K. Milinchuk. Photoradiation processes in polymers.M.: NIITEKHIM, 1980, p.60.
8. A.L. Buchachenko, P.Z. Sagdeev, K.M. Salikhov. Magnetic and spin effects in chemical reactions. Novosibirsk,1978,p.295.
9. G.S. Zhdanov, E.R. Klinshpont, P.Yu. Apel, V.K. Milinchuk. Orientation of polytetrafluroethylne macromolecules under heavy ion irradiation. Abstr. SHIM 95,1995,p.36.
10. P.Yu.Apel et al. Registration temperature effect in polymers: physico-chemical aspects. Radiation Measurements, 1997, Vol. 28, Nos. 1-6, pp.19-24.

Fission Fragments Track Formation in Polymer

A.A. Tumanov

The task to create ultrafiltration track membranes with a pore diameter less than 0,05 μm requires the knowledge of processes which occur in the area of a latent track. Currently there is no theory or models which can satisfactorily describe the available experimental results. It specifically refers to track formation by fission fragments when polymer is irradiated by strongly excited particles under the conditions of impact of many radiation factors (neutrons, electrons, γ -quanta) and non-radiation ones (temperature, atmosphere gas composition, electric field, etc.).

In this respect it is of a crucial importance to get a complete knowledge about the current feasibility to calculate energy losses on the way of multicharged ions through the substance. The analysis of literature data shows that the Bete-Bloch theory is the basis for calculations of dE/dx energy losses when the ion velocity is higher than the velocity of shell electrons. At a lower energy the dE/dx value is determined by the Lindhard theory. The calculation according to this algorithm was implemented in the OD-1 code. The significant scope of calculations is carried out by means of the Brant-Kitagava theory instead of the Bete-Bloch algorithm (codes of the TRIM-SRIM family). In order to directly compare these methods the energy losses and ranges (R) of U-235 fission fragments were calculated in polyethylene terephthalate (PET) by means of such codes as OD-1, TRIM-91 and SRIM-98. Along with the general agreement of the results obtained the pronounced specific features were found both in various algorithms and in the TRIM and SRIM codes. TRIM-91 cannot be used for the calculations related to Xe and I ions because these calculations appear absolutely wrong (it refers to dE/dx , R and Monte-Carlo blocks calculation). The results of dE/dx and R calculations based on TRIM-91 and SRIM-98 show significant differences. For instance, a relative decrease in the ranges for ions from Kr-90 to Ba-143 is equal to 3-18% when changing over from the first code to the second one. Besides the ion distribution in the range becomes also different: the slope of distribution becomes steeper at higher R values with the SRIM-98 code.

On the whole, the analysis of the results obtained does not allow the SRIM code to be considered a preferable one as compared to the Bete-Bloch algorithm.

According to the literature data the latent track core and halo are formed in a different way. When generalizing the results of experiments related to track formation in PET for ions from Co to U [1] it is possible to get the expressions for latent track core and halo diameters, d_c and d_h ($d_c \sim dE/dx^{0.55}$). With the use of the results of dE/dx calculations for fission fragments the functions of track distributions were obtained in terms of the size at various depth of PET foils. The calculations show a pronounced structure of track distribution in terms of sizes with a significant variation of their diameters at the depth of 10 μm . However the experimental study with the use of electronic microscopy techniques and other techniques does not reveal such predictions. These results indicate that fission fragments have a significantly higher destruction property as compared to accelerated ions and that there may be a more complicated mechanism of track formation.

So the chosen direction seems promising and requires further investigations.

This work was supported by Russian Foundation for Basic Research and the Government of Kaluga Region (grant no. 00-03-96004).

Reference

1. P.Apel et al. Track size and track structure in polymer irradiated by heavy ions. Nucl. Instr. and Meth. in Phys. Res. B 146 (1998) 468-474.

Wear Study of Ceramic Bearings Using Thin Layer Activation Technique

V.V. Sokovikov , I.O. Konstantinov

Wear study of ceramic sliding bearings was carried out using thin layer activation technique. The most proper activation conditions for the thin labels producing in ceramics with ZrO_2 and Si_3N_4 as the basic matrices were determined. Wear tests were carried out at the plant test bench and running-in curves were obtained. Some reasons concerning the applicability of the technique to ceramics are considered.

Thin-layer activation (TLA) technique of wear and corrosion monitoring for large variety of machine parts and materials is a well known field of accelerator applications. Having a lot of advantages this technique has become a reliable non-destructive method of monitoring and nowadays is widely spread in many countries [1 – 4].

The main engineering materials studied by this technique are metals and alloys. The attention of designers is now attracted to different ceramic materials having high corrosion and wear resistance. TLA application to this material research meets some problems associated with their specific properties

The specific task of this work was wear study of plunging pumps ceramic sliding bearings. These units may be manufactured from two types of ceramics with Si_3N_4 and ZrO_2 as the basic matrices. The object of our investigation is to study the beginning stage of the wear process being of very low rate, and to consider some reasons substantiating the use of the TLA technique for this purpose.

Activation of other ceramics based on ZrO_2 is not more complicated.. Proton induced reactions with the main component – zirconium, produce long-living radionuclides of Nb. The most suitable for wear measurements is ^{92m}Nb the fraction of other radionuclides, mainly ^{89}Zr , in 3-4 weeks of time delay being rather low. The thick target yield of ^{92m}Nb from pure Zr at $E_p = 7.6$ MeV was measured to be equal to (32 ± 4) kBq/ μAh , consequently for ceramics it was about 17 kBq/ $\mu A.hr$.

The label thickness is expected to be ~ 20 μm . After 3 weeks delay the fraction of ^{89}Zr decreases to ~ 2.5 %, furthermore its depth distribution nearly coincides with the distribution of ^{92m}Nb . This situation practically excludes the error of combined radiometry during testing.

A label necessary for wear measurements should be ring-shaped and located at the inner cylindrical surface of the outer bush spacing 5-7 mm from the edge. The irradiation was carried out by a proton beam extracted in the air through 50 - μm Mo foil. The samples $\varnothing 10 \times 4$ mm of the same ceramics were irradiated in the same conditions along with the components. These samples were used for determination of calibration curves and for studying possible irradiation effect on the material properties.

Calibration curves were obtained by a usual technique of abrading the irradiated samples and measuring the residual activity and the thickness removed. Consecutive removing of the surface layers from the sample was performed by grinding on the water-resistant emery cloth. After careful flushing thickness of the sample was measured by an optic head with graduation of 0.2 μm . Calibration curves should be obtained in the same measuring conditions which are to be encountered in real tests. Therefore γ - intensity was measured using scintillation detector NaJ(Tl) 40 \times 40 mm and single-channel analyzer NC-482B (Hungary). The curves and experimental points are given in Fig. 1

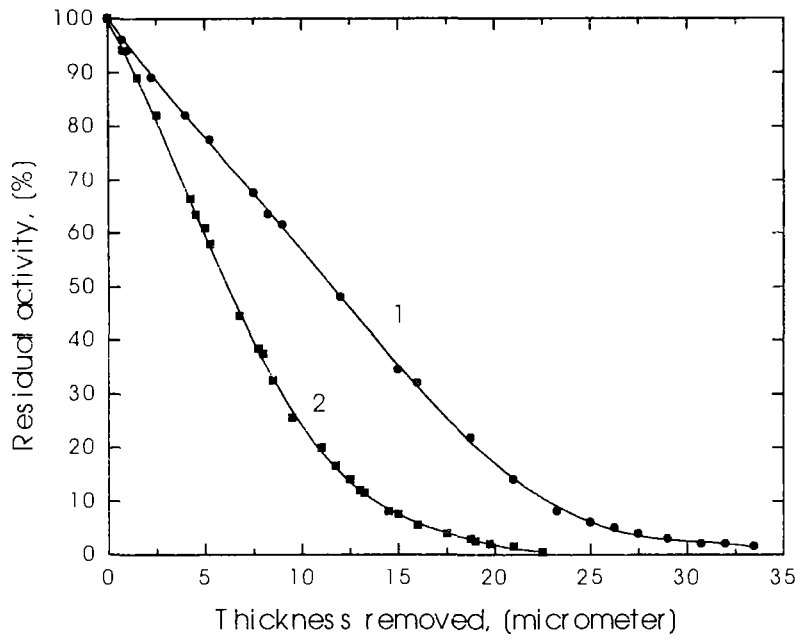


Fig.1 Calibration curves
 1 – for ceramics on the base of Si₃N₄ ,
 2 – for ceramics on the base of ZrO₂

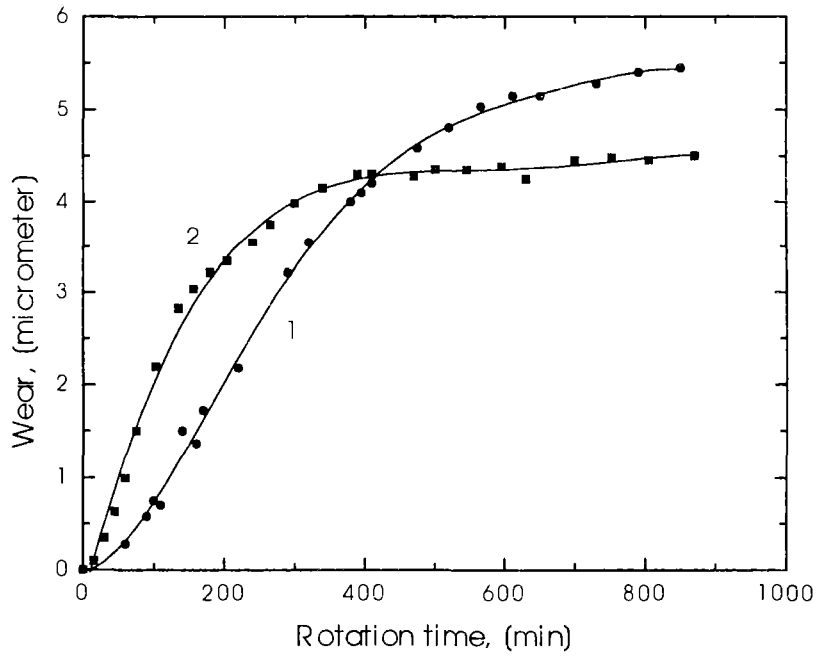


Fig.2 Wear curves of sliding bearings
 1 – from ceramics on the base of Si₃N₄ ,
 2 – from ceramics on the base of ZrO₂

Testing was carried out at the test benches of the plant “Borets” and ORPE “Technologiya”. The test conditions were different. At the plant the friction medium was a special oil and γ - intensity was measured during short stops and the pump shaft extraction out of the well without disassembling of the friction unit. In “Technologiya” it was dry friction and every 30-40 min of rotation the bearing was disassembled and carefully washed before measuring. The rotation speed in both cases equal to 3000 rpm.

The measurements were performed by use of the scintillation detector and single-channel γ - spectrometer described above. The reproducibility of measuring geometry was better than 2-3%. The testing results for both types of ceramic bearings are shown in the Fig. 2. The general conclusions are as follows :

a) The employed technique allows to investigate the wear of ceramics on the base of Si_3N_4 and ZrO_2 with great sensitivity. The determination limit in the realized conditions is equal to 0.1–0.2 μm , that enables to determine low rates of destruction. In this specific case it is the beginning stage of the wear process.

b) Running-in of bearings makes up 4–5 μm , that is about the grain size, and it lasts ~400 min for ZrO_2 and ~600 min for Si_3N_4 .

c) In our investigation we have not noticed appreciable changes of material operating properties, i.e. the irradiation conditions chosen proved to be satisfactory. Nevertheless it is obvious that while using the thin layer activation technique for measuring the wear of ceramic articles one must examine the irradiation effect on the properties of material in every case.

References

1. T.W.Conlon, *Wear*, 29 (1974) 69
2. P.Fehsenfeld, A.Kleinrahm ,H.Schweikert , *J. of Radioanal. and Nucl.Chemistry* , 160(1) (1992) 141
3. I.O.Konstantinov, *Isotopes in USSR*, 73 (1988) 5.
4. The thin layer activation method and its applications in industry. IAEA-TECDOC-924, 1997.

2.8 HIGH-VOLTAGE ACCELERATORS

Recent Developments at the IPPE EGP-15 Tandem for Fundamental and Applied Researches

*A.I. Glotov, S.V. Bazhal, V.S. Bashmakov, V.I. Volodin, V.K. Debin,
B.V. Kupriyanov, A.A. Malygin, V.A. Nikitin, V.A. Romanov, V.I. Spirin,
A.S. Feigin, Yu.R. Chaly*

Abstract

In this article we describe the reconstruction of the IPPE EGP-15 tandem that was necessary to fulfill the requirements on fundamental researches in nuclear and solid state physics. Until recently the accelerator was used for applied researches and the accelerator injector was equipped only with one sputter-type ion source for negative heavy ions. In order to increase the accelerator capabilities for fundamental researches, the availability of both continuous as well as nanosecond pulsed beams of hydrogen and other light ions was required. Therefore the injector upgrading was aimed to have two independent ion sources and a special chopping and bunching system. The hydrogen negative ion source is a duoplasmatron and will be positioned after reconstruction at the direct (vertical) mass-separator channel. At the high energy end of the accelerator an additional beam line equipped with lenses and beam position control equipment was installed for experiments in a separate target chamber. The upgrading carried out allowed to design a fast neutron time-of-flight spectrometer and to study radiation damage in engineering and optical materials including its dynamics.

1. Introduction

Last two years the EGP-15 tandem was mainly used for the production of track membranes. Irradiation of mylar films of 8-12 μm thickness with Si beam of up to 45 MeV was employed for the improvement of film technology. Such experiments required a terminal voltage of up to 6.5 MeV and special emphasis has been paid to the reliability of the accelerator and the intensity stability and dose uniformity of the beam.

Recently, our research program was extended with fundamental research in nuclear physics and solid state physics using isotopic hydrogen beams. For this, continuous and nanosecond pulsed beams with high intensity are needed, that makes possible fast neutron time-of-flight spectrometer having high resolution and sensitivity. The experiments on solid state physics also require external beam experiments.

Such works require a modification of the present injector, a development of beam lines and a creation of new working sites for the successful research performance.

2. The injector adaptation

In order to shorten a time required for the formation of "hydrogen" regimes, the reconstruction of an injector is employed step by step. In the first stage, the sputtering type ion source on the horizontal ray was replaced by a duoplasmatron. At the same time, the vertical beam line was reconstructed in order to improve the acceptance of pulsed beams (Fig. 1).

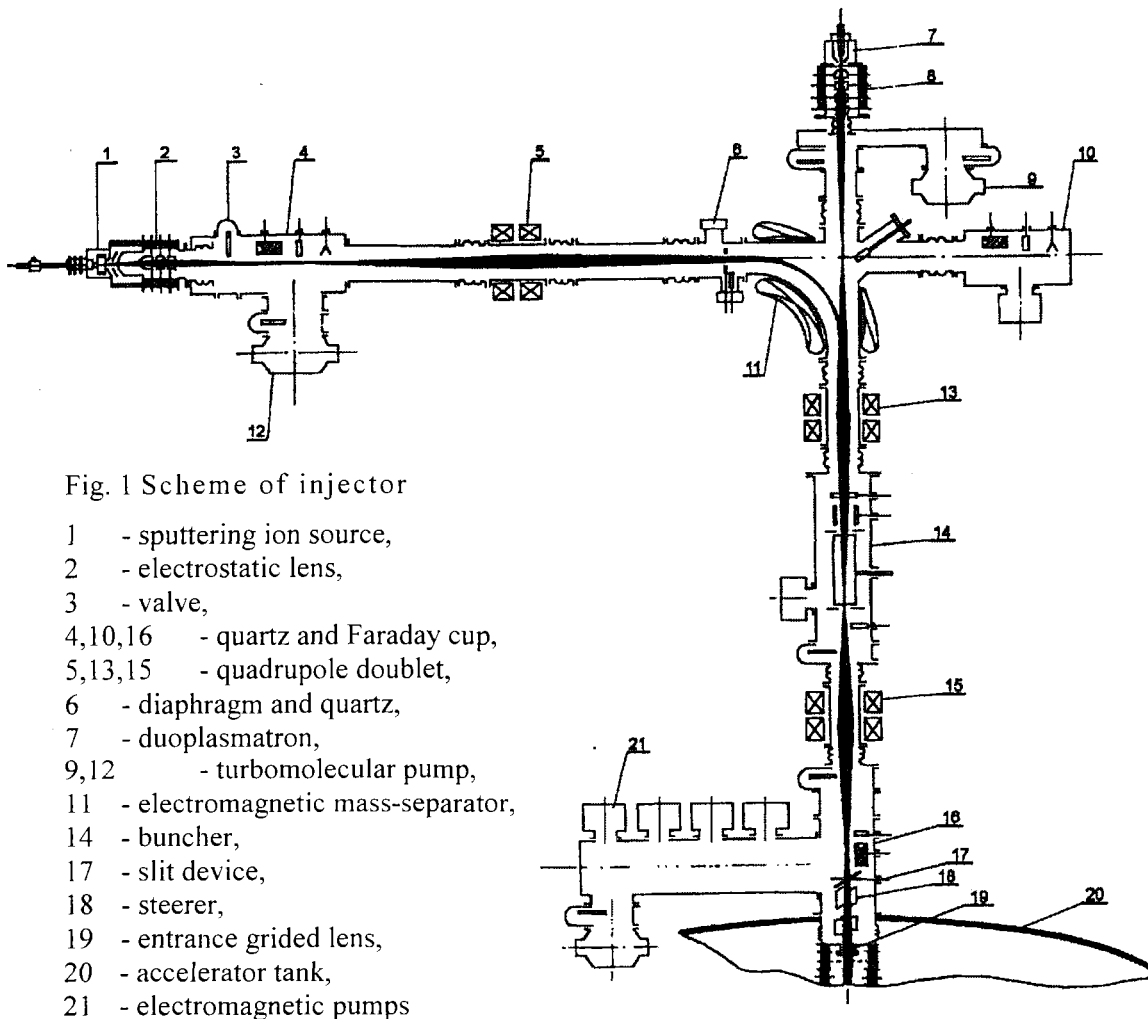


Fig. 1 Scheme of injector

- 1 - sputtering ion source,
- 2 - electrostatic lens,
- 3 - valve,
- 4,10,16 - quartz and Faraday cup,
- 5,13,15 - quadrupole doublet,
- 6 - diaphragm and quartz,
- 7 - duoplasmatron,
- 9,12 - turbomolecular pump,
- 11 - electromagnetic mass-separator,
- 14 - buncher,
- 17 - slit device,
- 18 - steerer,
- 19 - entrance grided lens,
- 20 - accelerator tank,
- 21 - electromagnetic pumps

The created injector optical system provides the formation of continuous and pulsed beams using two ion sources. A sputter-type ion source is situated at the entrance of the injector magnet in horizontal plane. The second, a duoplasmatron, is installed at the entrance of the magnet, in the vertical plane. The crossover of continuous and pulsed beams obtained from any of two ion sources is maintained at the buncher exit diaphragm. Along the horizontal beam line a diaphragm with controlled aperture and a quartz disk can be inserted to examine the beam position and measure the beam intensity.

Because the beam energy in the injector is only 27-50 keV, high particle losses are present as a result of recombination on permanent gas. Besides, this results in a high sensitivity of a beam to stray magnetic fields of lenses, magnets, etc.

To optimize particle transmission through the accelerator, the first electrode of the accelerator tube is equipped with a grid.

3. High energy beam line for isotopic hydrogen beams

Interaction of protons and neutrons with nuclei are investigated in a separate target camera having a specify radiation protection. An extended beam line for transporting ion beams into this camera was developed (Fig.2). The beam line is equipped with two Q-poles lenses transporting the beam from crossover to crossover by monitors and steerers of the beam position. The beam position and its dimensions at the entrances into quadrupole lenses are monitored with special devices and quartz disks.

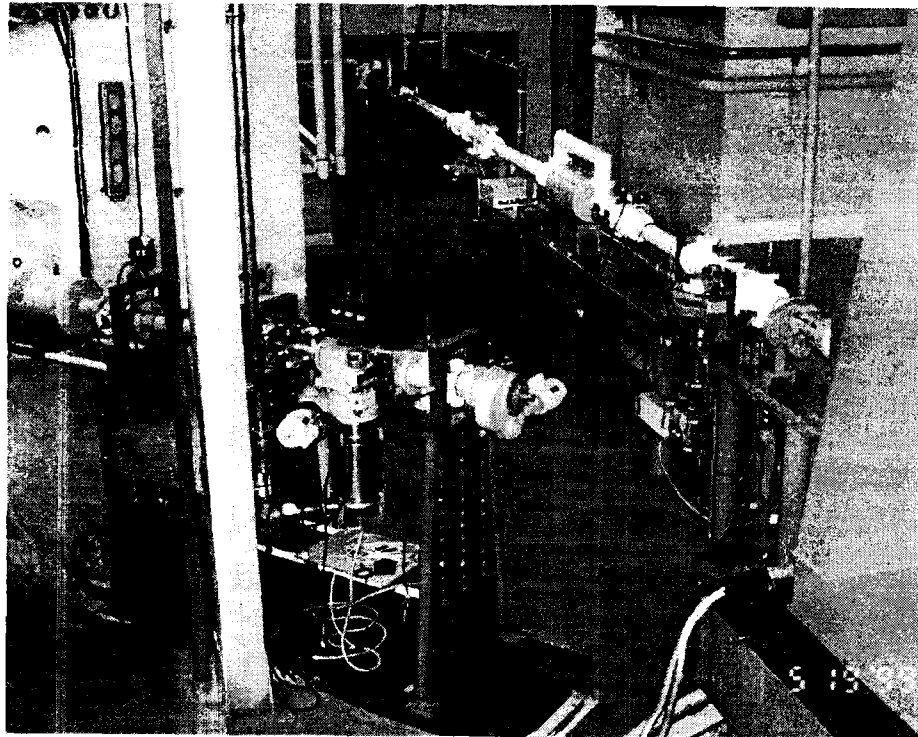


Fig. 2

The interconnection of an accelerator mass-separator and a beam line is effected by rotation of the magnet about vertical axis. This procedure is accompanied by time losses required for magnet rotation, beam line connection, electrical circuits interconnection and the mass-separator camera pumping.

4. Beam optics and experimental results

At the entrance of the low energy accelerator tube in the EGP-15 tandem a flat metal grid is present that determines the shape of the electrostatic field boundary. Opposite to the grid a cylindrical electrode is located. A potential was applied between them, and this way a controlling immerse lens was formed. During operation of any of the two ion sources, the injectors quadrupole lens produces a beam cross-over at the buncher exit diaphragm (Fig. 1). It was supposed that low emittance continuous beam after the buncher would be drifted to the grid lens at the entrance of the accelerator tube. This lens had to focus the beam into the stripping target of the accelerator. An additional quadrupole lens is installed at the injector outlet for pulsed beams or heavy ion beams having large emittance. The calculated beam envelopes for these both situations are presented in Fig. 3. This time, the works on beam transport is performed only for one ion source, without using the vertical ray of a mass-separator.

Experiments on a beam transport through the accelerator in the absence of the lens supplied by a grid were performed. The transmission of continuous beams was equal 30-40% for the injection energy of 30 keV. The transmission of pulsed proton beam was equal 20%.

The time dependent characteristics of pulsed beam were measured using the depth of the γ -peak from the target (Fig. 4). Taking into account the used instrument resolution time (~ 1 ns), the duration of the pulsed beam was equal ~ 1 ns.

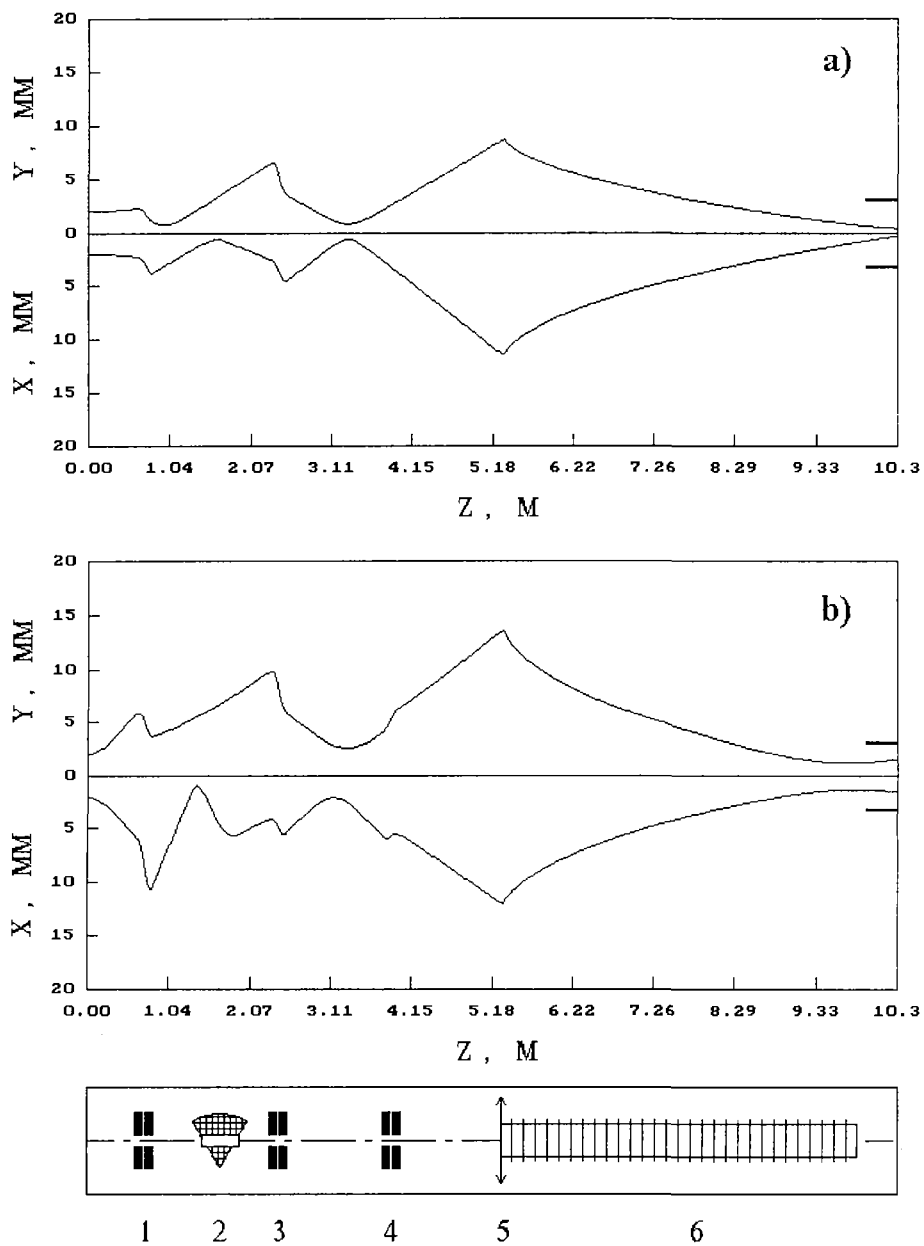


Fig. 3. Beam envelopes of a) H⁺ ions and b) Si⁺ ions in the low energy stage of the EGP-15 tandem. The entrance gridded lens is switched on. 1,3,4- quadrupole lenses; 2- analysing magnet; 5- immersion lens; 6- low energy accelerating tube.

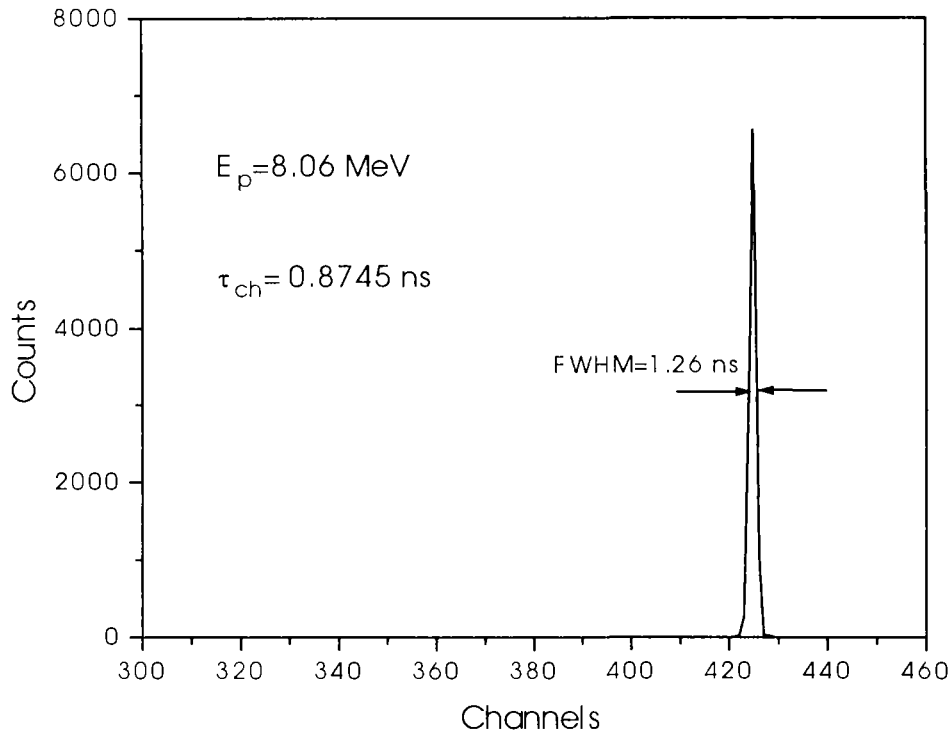


Fig. 4. The γ -rays spectrum from Al target.

5. Solid state physics study preparation

At the EGP-15 tandem the activity is aimed to design two additional beamlines for the solid state physical experiments. One of them is intended for the material radiation damage study. Another similar beam line is developed for the investigation of material. In this beamline the proton beam will be transmitted through a window into the air and will irradiate samples. Radiation stimulated changes in Young modulus and microplastic properties of metals and dielectrics will be studied. Besides, mirror and dielectrics optical properties used in thermonuclear facilities will be studied. In situ and post radiation measurements are planned. Optical and acoustic properties of samples will be measured simultaneously. Similar study was performed at the EGP-10M tandem [2].

References

1. B.V.Kuprijanov, V.S.Bashmakov, A.I.Glotov, V.A.Romanov, Yu.R.Tchaly, Low energy injector for the IPPE EGP-15, Obninsk, Proc. of the 12-th Conf. Of Electrostatic accelerators, November 25-28, 1997, Obninsk, Russia, 1999.
2. V.A.Stepanov, V.M.Chernov, A.I.Glotov, B.K.Kardashev, Plaksin, V.A.Romanov, Accelerators of SSC RF-IPPE for in-situ irradiation testing of mechanical and optical properties of materials, Report paper on ICFRM-9, Colorado Springs, Colorado, October 1999.

Quantitative Estimation of Effect of Polarity on the Accelerator Gas Gaps Breakdownvoltage

Proceedings of the XIII International Conference on Electrostatic Accelerators, Obninsk, 25–28th of May 1999, Obninsk: IPPE (in print)

K.A. Rezvykh, A.I. Glotov

Abstract

Effect of polarity is connected in great extent with appearance of volume charges which change radically the electrostatic field of electrodes. Therefore this problem is on the verge of possibility.

Negative polarity coefficient k_{pol} (negative and positive breakdown voltages ratio) can have one of three values: $k_{pol} = 1$, $k_{pol} < 1$, $k_{pol} > 1$. The developed theoretical model shows that the polar effect and phenomena connected (an «abnormal» breakdown with positive polarity, dominant influence of photoeffect near negative electrode surface, positive leader breakdown at electrostatic macrofield and at surface microstructure) depend first of all upon two special arguments: gas pressure and field nonuniformity coefficient. On the second stage of estimation the polarity coefficient value and calculated area boundaries are obtained in general form, as a function of high-voltage structure parameters.

Published experimental findings are included in files used at empirical formulae verified by other experimental results.

Besides polar effect estimation the reliability limits were verified for the breakdown voltage calculation by the method of the base if a volume charge is taken into account.

Figs. 10, Tables 3, Refs. 27.

Gases Breakdown Voltage Calculation for the Case of Accelerator Nonuniform Fields by Method of the Base

Nuclear Instruments and Methods in Physics Research A 423 (1999) 203–212

K.A. Rezvykh, V.A. Romanov

Abstract

The method for calculating the breakdown voltage of gas insulation of gaps in an accelerator has been developed. Firstly a new model of the insulation system element has been proposed according to the results of tests for the EG-2.5 Van de Graaff accelerator, IPPE. Then a complete-enough set of causes (factors) for the gas breakdown has been defined based on the experimental and calculation study. The calculation method includes a combination of some analytical equations coupled with the results of a special experiment with breakdown. A conclusion is made based on the comparison of experimental and calculated findings for the EG-2.5, MP and FN accelerators and other insulation structures that the accepted element model and the dependencies of the breakdown voltage on the main factors used here are adequate to the gas discharge nature of different gases. Since the calculation error is within the limit for the input data, the method described allows to predict the breakdown voltage for insulation gaps of an accelerator with accuracy of 1-5% . Figs. 2, table 1, Refs. 35.

Upgrading of EGP-15 Tandem High-Voltage Structure

Proceedings of the XIII International Conference on Electrostatic Accelerators,
Obninsk, 25–28th of May 1999, Obninsk: IPPE (in print)

K.A. Rezykh, V.A. Romanov

Abstract

Seven accelerators are compared for tank diameter 1.2 and 2.0 m. The upgrading effect is 1.53 and 1.17 for EN tandem and FN tandem respectively. Upgrading of the high-voltage structure must be complex. Economic calculations show that upgrading of EGP-15 terminal form costs 4–5 times cheaper than the year input of SF₆. Nowadays the most inexpensive structure modification is considered. Figs. 5, Tables 2, Refs. 10.

2.9 INSTRUMENTS AND METHODS

The Detector of Low Energy Neutrons with Thick Lithium Glass

*V.A. Talalaev, S.P. Simakov, B.V. Devkin, M.G. Kobozev, U. von Möllendorff**

**Forschungszentrum Karlsruhe, Institut für Kern- und Energietechnik,
Karlsruhe, Germany*

The purpose of the present experimental studies was to investigate properties of the detector, based on the ${}^6\text{Li}$ glass scintillators of different types and thickness: NE-905 ($\text{Ø}25 \times 3$ mm) and KG2L ($\text{Ø}51 \times 25$ mm). So far as the thresholds of the detectors, based on the organic scintillators, are above 30–50 keV, therefore, the necessity of studies neutrons in the keV energy range by the time-of-flight technique have involved the use ${}^6\text{Li}$ glass scintillators. The detectors haven't the threshold, they have reasonable time resolution and their efficiency grow up with the increase of the thickness of glass [1, 2]. The major difficulty the use of these detectors has been that their efficiency was not always known accurately, because of increase neutron multiple scattering and self-screen, and so the calculations of the efficiency are limited by that.

The main problem of this work was to investigate thick ${}^6\text{Li}$ glass KG2L ($\text{Ø}51 \times 25$ mm) with low-level fluor, which was coupled to $\Phi\text{ЭY-143-1}$ photomultiplier tube.

In our experiments amplitude characteristics were following: pulse height resolution varied from 20% FWHM for NE-905 up to 40% FWHM for KG2L. For purposes of the optimization detector's characteristics, filters from polyethylene and lead were placed in front of detector. We have found, that polyethylene filters with thickness 10 mm and 20 mm result in small changes in the amplitude of the neutron peak, and filter 40 mm thickness increase they significantly. The lead filter with 40 mm thickness decreases significantly γ -ray background at insignificant decreasing of the neutron peak. The timing characteristics were obtained by the time correlation method with ${}^{60}\text{Co}$ γ -source. For the NE-905 the time resolution was ~ 3 ns, and for KG2L – 4 ns, that suit that for organic scintillators at threshold ~ 100 keV.

The detector efficiency was defined relatively to the fission spectrum ${}^{252}\text{Cf}$, smoothed by the polyethylene filter, Fig. 1. Absolute value of the efficiency varied in the energy region 10 keV – 1 MeV from 1% up to 10%. For the true calibration we, also, had carried measurements with aluminium filter, which has some narrow resonances in the energy region under investigation, Fig. 2. The calculations of the efficiency were made with the MCNP-4b code, using ENDF-B6 nuclear data library, which predicts efficiency satisfactory.

The analysis of the characteristics of the detector, based on the thick lithium glass KG2L, allows to conclude, that it can be used for the investigations by time-of-flight technique the spectra of the secondary neutrons from the reactions (n,n'), (n,2n) and (n,fn).

References

1. J.M. Neil, D. Huffman et al. Nucl. Instr. and Meth., 1970, v. 82, p. 162
2. V.N. Kononov et al. Nucl. Instr. and Meth., 1985, v. A234, p. 36

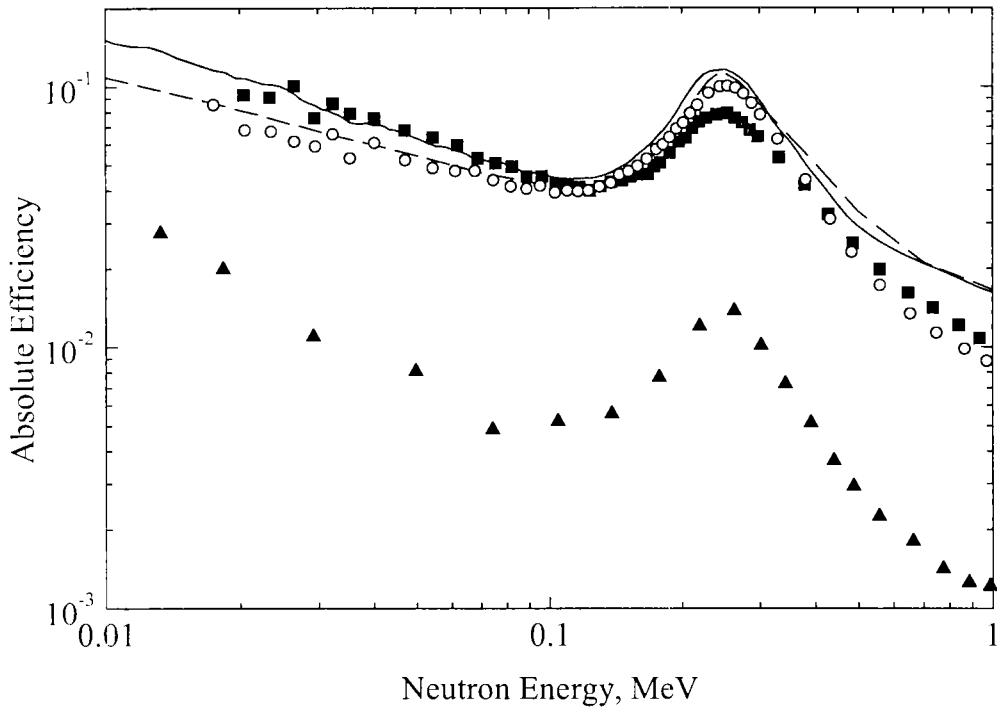


Fig. 1. Efficiency of Li-glass detector versus neutron energy: KG2L with polyethylene filter of 5 mm thickness (■) and without (○). Curves – calculation with filter (—) and without (- - -); NE-905 without filter (▲)

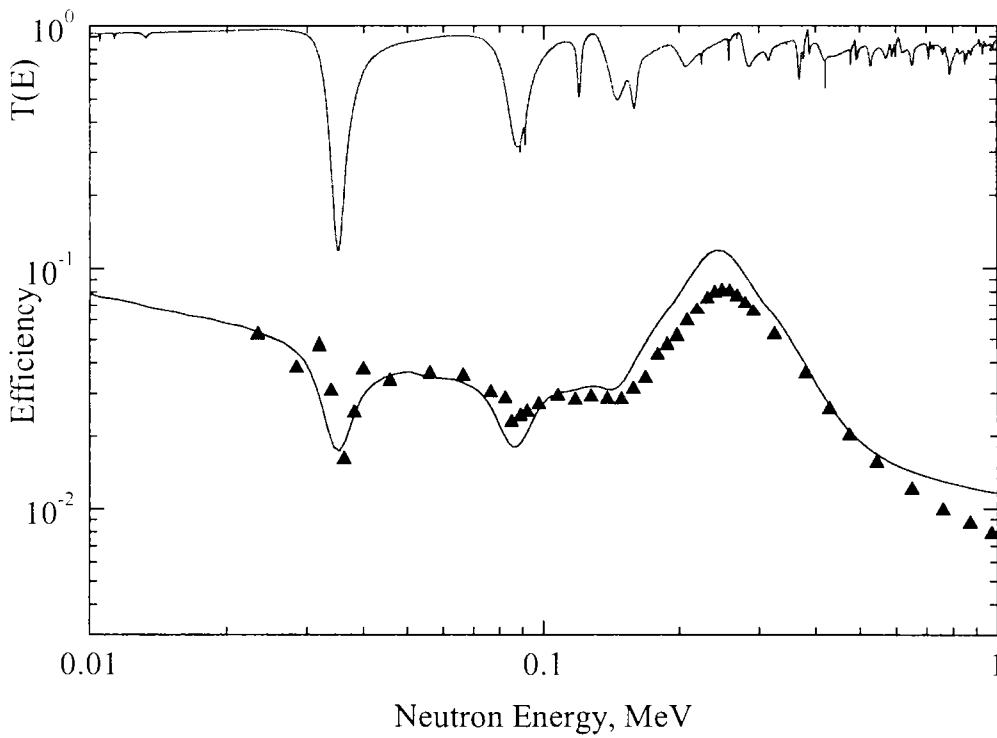


Fig. 2. Efficiency of Li-glass (KG2L) detector versus neutron energy with aluminum filter of 10 mm: ▲ – experiment, — – calculation. Transmission of aluminum filter (—)

Low Background Spectrometer for the Study of Fast Neutron Induced (n, α) Reactions

V.A. Khriachkov, V.V. Ketlerov, V.F. Mitrofanov, N.N. Semenova

Cross-section data for neutron-induced (n, α) reactions are of prime importance to evaluate radiation damage, nuclear heating in fusion and reactors, and for the selection of structural materials. At present, gridded ionization chambers are very popular for the investigation of neutron-induced reactions like (n, α) owing to their large geometrical efficiency (close to 100%), capability of energy-angle determination, good energy resolution and radiation durability [1-5]. However, under fast neutron bombardment the counting gas of the ionization chamber itself becomes an α -particle source.

The combination of the gridded ionization chamber and a waveform digitizer is a further development of this method of simultaneous measurements of the signal amplitudes from the ionization chamber electrodes. However applying the waveform digitizer we have much more information on charged particle properties. From the amplitude and the shape of the digitized anode signal we can derive information both on energy and emission angle of the particles originating from the cathode and on the location and the track direction of α -particles originating from a gaseous target. The latter can be used for the suppression of background events due to neutron interactions with the counting gas.

The α -particle spectrometer is based on the classical parallel plate ionization chamber with Frisch grid. The experimental setup is shown in Fig. 1. The anode signals after charge-sensitive preamplifier and fast amplifier are digitized by a LeCroy Waveform Digitizer 2262 (with a sampling time of 12,5 ns). The cathode signals are used as stop signals for the digitizer after a delay of 4 μ s. The host computer (PC386) reads the digitized signal as an array of 512 samples spaced by 12,5 ns. The data are sent to another computer via a local area network for storage and processing.

Each digital oscillogram of the anode signal contains practically the complete

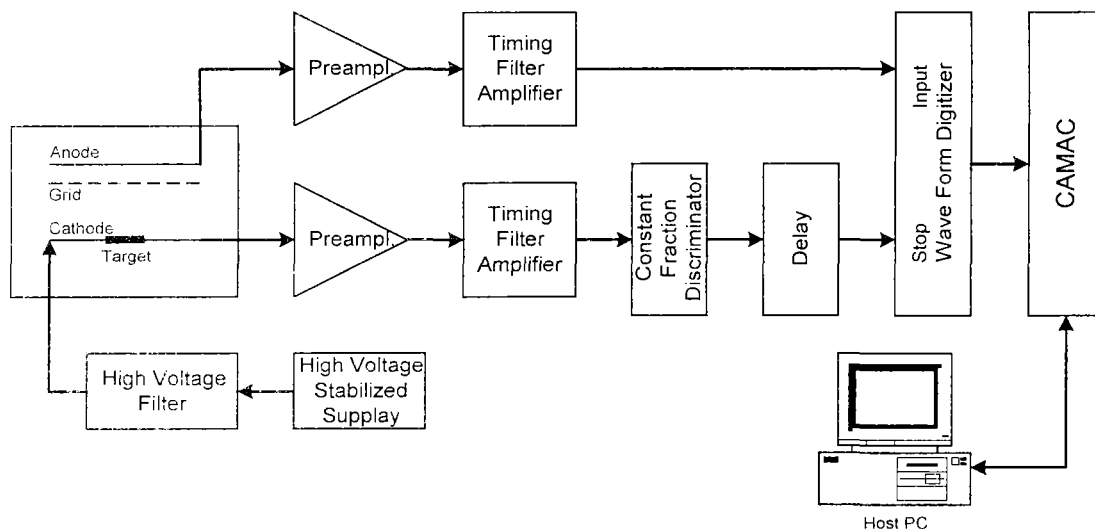


Fig.1. Scheme of the experimental setup for α -particle spectroscopy.

information both about the α -particle and about the conditions of the registration process. Thus, the amplitude of the anode signal is proportional to the energy of the α -particle. For a precise determination of the energy it is necessary to take into account the Frisch grid inefficiency and the energy loss in the sample. The rise time of the anode signal for α -particles of fixed energy is proportional to $\cos\theta$. The geometrical efficiency of the detector is close to 100% including the effect of self-absorption of the α -particles in the source. For the spontaneous alpha decay of ^{252}Cf ($E_\alpha=6,12$ MeV) we have obtained an energy resolution of 40 keV for the angular cone $\cos\theta > 0,7$.

Let us consider a chamber in which both the solid target on the cathode and the working gas are the alpha-particle sources. Depending on the track position in the volume of the chamber, all α -particles can be divided into three groups: the “cathode” α -particles (which are emitted from the solid target), the “false-cathode” α -particles (which are born in the working gas and hit the cathode) and the “gaseous” α -particles (which are born in the working gas and do not hit the cathode). The separation method for these α -particle groups is based on the analysis of the arrival time of the last electron to the anode. For “cathode” particles this time is fixed, while for “gaseous” particles this time can change over a wide range. Therefore the analysis of the arrival time of the last electron from the ionization track τ allows rejecting a large part of “gaseous” α -particles.

The shape of the anode signal contains information about the ionization density along the track. It is known that for α -particles the ionization power has its maximum at the end of the track. It means that we can determine the direction of the particle movement and also reject the part of the “false-cathode” α -particles moving to the cathode.

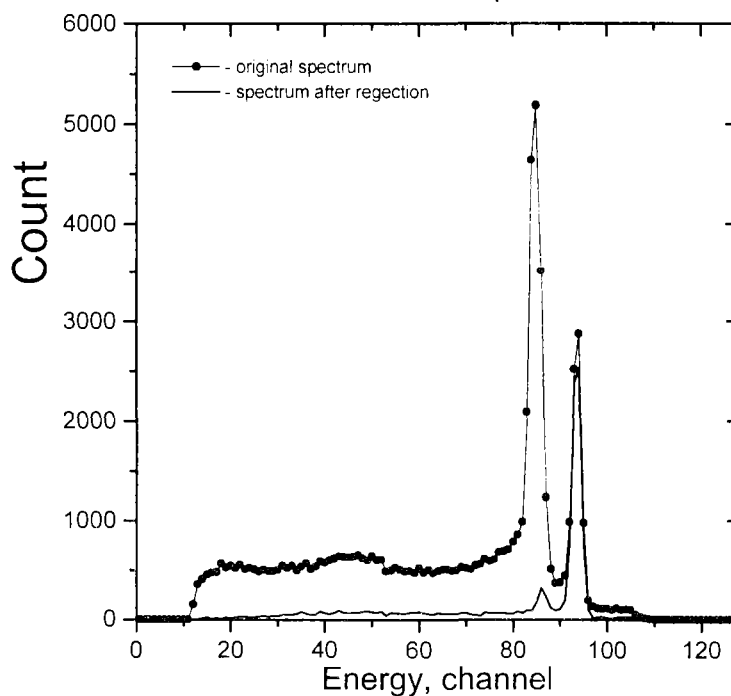


Fig.2. Original pulse height spectrum of α -particles of ^{218}Po and ^{222}Rn (symbols with line) and after rejection of “gaseous” α -particles (thin line)

In order to get the situation when both the “cathode” α -particles and “gaseous” α -particles are present in the ionization chamber, the gaseous ^{222}Rn was added to the working gas. The α -particles of radon are born at any point of the chamber volume with equal probability. ^{218}Po which is the product of the ^{222}Rn α -decay was absorbed on the cathode making a thin solid target of α -particles (half-life 3.1 min). We can reject the main part of the “gaseous” α -particle background by selecting only those events inside the $\Delta\tau$ – window near the maximum value of τ . In order to separate the “cathode” and “false-cathode” α -particles having both the maximum value of τ it is necessary to analyze the shape of the anode pulses. It has been already noted that for α -particles the ionization power has its maximum at the end of the track. It means that for “cathode” α -particles moving to the anode the first part of the rise time must be steeper than the last one. For the “false – cathode” α -particles moving to the cathode the situation must be the opposite. Fig. 2 shows the original pulse height spectrum of α -particles and the one after rejection. From the corresponding peak areas one can conclude that the gaseous fraction of the α -particles was suppressed by a factor of 30.

References

1. C. Budtz-Jørgensen and H.-H. Knitter, Nucl. Instr. and Meth. 223 (1984) 295-302.
2. A.A. Goverdovsky, V.V. Ketlerov, V.A. Khriachkov, V.F. Mitrofanov, H. Vonach and R.C. Haight, Proc. Int. Conf. on Nucl. Data for Sci. and Technol., Gatlinburg, USA (1994) ed. J.K. Dickens, pp. 117-123.
3. N. Ito, M. Baba, S. Matsuyama, I. Matsuyama and N. Hirakawa, Nucl. Instr. and Meth. A 337 (1994) 474-485.
4. Yu.M. Gledenov, V.I. Salatski, P.V. Sedyshev, P.J. Szalanski, J. Andrzejewski and A. Zak, Proc. Int. Conf. on Nucl. Data for Sci. and Technol., Trieste, Italy (1997) ed. G. Reffo, pp.511-516.
5. V.A. Khryachkov, A.A. Goverdovskij, V.V. Ketlerov, V.F. Mitrofanov and N.N. Semenova, Instruments and Experimental Techniques Vol.41, No.2 (1998) pp. 171-175.

3. ACCELERATORS COMPLEX

During 1999 four accelerators were operated providing the necessary experimental base for researches in the Nuclear Physics Department. The main parameters of accelerators are given in Table.

Accelerator type	Singly-charged ion energy (MeV)	Ions type	Operation conditions	Ion beam parameters	Operation time
EG-1	1,5-4,0	p,d	Pulsed	Pulse duration-2ns Pulse repetition-1; 2MHz Pulse beam current-2,5mA	2000h
KG-2,5	0,2-2,0	p,d	Continuous	Beam current 10-100 μ A	2100h
EGP-10M	4,0-9,2	p,d	Continuous Pulsed	Beam current 0,1-2,0 μ A Pulse duration-1,0ns Pulse repetition-2,5MHz Pulse beam current-0,2mA	120h 900h $\Sigma=920h$
EGP-15	5,0-11,5	p	Continuous Pulsed	Beam current 0,1-2,0 μ A Pulse duration-1,0ns Pulse repetition-2,5MHz Pulse beam current-0,2 μ A	50h 150h $\Sigma=200h$

During 1999 accelerator EGP-15 was operated for nuclear physics tasks fulfillment.

4. PUBLICATIONS

THEORETICAL NUCLEAR PHYSICS DIVISION

1. I.N Borzov. Theoretical weak rates for astrophysics. Proc. Conf. on beta-decay. from weak interaction to nuclear structure, Strasbourg, France, 17-19.03.99, p.43-50.
2. A Bobyk, I.N Borzov, W.A. Kaminski Gamow-Teller beta-decay strength of neutron-deficient tin isotopes: comparison of FFST and pnBCS+QRPA results. Acta Physica Polonica, 1999, to be publ.
3. I.N Borzov, S Goriely, J.M Pearson. Weak rates of neutron-rich nuclei and r-process nucleosynthesis. Phys.Rev.C, 1999, submitted.
4. I.N. Borzov. Nuclear structure effects in charged current neutrino capture rates of heavy nuclei. Phys.Lett. B, 1999, submitted.
5. S.Kamerdzhiev, J.Speth, G.Tertychny. Microscopic analysis of the breathing mode in ^{40}Ca and ^{58}Ni . Euro. Phys. J., ser. A, submitted.
6. S.Kamerdzhiev, J.Speth, G.Tertychny, No missing isoscalar monopole strength in ^{58}Ni : final result?. IKP-Annual Report 1999, submitted.
7. А.В. Авдеенков А.В., Камерджиев С.П. О механизмах сверхтекучести в атомных ядрах. Письма в ЖЭТФ, 1999, т. 69, с. 669.
8. Авдеенков А.В. Микроскопическое описание одночастичных характеристик немагических ядер. Автореф. дисс. канд. физ.-мат. наук, Дубна, ОИЯИ, 1999.
9. S.P.Kamerdzhiev, E.V.Litvinova, D Zawisha Role of quasiparticle-phonon interaction in non-magic nuclei. Phys. Rev. C, 1999, submitted.
10. A.V.Ignatyuk, V.P.Lunev, Yu.N.Shubin Yu.N., Yu.N Gai, N.N Titarenko, A.Ventura, W.W Gudowski. Neutron Cross Section Evaluations for U-238 up to 150 MeV. Nucl. Sci. Engin., 1999, to be publ.
11. Shubin Yu.N., Ignatyuk A.V., Lunev V.P. et al. Experimental and theoretical study of the yields of radionuclides produced in ^{nat}U thin targets irradiated by 100 and 800 MeV protons. In: Proc. 3d Conf. on Accelerator Driven Transmutation Technology and Applications (Prague, June 1999), to be publ.
12. Yu.N Shubin, A.V Ignatyuk, V.P Lunev et al. Experimental and theoretical study of the yields of radionuclides produced in ^{232}Th thin targets irradiated by 100 and 800 MeV protons. Ibid.
13. A.V.Ignatyuk, V.P.Lunev, Yu.N.Shubin, E.V.Gai, N.N.Titarenko, W.Gudowski W. Neutron cross section Evaluations for ^{232}Th up to 150 MeV. Ibid.
14. E.V Gai, A.V.Ignatyuk, V.P Lunev, Yu.N Shubin. Safety aspects of targets for ADT: activities, volatile products, residual heat release. Ibid.
15. V.N.Mikhailov, S.T.Belyaev, Yu.A.Sokolov, O.V.Shvedov, N.S.Rabotnov, Yu.N.Shubin Russian Minatom Program on ADT Research. Ibid.
16. V.I Levanov, V.I Pankratov, E.I Efimov, Yu.N Shubin. Radiological properties of heavy liquid metal targets of accelerator driven systems. Ibid.
17. G.L.Khorosanov, A.P.Ivanov, A.I.Blokhin et al. Lead and tin targets for reducing polonium waste. Ibid.
18. E.V.Gai., A.E.Ivanov, A.L.Kochetkov, N.S Rabotnov. On Criteria of minor actinides transmutation efficiency. Ibid.

19. E.V.Gai, A.E.Ivanov, A.L.Kochetkov, N.S.Robotnov. Calculations of Isotopic Composition, Residual Heat and Helium Content of Spent AMOX Fuel of BOR-60 Reactor. In: Proc. Conf. on Future Nuclear Systems: GLOBAL'99 (Wyoming, August 1999), USA, CD-edition.
20. V.P.Lunev, V.P.Shubin, C.Grandi, B.Poli, A.Ventura. Effect of the level density and reaction mechanisms on cross section calculations at intermediate energies. *Il Nuovo Cimento*, vol. 112 A, 743 (1999).
21. S.A.Badikov, E.V.Gai, N.S.Robotnov. An efficient way of the representation of covariance data in ENDF-6 format for fast neutron reaction cross sections. In: Proc. BNL Covariance Workshop (Brookhaven, April 1999), to be publ.
22. Е.В.Гай, А.Е.Иванов, А.Л.Кочетков, Н.С.Работнов. Расчет нуклидных характеристик топлива с высоким содержанием америция после его облучения в БОР-60. *Атомная энергия*, 1999, в печати.
23. С.А.Бадиков, Е.В.Гай, Н.С.Работнов. Одновременный статистический анализ больших массивов коррелированных нейтронных измерений. Направлена в Атомную энергию, 1999.
24. А.В.Субботин, Б.С.Родченков, Н.А.Дёмин, А.В.Целищев. Анализ возможности прогнозирования работоспособности конструкционных материалов ТЯР посредством облучения их в исследовательских реакторах. (Часть 1). Отчет НИКИЭТ 070-248-5357, 1999.
25. Н.А.Дёмин, Э.А.Коптелов, Е.Ю.Ривкин, Е.Ю.Семёнов, А.В.Субботин, А.В.Целищев. Анализ фундаментальных процессов радиационно-стимулированной эволюции микроструктуры и изменения свойств реакторных корпусных сталей. Отчет НИКИЭТ 070-248-5381, 1999.
26. Н.А.Дёмин, А.В.Субботин. Нарботки гелия и водорода в никеле за счет двухстадийных реакций в реакторе ИВВ-2М. Отчет НИКИЭТ 070-248-5382, 1999.
27. А.В.Субботин, Б.С.Родченков, Н.А.Дёмин, Н.А.Целищев. Анализ возможности прогнозирования работоспособности конструкционных материалов ТЯР посредством облучения их в исследовательских реакторах. (Часть 2). Отчет НИКИЭТ 070-248-5383, 1999.
28. V.N.Manokhin. Some considerations concerning $^{58}\text{Ni}(n,\alpha)$ reaction. *Вопросы атомной науки и техники, Сер. Ядерные константы*, 1999, №1, с.39.
29. A.I.Blokhin, A.S.Badikov, A.V.Ignatyuk, V.P.Lunev, V.N.Manokhin, G.Ya.Tertychnyi, K.I.Zolotarev. Evaluation of cross sections for Cm-242,-243,-244. *Вопросы атомной науки и техники, Сер. Ядерные константы*, 1999, №2.
30. V.N. Manokhin, A.I.Blokhin, Empirical systematics for the analysis of threshold reaction excitation functions. Report to Symposium on Nuclear Data (18-19 November, Japan).
31. A.V.Ignatyuk. Level density systematics for astrophysical applications Proc. 10th. Symp. on gamma-ray spectroscopy and related topics. (Santa Fe, September 1999), to be publ.
32. A.V.Ignatyuk, A.I.Blokhin, V.P.Lunev, V.N.Manokhin, S.P.Simakov, G.Ya.Tertychnyi, K.I.Zolotarev. New evaluation of gamma-ray production cross sections for lead and bismuth. *Ibid.*

33. A.G.Zvenigorodskii, M.S.Shvetsov, A.M.Shvetsov, M.V.Savin, Yu.Ya.Nefedov, A.I.Blokhin. Evaluation of gamma-ray production cross-sections for inelastic neutron interaction with aluminium and lead. Proc.of the 9th International Conference on Radiation Shielding (Japan, October 1999).
34. M.V.Savin, A.V.Livke, Yu.Ya.Nefedov, M.S.Shvetsov, A.G.Zvenigorodskii, A.I.Blokhin. Evaluation of angular distributions and gamma-ray production cross sections for iron. Proc. of the 9th International Conference on Radiation Shielding (Japan, October 1999).
35. A.I.Blokhin, A.V.Ignatyuk, L.A.Trykov, G.Ya.Tertychnyi, K.I.Zolotarev Integral test of evaluated nuclear data for zirconium, lead and bismuth materials. Proc. of the 9th International Conference on Radiation Shielding (Japan, October 1999).
36. Г.Л.Хорасанов, А.П.Иванов, В.В.Коробейников, А.И.Блохин, А.Л.Шимкевич. Свинцовый теплоноситель для быстрого реактора-выжигателя с жестким спектром нейтронов. // Известия ВУЗ'ов. Ядерная энергетика, 1999, №1, с.80.
37. G.L.Khorosanov, A.P.Ivanov, A.I.Blokhin, A.L.Shimkevich, M.V. Mikhailyukova, V.A.Apse, A.N.Shmelev, G.G.Koulikov, A.A.Glazkov, A.D.Kolyaskin. Low-activation materials with isotopic tailoring for future NPPs. In: Proceedings of the Int.Conf. on Future Nuclear Systems GLOBAL'99, August 29-September 3, 1999, Jackson Hole, Wyoming, USA, Paper N345.
38. Г.Л.Хорасанов, А.П.Иванов, А.И.Блохин, А.Ю.Конобеев, М.В.Михайлюкова, А.Д.Коляскин, А.А.Глазков. Проблема накопления радионуклида Bi-207 в свинцовых мишенях электроядерных систем. В сб.: Труды Международного семинара "Электроядерные системы в перспективной ядерной энергетике". 11-16 октября 1999 г., Москва. М.: ИТЭФ, 1999.
39. G.L.Khorosanov, A.P.Ivanov, A.I.Blokhin, M.V.Mikhailyukova, A.A.Glazkov, A.D.Kolyaskin. Molten lead enriched with isotope Pb-206 as a low-activation coolant for emerging nuclear power systems. Paper#8385 accepted at the 8th Int. Conf. on Nuclear Engineering ICONE-8, April 2-6, 2000, Baltimore, Maryland, USA. (in press)

EXPERIMENTAL NUCLEAR PHYSICS DIVISION

1. S.P. Simakov, G.N. Lovchikova, A.M. Trufanov, V.A. Vinogradov, M.G. Kobozev. Spectrum of Neutron Source Based on a Solid Tritium Target. // Pribory i Technika Experimenta, 1999, № 6, стр. 5-12
2. S.P. Simakov, B.V. Devkin, M.G. Kobozev, U. von Moellendorff, D. Chuvilin. Benchmarking of the evaluated data for nickel by a 14 MeV spherical shell transmission experiment. // Fusion Technology, 1999, v. 36, no 2, p. 173
3. S.P. Simakov, B.V. Devkin, M.G. Kobozev, V.A. Talalev, U. von Moellendorff. Benchmarking of evaluated nuclear data for bismuth by spherical shell transmission experiments with central T(d,n) and Cf-252 neutron sources. // Fusion Engineering and Design, 1999, v. 46, no. 1, p. 99
4. B.V. Devkin, M.G. Kobozev, A.A. Lychagin, S.P. Simakov, V.A. Talalaev. Differential Cross Sections of U(n,xn) Reaction at 14.3 MeV Neutron Energy. // Voprosy Atomnoy Nauki i Techniki, Seriya Yadernye Konstanty, 1999, vol. 2
5. V.A. Talalaev, S.P. Simakov, B.V. Devkin, M.G. Kobozev, U. von Moellendorff. The Detector of Low Energy Neutrons with Thick Lithium Glass. // Preprint FEI-2765, Obninsk, 1999

6. U. von Moellendorff, S.P. Simakov. Integral experiments for validating fusion relevant nuclear data of vanadium. // Межд. семинар «Потенциал российских ядерных центров и МНТЦ в тритиевых технологиях», Саров, 1999
7. S. Hlavac, M. Benovic, E. Betak, L. Dostal, I. Turzo, S.P. Simakov. Cross Sections for Discrete γ Ray Production in Interactions of 14.6 MeV Neutrons with Light and Medium Heavy Nuclei. // Report INDC(NDS)-412, IAEA, Vienna, 1999, p.12

CONDENSED MATTER PHYSICS LABORATORY

1. A.G.Novikov, M.N.Rodnikova, J.Barthel, O.V.Sobolev, Quasielastic neutron scattering of aqueous tetrabutylammonium chloride solutions, J.of Mol.Liquids, 79(1999)203-212.
2. A.G.Novikov, M.N.Rodnikova, O.V.Sobolev. The study of hydration effects in aqueous solutions LiCl and CsCl byinelastic neutron scattering. J. of Mol. Liquids. 82(1999)83-104.
3. А.Г.Новиков, М.Н.Родникова, О.В.Соболев. Эффекты гидрофобной гидратации из экспериментов по неупругому рассеянию. // Ж. физ. химии. 72(1998)2232-2234.
4. A.G.Novikov, V.V.Savostin, A.L.Shimkevich, M.V.Zaezjev, «Oxygen microscopic dynamics in liquid potassium studied by inelastic neutron scattering», J. of Non-Cryst. Solids. 250-252(1999)124-128.
5. M.V.Zaezjev, A.G.Novikov, V.V.Savostin, «Isochoric specific heat and anharmonicity for liquid potassuim», J. of Non-Cryst. Solids 250-252(1999)12-123.
6. A.Novikov, M.Rodnikova, O.Sobolev. «Comparative analysis of ionic and hydrophobic hydration effects», FLNF Annual Report 1998, p.87.
7. A.Novikov, D.Seliverstov, O.Sobolev. «Some structural and dynamical properties of liquid POCl₃», FLNF Annual Report 1998, p89.
8. A.Novikov, I.Padureanu, V.Savostin «Atomic dynamics in liquid gallium», Abstracts of ECNS'99, Budapest, 1999, p.141.
9. I.Padureanu, A.Radulescu, A.Beldiman, M.Ion, A.G.Novikov, V.Savostin, Zh.A.Kozlov «Inelastic neutron scattering on liquid gallium», Abstracts of ECNS'99, Budapest, 1999, p.140.
10. A.G.Novikov, M.N.Rodnikova, O.V.Sobolev, The investigation of hydrophobic hydration effects, Abstracts of ECNS'99, Budapest, 1999, p.269.
11. А.Г.Новиков, М.Н.Родников, О.В.Соболев, Тезисы доклада «Метод нейтронного рассеяния и кинетика гидратации», 10-я Всероссийская конференция по межмолекулярным взаимодействиям, Казань, 30 июня-3 июля 1999.
12. А.В.Кнотько, В.И.Путляев, С.И.Морозов «Исследование фононного спектра Nd-содержащих твердых растворов на основе Bi₂Sr₂CaCu₂O₈ методом неупругого рассеяния нейтронов» направлена в ФТТ.
13. S.I.Morozov, Band and local modes of hydrogen in V-O-H interstitial phases, Abstracts of ECNS'99, Budapest, 1999, p.82.
14. О.А.Дубовский. Кинематический квазивакансионный биэкситон Френкеля в лавыдовском мультиплете. // ФТТ 41(1999)423.
15. О.А.Дубовский, А.В.Орлов. Локальные поляритоны нового типа на границе раздела гиротропных энантиоморфных кристаллов. // ФТТ 41(1999)337.

16. О.А.Дубовский, А.В.Орлов, Солитоны в двумерных и трехмерных кристаллах при Ферми-резонансе оптических колебаний, ФТТ 41(1999)712.
17. I.V.Bogoyavlenskii, A.V.Puchkov and A.Skomorokhov, "The correlation between Bose condensation and helium excitations in neutron scattering study," Abstracts of ECNS'99, Budapest, 1999, p.141.
18. I.V.Bogoyavlenskii, A.V.Puchkov and A.Skomorokhov, "Study of the Phonon-Maxon region of the liquid helium dispersion curve - the latest results" Abstracts of XXII Intern.Conf.on Low Temp.Physics, LT22, Helsinki, p.297, 1999.
19. С.А.Данилкин, А.Г.Новиков, А.В.Пучков, «О возможной модификации спектрометра ДИН-2ПИ»: Препринт ФЭИ-2760, Обнинск, 1999.
20. A.Beskrovni, S.Danilkin, H.Fuess, E.Jadrowski, M.Neova-Baeva, T.Wieder: "Effect of Cr Content on the Crystal Structure and Lattice Dynamics of FCC Fe-Cr-Ni-N Austenitic Alloys", J. of Alloys and Compounds, 1999, v.291, pp.262-268.
21. M.Baeva, A.Beskrovni, S.Danilkin, H.Fuess, E.Jadrowski, T.Wieder: X-Ray and Neutron Study of Crystal Structure and Lattice Dynamics of Fe-Cr-Mn-and Fe-Cr-Ni-Nitrogen Steels with Different Mn and Cr Content, Deutsche Neutronenstreutagung, 25-27 May, 1999, Potsdam, Germany.
22. S.Danilkin, D.Delafosse, H.Fuess, V.Gavriljuk, A.Ivanov, T.Magnin, H.Wipf Hydrogen vibrations in austenitic stainless steels, ILL Experimental Reports and Theory Activities, 1998.
23. S.Danilkin, D.Delafosse, H.Fuess, V.Gavriljuk, A.Ivanov, T.Magnin, H.Wipf: Hydrogen vibrations in austenitic stainless steels, Abstracts of ECNS'99, Budapest, 1999, p. 281.
24. A.Beskrovni, S.Danilkin, H.Fuess, E.Jadrowski, M.Neova-Baeva, T.Wieder: Crystal Structure and lattice dynamics of Fe-Cr-Mn-Ni-N austenitic steels, Abstracts of ECNS'99, Budapest, 1999, p. 281.
25. A.Radulescu, I.Padureanu, S.N.Rapeanu, A.Beldiman, Zh.A.Kozlov, V.A.Semenov. Low-frequency excitations in zirconium hydrides. Preprint JINR, E14-99-165, 1999.
26. A.Radulescu, I.Padureanu, S.N.Rapeanu, A.Beldiman, M.Ion, Zh.A.Kozlov, V.A.Semenov. Low-frequency collective modes in the superionic phase of lead fluoride studied by quasielastic cold neutron scattering. Physical Review B59(1999)3270.
27. A.Radulescu, I.Padureanu, A.Beldiman, S.N.Rapeanu, Zh.A.Kozlov, V.A.Semenov. Observation of Low-Frequency Excitations of Hydrogen in Zirconium. Abstracts of ECNS'99, Budapest, 1999, p.267.
28. S.N.Ishmaev, Y.V.Lisichkin, A.V.Puchkov, V.A.Semenov, E.Svab, G.F.Syrykh, Neutron scattering law study of isotopic Ni-B metallic glasses, Abstracts of ECNS'99, Budapest, 1999, p.142.
29. S.Danilkin V.Konstantinov, A.Kustov, A.Novikov, A.Puchkov, B.Solovjev, "Velocity Selector for SANS Spectrometer" Abstracts of ECNS'99, Budapest, 1999, p.26.
30. S.Danilkin, V.Konstantinov, A.Novikov, A.Puchkov, B.Solovjev, Sh.Zeinalov, A.Wiedenmann, "SANS Spectrometer for 1 MW NUR Reactor at URGN, Algeria" Abstracts of ECNS'99, Budapest, 1999, p.27.
31. В.В.Кузин, А.Г.Новиков, В.В.Савостин, И.Ю.Шимкевич, А.Л.Шимкевич, «Цепочечные кластеры растворенного кислорода в расплаве калия», Теплофизические исследования. Сборник статей к 80-летию академика РАН В.И.Субботина, Обнинск, 1999, с.171.

MATHEMATICS AND SOFTWARE DIVISION

1. A.Kartavykh, M.Mil'vidskii, V.Rakov, V.Ginkin, V.Artemyev, N.Gusev, V.Folomeev, T.Lyukhanova. Numerical Simulation of Anomalous Doping Effect in Ge Single Crystals Grown by FZ-Technique Aboard the Space Crafts. Third International Conference "Single Crystal Growth, Strength Problems, and Heat Mass Transfer", Obninsk, Russia, September 21-24, 1999. Abstracts, Obninsk, 1999, p.175-176.
2. V.P.Ginkin, A.I.Zinin, A.A.Izotov. The Numerical Simulation of a 2D Stefan Problem for the Directional Crystallization Method under the Microgravity Conditions. Third International Conference "Single Crystal Growth, Strength Problems, and Heat Mass Transfer", Obninsk, Russia, September 21-24, 1999. Abstracts, Obninsk, 1999, p.181.
3. I.P.Sviridenco, V.P.Shishulin, V.V.Kumskoy, Yu.N.Pokrovsky, V.K.Artemyev, V.P.Ginkin, N.V.Gusev. The Numerical and Experimental Research of High Temperature Zone in Floating Zone and Bridgman Installations for Crystal Growth. Third International Conference "Single Crystal Growth, Strength Problems, and Heat Mass Transfer", Obninsk, Russia, September 21-24, 1999. Abstracts, Obninsk, 1999, p.228-229.
4. I.P.Sviridenco, V.P.Ginkin. Thermophysical Research and Computer Software to Provide Development of Processing Equipment for Microelectronics. Third International Conference "Single Crystal Growth, Strength Problems, and Heat Mass Transfer", Obninsk, Russia, September 21-24, 1999. Abstracts, Obninsk, 1999, p.30.
5. V.K.Artemiev, V.P.Ginkin, T.M.Lukhanova, V.I.Folomeev. Numerical Benchmark for Calculation of Convective Heat Transfer During Crystal Growth by the Floating Zone Method under the Null Gravity Conditions. Proceedings of the International Conference on Computational Heat and Mass Transfer, Eastern Mediterranean University, G.Magusa, April 26-29, 1999, p.195-200.
6. V.P.Ginkin. Problems of Numerical Simulation in Crystal Growth Process. Proceedings of the International Conference on Computational Heat and Mass Transfer, Eastern Mediterranean University, G.Magusa, April 26-29, 1999, p.32-37.
7. V.K.Artemiev, N.A.Verezub, V.P.Ginkin, N.V.Gusev, A.Z.Mjal'dun, A.I.Prostomolotov. The Numerical and Experimental Study of the Bridgman Crystal Growth on a Model Device. Proceedings of the International Conference on Computational Heat and Mass Transfer, Eastern Mediterranean University, G.Magusa, April 26-29, 1999, p.201-206.
8. V.P.Ginkin. Numerical Simulation of the Single Crystal Growth Process. Book of Abstracts, PCC-99 Workshop on Phase Change with Convection Modelling and Validation, June 24-26, 1999, Warsaw, Poland, Instytut Podstawowych Problemow Techniki PAN, p.85-86.
9. E.Kornienko, Y.Kornienko. Generalized Integral Forms of Wall Friction, Heat and Mass Transfer Factors for Drift Flux Model of Two-Phase Flow in Axisymmetrical Channels." Book of Abstracts, PCC-99 Workshop on Phase Change with Convection Modelling and Validation, June 24-26, 1999, Warsaw, Poland, Instytut Podstawowych Problemow Techniki PAN, p.105.
10. В.П.Гинкин, А.В.Кулик. Оптимальный предобуславливатель в методе сопряжённых градиентов для трехмерной HEX-Z геометрии. Препринт ФЭИ-2786, Обнинск, 1999, 20с.

11. В.П.Гинкин, А.В.Кулик. Оптимальный предобуславливатель в методе сопряжённых градиентов для трехмерной HEX-Z геометрии. Доклад на отраслевом семинаре "Нейтроника-99", Обнинск, 27-30 сентября 1999.
12. В.К.Артемьев, В.П.Гинкин, Н.В.Гусев, И.П.Свириденко, В.П.Шишулин. Разработка и расчетное обоснование участка для ультразвуковой диагностики фронта кристаллизации в расплаве Ge в ростовой установке типа "Зона". //I-ая Российская конференция по космическому материаловедению. Изд-во НИЦ "Космическое материаловедение" ИК РАН, Калуга, 1999, с.38.
13. В.К.Артемьев, С.И.Зайцев, Ю.Н.Корниенко. Усовершенствование модели алгоритма расчета динамики аварийных режимов кода "ТРАП-97". Тезисы докладов на отраслевой конференции "Теплофизика-99", Обнинск, 28-30 сентября, с. 77.
14. V.K.Artemyev, V.P.Ginkin, V.D.Golyshev, M.A.Gonik and V.B.Tsvetovsky. Influence of Three Dimensional Flow on a Cross Section Impurity Distribution During Ge Single Crystal Growth by AHP-Method. Third International Conference "Single Crystals Growth, Strength Problems, and Heat Mass Transfer", Obninsk, 1999, p.215.
15. V.K.Artemyev, V.P.Ginkin, N.A.Gorev, N.V.Gusev, T.M.Lukhanova, A.Yu.Rakitin, A.S.Senchikov, I.V.Sleptsova, V.I.Folomeev. Numerical and Experimental Study of Heat Transfer Processes in Modular Furnace Polizon. Third International Conference "Single Crystal Growth, Strength Problems, and Heat Mass Transfer", Obninsk, 1999, p.222.
16. Проведение среднесрочных прогнозных расчетов миграции радиоактивных отходов от глубинного захоронения отходов на полигоне НИИАР с учетом анизотропии проводимости пород. Отчет ФЭИ-10092, 1999, с.43. -Исполн. А.И.Зинин, Г.А.Зинина.
17. C.Cole, M.Williams, M.Foley, K.Hoover, E.Drozdko, L.Samsonova, N.Vasilkova, A.Zinin, G.Zinina. Development and Calibration of a Three-Dimensional Regional Hydrogeologic Model of the Majak Site, Urals. Book of Abstracts of the Forth Joint Conference on Environmental Hydrology and Hydrogeology, 1999, San -Francisco.
18. E.Drozdko, I.Ivanov, J.Mokrov, L.Samsonova, N.Vasilkova, A.Zinin, G.Zinina. Experience of Contaminant Transport Forecasting at the Mayak Site (GEON-3D Model). Book of Abstracts of the Forth Joint Conference on Environmental Hydrology and Hydrogeology, 1999, San -Francisco.
19. Ю.Н.Корниенко. К разработке аналитических замыкающих соотношений коэффициентов пристенного трения, тепло- и массообмена для кольцевой и субканальной геометрии. // Труды отрас. конф. "Теплофизика-99". Обнинск, 1999, стр.62-65.
20. Y.Kornienko, H.Ninokata. Influences of the Transversal Non-Homogeneous Parameter Distribution on Wall Friction, Heat and Mass Transfers in Single- and Two-Phase Flows in Vertical Annular and Subchannel Geometries. Proc. of ICONE-7, Trac.7, CD-Room, 19-23 April 1999, Tokyo, Japan.
21. Y.Kornienko, H.Ninokata. "Development of Generalized Integral Forms of Local and Subchannel Wall Friction, Heat and Mass Transfer Coefficients in Single- and Two-Phase Flows", Препринт ФЭИ-2791, Обнинск, 1999, 27с.

22. Развитие методов построения замыкающих соотношений неравновесных двухфазных парожидкостных потоков для кодов «улучшенных оценок» для расчетов аварийных режимов ЯЭУ: Отчет ФЭИ-10089, 1999. - Исполн. Е.В.Корниенко, Ю.Н.Корниенко.
23. Y.Kornienko. "Analytical model for estimation of friction and heat transfer in two-phase flow with saddle-shape void fraction profile." Fourth International Information Exchange Forum "Safety Analysis for NPPS of VVER and RBMK type", Obninsk, Russian Federation, 11-15 October, 1999.
24. V.K.Artemyev, S.I.Zaytsev, Y.N.Kornienko. "Modernization of numerical scheme and algorithm of emergency calculation for "TRAP-97" code." Fourth International Information Exchange Forum "Safety Analysis for NPPS of VVER and RBMK type", Obninsk, Russian Federation, 11-15 October, 1999.
25. Single Crystal Growth, Strength Problems, and Heat Mass Transfer, Book of Abstracts of Third International Conference, Institute for Physics and Power Engineering, Obninsk, 1999, 272 p.
26. A.A.Bezborodov, A.V.Volkov, S.M.Ganina, V.P.Ginkin, I.A.Kuznetsov, N.M.Troyanova, Yu.E.Shvetsov. Spatial and Time-Dependent Calculation of Fast Reactor Transients. The Fourth International Congress on Industrial and Applied Mathematics, July 5-9, 1999, Edinburgh, Scotland.
27. Разработка расчетного кода деградации активной зоны реактора типа ВВЭР-1000 в условиях тяжелой аварии "ТАРПАЗ": Отчет ФЭИ-10146, 1999, с.30. - Исполн. Г.А.Мякишев, И.М.Бондаренко, А.И.Коваль, А.А.Изотов, О.М.Науменко.
28. Разработка тепловых зон для отработки ультразвуковой диагностики параметров процесса кристаллизации из расплава методами Бриджмена и зонной плавки. Математическое моделирование тепловых процессов и проведение вариантных расчетов по обоснованию оптимальных параметров конструкций: Отчет ФЭИ-10002, Обнинск, 1999. – Исполн. В.П.Шишулин, И.П.Свириденко, В.К.Артемьев и др.
29. Развитие численной методики и программ решения двумерных и трехмерных задач гидродинамики и тепломассообмена: Отчет ФЭИ-10237, Обнинск, 1999. – Исполн. В.К.Артемьев, Е.О.Руденская.
30. Развитие методов вычисления аналитического решения системы линейных уравнений кинетики реактора: Отчет ФЭИ-10252, Обнинск, 1999, 20с. - Исполн. Д.М.Бабанаков.
31. Разработка нового варианта метода неполной факторизации для решения двумерных и трехмерных уравнений эллиптического типа со смешанными производными: Отчет ФЭИ-10238, Обнинск, 1999, 21с. - Исполн. В.П.Гинкин, А.А.Кулик, О.М.Науменко.
32. П.А.Андросенко, Д.Л.Жолудов, А.В.Компаниец, О.А.Смирнова. Моделирование экспериментов по измерению утечки нейтронов и фотонов непосредственно по данным из файлов оцененных данных. Семинар "Алгоритмы и программы для нейтронно-физических расчетов ядерных реакторов", ИАТЭ, 26-28 октября 1999.
33. П.А.Андросенко, А.В.Компаниец. "Алгоритмы и программы для нейтронно-физических расчетов ядерных реакторов" Моделирование сферических benchmark-экспериментов непосредственно по данным различных библиотек оцененных данных.

34. И.Ю.Шимкевич, А.Л.Шимкевич. Молекулярно-динамическое исследование влияния параметров эффективного парного потенциала на структуру и динамику жидкого натрия. Препринт ГНЦ РФ-ФЭИ, № 2803.
35. В.А.Блохин, М.Н.Ивановский, Т.А.Кувшинчикова, В.В.Кузин, Н.И.Логинов, В.А.Морозов, А.Г.Новиков, С.С.Плетенец, В.В.Савостин, А.Л.Шимкевич, И.Ю.Шимкевич, Б.А.Шматко. Структура, атомная динамика, термодинамики и примесное состояние расплавов свинца и висмута (современное состояние проблемы). Обзор ГНЦ РФ-ФЭИ, №0290, с.1-77.
36. Расплав калия – модельная жидкость щелочно-металлических теплоносителей ЯЭУ. Отчёт ФЭИ-10168, Обнинск, 1999. Исполн. А.Л.Шимкевич, М.Н.Ивановский, В.В.Кузин, Т.А.Кувшинчикова, В.А.Морозов, И.Ю.Шимкевич.
37. A.L.Shimkevich, I.Yu.Shimkevich, and V.V.Kuzin, Molecular Dynamics Study of Ternary System, $K+K^q+O^{-2q}$ // Condensed Matter Physics, 1999, vol.2, №2(18), pp.329-337.
38. I.Yu.Shimkevich, V.V.Kuzin, and A.L.Shimkevich, Dynamic Structure of Oxygen in Liquid Potassium Studied by MD Method and Statistical Geometry // Journal of Non-Crystalline Solids, 1999, vol.250-252, pp.129-134.
39. М.В.Заезжев, В.В.Кузин, А.Г.Новиков, В.В.Савостин, А.Л.Шимкевич, И.Ю.Шимкевич. Микродинамика кислорода в жидком калии, исследованная методами неупругого рассеяния нейтронов и молекулярно-динамического моделирования. Тезисы докладов на конференции РНИКС-99, Обнинск, 13-17 сентября 1999.
40. В.В.Кузин, А.Г.Новиков, В.В.Савостин, А.Л.Шимкевич, И.Ю.Шимкевич. Цепочечные кластеры растворённого кислорода в расплаве калия. Статья в сб.: Теплофизические исследования, Обнинск, ГНЦ РФ-ФЭИ, 1999, с.171-178.
41. В.В.Кузин, А.Г.Новиков, В.В.Савостин, И.Ю.Шимкевич, А.Л.Шимкевич, М.В.Заезжев. Атомная динамика жидкого калия и расплава калия с кислородом // Известия вузов, Ядерная энергетика, Изд. Высшей школы, 2000, №1.

HIGH-VOLTAGE ACCELERATORS DIVISION

1. В.А.Романов, А.А.Малыгин, А.С.Фейгин, Г.С.Жданов, Т.А.Красавина, Д.Л.Загорский, А.И.Виленский, Б.В.Мчедlishvili, Производство трековых мембран на ускорительном комплексе ЭПП-15. Характеристики и свойства. Доклад на XII Международной конференции по электростатическим ускорителям. Обнинск, 25-28 мая 1999 г. (в печати).
2. В.А.Романов, В.В.Экомасов, С.В.Бажал, А.С.Фейгин, Ускоряющая трубка для электростатического ускорителя ЭГ-1, там же.
3. А.И.Глотов, В.С.Башмаков, С.В.Бажал, В.И.Володин, В.К.Дебин, Б.В.Куприянов, А.А.Малыгин, В.А.Никитин, В.А.Романов, В.И.Спирин, А.С.Фейгин, Ю.Р.Чалый, Получение пучков изотопов водорода на ускорителе ЭПП-15 ФЭИ, там же.
4. С.В.Бажал, В.А.Романов, С.-Е.Магнуссон, Р.Хеллборг, М.Фаринен, Конструкция ионно-оптического тракта нового инжектора пеллетрона в Лунде, там же.

5. Б.В.Куприянов, В.С.Башмаков, С.В.Бажал, А.И.Глотов, В.М.Матвеев, Ю.Р.Чалый, Первые результаты реконструкции инжектора ускорителя ЭПП-15, там же.
6. В.Н.Канаки, Н.И.Дудкин, Ю.Р.Чалый, Спектрометр быстрых нейтронов на базе электростатического ускорителя ЭГ-1 ГНЦ РФ-ФЭИ, там же.
7. К.А.Резвых, А.И.Глотов, Влияние полярности на пробивное напряжение промежутков ускорителя (количественная оценка), там же.
8. К.А.Резвых, В.А.Романов, Модернизация высоковольтной структуры перезарядного электростатического ускорителя ЭПП-15, там же.
9. В.В.Соковиков, И.О.Константинов, О возможности изучения износа и коррозии керамики методом поверхностной активации, там же.
10. V.V.Sokovikov, I.O.Konstantinov, V.I.Novikov, I.L.Shcharupa, Wear study of ceramic bearings using thin layer activation technique, Report at the Int.Conf. IBA-14 and ECAART-6, Dresden, Germany, July 26-30, 1999 (in print).
11. K.A.Rezvykh, V.A.Romanov, Gases Breakdown Voltage Calculation for the Case of Accelerator Nonuniform Fields by Method of the Base, Nuclear Instruments and Methods in Physics Research A 423 (1999) 203-212.
12. G.L.Khorasanov, A.P.Ivanov, A.I.Blokhin, A.L.Shimkevich, Lead and Tin Targets for Reducing Polonium Waste. In: Proceedings of the Third Int. Conf. on Accelerator Driven Transmutation Technologies and Applications ADTTA'99, June 7-11, 1999, Praha, Czech Republic, Abstracts, p. 46, Published by ICARIS Ltd, Praha, 1999.
13. G.L.Khorasanov, A.P.Ivanov, A.I.Blokhin, A.Yu.Konobeyev, M.V.Mikhailyukova, V.A.Apse, A.N.Shmelev, G.G.Koulikov, A.A.Glazkov, A.D.Koljaskin, Low-Activation Materials With Isotopic Tailoring for Future NPPs. In: CD-ROM Proceedings of the Int.Conf.on Future Nuclear Systems, GLOBAL'99, Jacson Hole, Wyoming, USA, Aug.30-Sept.2, 1999.
14. G.L.Khorasanov, A.P.Ivanov, V.V.Korobeinikov, A.I.Blokhin, and A.L.Shimkevich. Lead Coolant for Fast Reactor-Burner With Hard Neutron Spectrum. Ibid.
15. A.N.Didenko, A.A.Glazkov, A.D.Koljaskin, A.N.Shmelev, G.L.Khorasanov. Parameters of Electronuclear Facility for Radiowaste Transmutation. Ibid.
16. G.L.Khorasanov, A.P.Ivanov, A.I.Blokhin, A.Yu.Konobeyev, M.V.Mikhailyukova, A.A.Glazkov, A.D.Koljaskin. Bi-207 accumulation problem in lead target for ADS. В сб.: 'Электроядерные системы в перспективной ядерной энергетике' Труды Межд. конференции, (Москва, 11-15 окт.1999 г.),- М.:ИТЭФ, 1999, с.200-203.
17. A.P. Ivanov, V.V. Korobeinikov, G.L. Khorasanov, Lead coolant for ADS blanket with hard neutron spectrum. Там же. 138-141.
18. Г.Л.Хорасанов, А.П.Иванов, В.В.Коробейников, А.И.Блохин, А.Л.Шимкевич. Свинцовый теплоноситель для быстрого реактора – выжигателя с жестким спектром нейтронов. // Известия ВУЗов. Ядерная энергетика, 1999, №1, с.80.
19. Г.Л.Хорасанов. Легкоионные радиоактивные пучки на перезарядных ускорителях. Доклад на XIII Международной конференции по электростатическим ускорителям. Обнинск, 25-28 Мая 1999 г. (в печати).
20. Г.Л.Хорасанов, А.П.Иванов, А.И.Блохин, М.В.Михайлюкова, А.Д.Коляскин, А.А.Глазков, В.Н.Прусаков. Малоактивируемый теплоноситель на основе изотопа свинца Pb-206 для перспективных ЯЭУ. В Сборнике докладов 4-й Всероссийской научной конференции "Физико-химические процессы при

селекции атомов и молекул”, Звенигород, 4-8 окт.1999г., М.: ЦНИИАтоминформ, 1999, с.262-267.

21. A.I.Blokhin, A.P.Ivanov, V.V.Korobeinikov, V.P.Lunev, V.N.Manokhin, G.L.Khorasanov, Calculation and analysis of neutron and radiation characteristics of lead coolants with isotopic tailoring for future nuclear power facilities. In: Proceedings of the Int. Symposium on Nuclear Data, November 18–19, 1999, JAERI, Tokai-mura, Japan (in press).
22. В.В.Коробейников, А.П.Иванов, К.Ф.Раскач, Г.Л.Хорасанов. Анализ различных концепций подкритических реакторов-выжигателей с точки зрения эффективности и безопасности по сравнению с традиционным быстрым реактором . В сб.: “От Первой в мире АЭС к атомной энергетике XXI века”, Сборник тезисов докладов и сообщений. Обнинск: изд.ГНЦ РФ ФЭИ, 1999, стр. 119.

5. MEETINGS AND CONFERENCES

(These are Meeting and Conferences where NPD played a major role in the organization)

1. XVI Workshop on neutron scattering application for condensed matter investigations, 13-17 September 1999, Obninsk, SSC RF IPPE.
About 140 participants from Russia and Former Soviet Union Countries.
Topic: neutron scattering study of solids and liquids, methods and instruments, theory and experiment, applications
2. XIII International Conference on Electrostatic Accelerators, 25-29 May, IPPE Obninsk.
About 120 participants from Russia and Foreign Parts.
Topic: physics and technology of high-voltage accelerators, ion sources, ion beam optics, application of accelerators.
3. Third International Conference "Single Crystal Growth, Strength problems, and Heat Mass Transfer" (ICSC-99), 21-24 September, IPPE, Obninsk.
About 250 participants from Russia and Foreign Parts.
Topics: growth of crystals and thin films, real structures and kinetics of crystallization, mechanics of deformation and fracture of single crystals and thin film structures, heat mass transfer processes in growth of crystals and thin film structures, crystal growth and heat mass transfer processes under microgravity conditions, problems of mathematical and physical modeling in crystal growth.

6. PARTICIPATION IN INTERNATIONAL AND NATIONAL CONFERNCES, SEMINARS AND ORGANIZATION

1.	XXII International Conference on Low Temperature Physics	August 4-11	Helsinki, Finland
2.	Deutsche Neutronenstreutagung	May 25-27	Potsdam, Germany
3.	2nd European Conference on Neutron Scattering	September 1-4	Budapest, Hungary
4.	XX National Conference on Molecules Interactions	June 30-July 3	Kazan, Russia
5.	14 th International Conference on Ion Beam Analysis jointly with 6 th European Conference on Accelerators in Applied Research and Technology	July 26-30 1999	Dresden, Germany
6.	The 3 th International Conference "Single Crystal Growth, Strength Problems, and Heat Mass Transfer"	September 21-24 1999	Obninsk, Russia
7.	International Conference on Computational Heat and Mass Transfer	April 26-29 1999	G. Magusa, N. Cyprus
8.	Workshop on Phase Change with Convection Modeling and Validation	June 24-26 1999	Warsaw, Poland
9.	Отраслевая конференция "Теплофизика-99"	28-30 сентября 1999	Обнинск
10.	Отраслевой семинар "Нейтроника-99"	26-28 октября 1999	Обнинск
11.	The 4 th Joint Conference on Environmental Hydrology and Hydrogeology	November 7-11 1999	San - Francisco
12.	ICONE-7, Trac.7, CD-Room	April 19-23 1999	Tokyo, Japan
13.	The 4 th International Information Exchange Forum "Safety Analysis for NPPS of VVER and RBMK type"	October 11-15 1999	Obninsk
14.	РНИКС-99	13-17 сентября 1999	Обнинск
15.	Intern. Workshop "Collective excitations in nuclei and other finite Fermi- systems"	June 14-24 1999	Dubna, Russia
16.	Intern. conference on nuclear physics "Nuclear shells - 50 years" (XLIL Meeting on Nuclear Spectroscopy and Nuclear Structure)	April 21-24, 1999	Dubna, Russia.
17.	Workshop on "Beta-decay: from weak interaction to nuclear properties"	March 17- 19 1999	Strasbourg, France

7. COOPERATION

1.	Condensed matter study and the neutron spectrometry methods development.	Frank Laboratory of Neutron Physics, Joint Institute on Nuclear Research	Dubna, Russia
2.	The partial dynamical structure factors study of the crystalline and amorphous compounds Ni-B by the inelastic neutron scattering.	Russian National Centre - "Kurchatov Institute"	Moscow, Russia
3.	Study of the microscopic dynamics of the aqueous and nonaqueous solutions by the inelastic neutron scattering.	Kurnakov Institute of General and Inorganic Chemistry, Russian Academy of Sciences	Moscow, Russia
4.	Investigation of the influence of high frequency nonlinear vibrations - biphonons, biexcitons, solitons - with the energy near the lattice stability barrier on the phase transition kinetic in the crystalline and the disordered solid materials.	Institute of Spectroscopy, Academy of Sciences of Russian Federation	Troisk, Moscow Region
5.	Study of lattice dynamic of high temperature superconductors.	Chemical faculty of MSU	Moscow, Russia
6.	The investigation of the quantum liquids fundamental properties by neutron scattering.	National Scientific Centre of Ukraine - "Kharkov Institute of Physics and Technology"	Kharkov, Ukraine
7.	The investigation of hydrogen effect on the crystal structure and lattice dynamics of the austenitic Fe-Cr-Mn steels by the neutron diffraction and inelastic neutron scattering.	Institute for Metal Physics, Ukraine Academy of Science	Kiev, Ukraine
8.	The investigation of the excitation spectrum of the superfluid helium.	Institute of Laue-Langevin,	Grenoble, France
9.	A study of the lattice dynamics of fast ion conductors with the fluorite structure at the transitions temperatures.	Institute for Physics and Nuclear Engineering,	Bucharest, Romania
10.	Interstitial atom effect on the crystal structure and lattice dynamics of the triple Nb-O-H(D) solid solutions and high nitrogen steels.	Darmshtadt University of Technology,	Darmshtadt, Germany
11.	X-ray diffraction and inelastic neutron scattering study of the substitutional alloying additions effect on the crystal structure and lattice dynamics of the austenitic steels.	Institute of Solid State Physics, Bulgarian Academy of Science,	Sofia, Bulgaria
12.	Small angle neutron scattering spectroscopy.	Unite de Recherche en Genie Nucleaire, URGN	Draria, Algeria

13.	Powder neutron diffractometry.	Centre de Developpement des Systemes Energetiques, CDSE	Ain-Oussera, Algeria
14.	Accelerator system "SPRUT" with overlapping low energy electron and proton beams for use in simulating complex KOBE.	Deutsches Zentrum für Luft-und Raumfahrt e.V. , Berlin	Germany
15.	Charging belt system for electrostatic accelerators.	Institute of Ion Beam Physics and Materials Research, Rossendorf	Germany
16.	Verification of fusion relevant nuclear data.	Institut für Kern- und Energietechnik, Forschungszentrum Karlsruhe	Germany
17.	Renormalized QRPA methods for fermionic-bosonic systems.	Laboratory of complex systems, Maria Curie-Sklodowska University, Lublin	Poland
18.	Nuclei far from the β -stability. Nuclear data for astrophysics.	Institut d'Astrophysique ULB, Bruxelles	Belgium

Подписано в печать 15.06.2000. Тираж 135. Заказ №100. Уч.-изд. л.10,6. Усл. печ. л. 7,9.
 Отпечатано на ротапринте ФЭИ с готового макета-оригинала.
 249020, Обнинск Калужской обл., пл. Бондаренко, 1.